

AD-A138 250

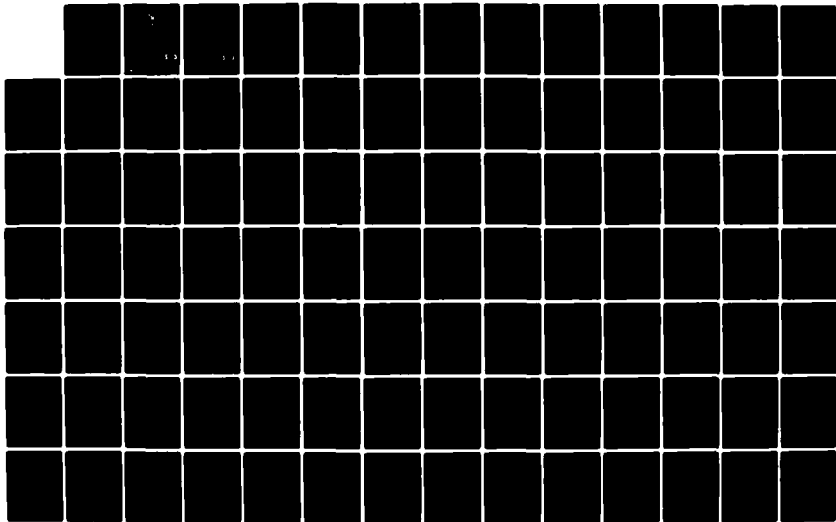
SPECTROSCOPY AND KINETICS OF LEAD OXIDE
CHEMILUMINESCENCE(U) AIR FORCE INST OF TECH
WRIGHT-PATTERSON AFB OH SCHOOL OF ENGINEERING
C M RITCHEY 12 DEC 83 AFIT/GEP/PH/83D-10

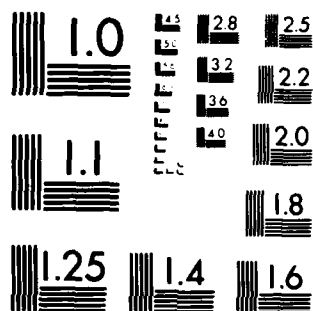
1/2

UNCLASSIFIED

F/G 7/2

NL



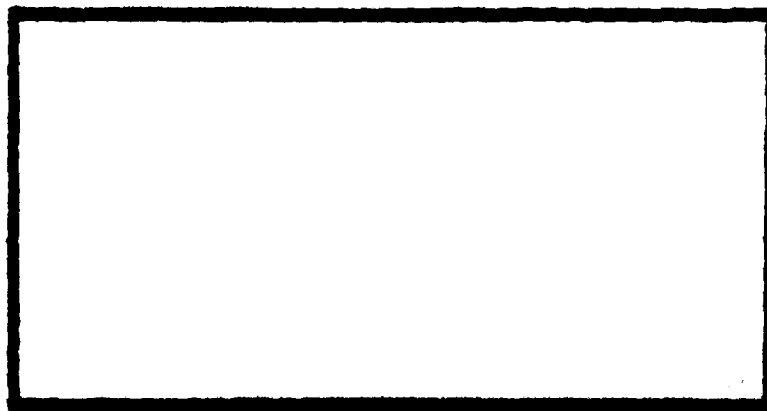


MICROCOPY RESOLUTION TEST CHART
NATIONAL BUREAU OF STANDARDS-1963-A

ADA138250



①



DISTRIBUTION STATEMENT A
Approved for public release;
Distribution Unlimited

DTIC
ELECTE
FEB 24 1984

DEPARTMENT OF THE AIR FORCE
AIR UNIVERSITY (ATC)

AIR FORCE INSTITUTE OF TECHNOLOGY

Wright-Patterson Air Force Base, Ohio

FILE COPY

84 02 21 164

AFIT/GEP/PH/83D-10

SPECTROSCOPY AND KINETICS
OF LEAD OXIDE CHEMILUMINESCENCE

THESIS

Conrad M. Ritchey
Captain, USAF

^P
AFIT/GEP/PH/83-10

DTIC
ELECTE
FEB 24 1984
S D
B

Approved for Public Release; Distribution Unlimited

AFIT/GEP/PH/83D-10

SPECTROSCOPY AND KINETICS
OF LEAD OXIDE CHEMILUMINESCENCE

THESIS

Presented to the Faculty of the School of Engineering
of the Air Force Institute of Technology
Air University
in Partial Fulfillment of the
Requirements for the Degree of
Master of Science

Conrad M. Ritchey, B.S.

Captain, USAF

12 December 1983

Approved for Public Release; Distribution Unlimited

Preface

This thesis is part of an on-going project by AFIT and Air Force Weapons Laboratory researchers to identify possible candidates for chemical lasers. I found this project to be both challenging and rewarding, and I am proud of my contribution to it.

I am especially grateful to Dr. E. A. Dorko for the many stimulating conversations and for his invaluable assistance in the preparation of this manuscript. I would like to thank Mr. Carl Shortt, Mr. David Paine, and Mr. John Brohas of the AFIT Fabrication Shop for their expertise and responsiveness in making flow tube modifications and on-the-spot repairs. I am deeply indebted to Mr. Robert Wade for his excellent craftsmanship in producing the Pyrex manifold. Finally, I wish to thank my loving wife, Nancy, for her patience and understanding throughout this project.

Conrad M. Ritchey

(This thesis typed by Sharon A. Gabriel)

Table of Contents

	<u>Page</u>
Preface-----	ii
List of Figures-----	v
List of Tables-----	vii
Abstract-----	viii
I. Introduction-----	1
Background-----	1
Problem-----	1
Approach-----	2
II. Theory-----	3
Overview of PbO Spectroscopy-----	3
Singlet Delta Oxygen-----	10
Kinetics-----	12
Literature Review-----	15
III. Experimental Equipment and Operational Procedures	22
Flow Tube System-----	22
Vacuum-----	22
Flow Tube-----	24
Optical-----	28
Detection and Recording-----	29
Experimental Procedures-----	30
Alignment-----	31
Calibration-----	32
Signal-to-Noise Ratio-----	33
Resolution-----	35
Spectra-----	35
Temperature Experiments-----	35
IV. Results and Analysis-----	37
System Modifications-----	37
Zirconia Felt Insulation-----	37
Flame Optimization-----	37
Vacuum Transition Section-----	39
Spectra-----	40
Kinetics-----	69
Presence of Excited Pb-----	69
Pb + O ₂ (³ Σ) Reaction Mechanisms-----	78
Pb + O ₂ (¹ Δ) Reaction-----	83

Table of Contents (Cont'd)

	<u>Page</u>
V. Conclusions and Recommendations-----	85
Conclusions-----	85
Recommendations-----	87
New Grating-----	87
New Manifold-----	87
Photon Counter-----	87
Modulated Spectra-----	98
Flame Measurements-----	88
Pb Concentrations-----	88
Activation Energies-----	88
Bibliography-----	89
Appendix A: Photographs-----	92
Appendix B: Power Supply-----	95
Appendix C: Grating Response-----	96
Appendix D: Photomultiplier Tubes-----	97
Appendix E: Start-up and Shut-down Steps-----	99
Appendix F: Pressure Variation Spectra-----	101
Appendix G: Temperature Measurements with Heater Off - O ₂ (³ Σ)-----	110
Vita-----	111



Accession For	
NTIS GRA&I	<input checked="" type="checkbox"/>
DTIC TAB	<input type="checkbox"/>
Unannounced	<input type="checkbox"/>
Justification	
PER CALL JC	
By	
Distribution/	
Availability Codes	
Dist	Avail and/or Special
A-1	

List of Figures

<u>Figure</u>		<u>Page</u>
1	Vertical Transitions-----	7
2	Overlapping Eigenfunctions-----	7
3	PbO Correlation Diagram-----	9
4	Energy Levels of O ₂ , Pb, and PbO-----	13
5	Reaction Process-----	15
6	Flow Tube System-----	23
7	Vacuum Transition Sections-----	25
8	Pyrex Oxidizer Manifold-----	27
9	Low Pass Filter-----	31
10	PMT Signal-to-Noise Ratios-----	34
11	Low Resolution Spectrum-----	41
12	Medium Resolution Spectrum-----	42
13	High Resolution Spectrum-----	43
14	Deslandres Table for the a - X Transition of the Pb + O ₂ (³ Σ) Reaction-----	59
15	Deslandres Table for the A - X Transition of the Pb + O ₂ (¹ Δ) Reaction-----	60
16	Deslandres Table for the B - X Transition of the Pb + O ₂ (¹ Δ) Reaction-----	61
17	Spectrum from 3000 Å to 4000 Å for the Pb + O ₂ (¹ Δ) Reaction-----	62
18	Deslandres Table of Intensities for the a - X Transition of the Pb + O ₂ (³ Σ) Reaction-----	64
19	Deslandres Table of Intensities for the A - X Transition of the Pb + O ₂ (¹ Δ)-----	64

List of Figures (Cont'd)

<u>Figure</u>		<u>Page</u>
20	Deslandres Table of Intensities for the B - X Transition of the $\text{Pb} + \text{O}_2(^1\Delta)$ Reaction-----	65
21	Low Dispersion Spectrum from the $\text{Pb} + \text{O}_2(^3\Sigma)$ Reaction-----	66
22	Low Dispersion Spectrum from the $\text{Pb} + \text{O}_2(^1\Delta)$ Reaction-----	67
23	Intensity and Temperature Decay Versus Time for $\text{Pb} + \text{O}_2(^3\Sigma)$ Reaction-----	72
24	Logarithmic Intensity Decay Versus Time for $\text{Pb} + \text{O}_2(^3\Sigma)$ Reaction-----	72
25	Excited State Energies and Reaction Exothermicities-----	81
A-1	Flow Tube System-----	92
A-2	Furnace Chamber-----	92
A-3	Oxidizer Manifolds-----	93
A-4	Discharge Cavity Assembly-----	93
A-5	Chemiluminescent Flame-----	94
B-1	Power Supply-----	95
B-2	Power Supply Schematic-----	95
D-1	PMT Characteristics-----	97
D-2	PMT Response-----	97
D-3	New PMT and Housing-----	98

List of Tables

<u>Table</u>		<u>Page</u>
I	Electronic State Energies-----	4
II	Lifetimes of Excited States of PbO-----	16
III	Observed PbO Bandheads and Their Assignments for the $\text{Pb} + \text{O}_2(^3\Sigma)$ Reaction-----	45
IV	Observed PbO Bandheads and Their Assignments for the $\text{Pb} + \text{O}_2(^1\Delta)$ Reaction-----	48
V	Intensity Ratios for the a - X, A - X and B - X Transitions-----	68
VI	Energy Levels of Pb-----	74
VII	Transition Probabilities Between Excited States of Pb-----	75
VIII	Heats of Formation-----	79
IX	Reaction Exothermicities of $\text{Pb}(^3\text{P}_n) + \text{O}_2(^3\Sigma)$ where $n = 0, 1, 2$ -----	79
X	Activation Energies-----	80

delta

Sigma

Abstract

Chemiluminescence from lead oxide has been observed from the reaction between lead (Pb) vapor and $O_2(^1\Delta)$. The spectrum obtained from this emission has been compared to that obtained from the chemiluminescence observed during the reaction between Pb and ground state $O_2(^3\Sigma)$. A significant enhancement of the A and B states over the a state was noted. Spectral analysis has led to the assignment of 225 transitions from the a, b, A, B, C, C', D and E excited states to the ground state. A simple kinetic analysis was performed for the two reactions in which a plot of the logarithm of the intensity of a spectral band vs $1/T^\circ K$ was prepared. From the slope of the straight lines produced, the activation energies of the two reactions were calculated. The activation energy for the $Pb + O_2(^1\Delta)$ reaction was found to be about 21 Kcal/mole with a strong inverse dependency on oven temperature. The activation energy for the $Pb + O_2(^3\Sigma)$ reaction was determined for two oxidizer pressure regimes. The activation energies ranged from 64 Kcal/mole at low oxidizer pressures to 115 Kcal/mole at high oxidizer pressures. The significance of these results is discussed.

SPECTROSCOPY AND KINETICS OF LEAD OXIDE CHEMILUMINESCENCE

I. Introduction

Background

The Air Force is currently involved in the development of Chemical Electronic Transition Lasers (CETL). These lasers depend on a chemical reaction to produce both the lasing species and the population inversion. Since the scale-up of such devices is not limited by large electrical power supplies, they are attractive for high power military applications (Ref 1:398).

Because of its chemiluminescent properties, lead oxide (PbO) is being investigated by AFIT researchers as a potential candidate for a CETL. The emission spectrum of PbO and the kinetic mechanisms of the chemical reactions involved must be fully characterized before the full lasing potential of PbO can be realized. A comparison of the spectra and kinetics of PbO using ground state oxygen, $O_2(^3\Sigma)$, and singlet delta (excited) oxygen, $O_2(^1\Delta)$, as the oxidizers, forms the basis for this thesis.

Problem

The purpose of this thesis was to compare the relative intensities of the spectral emissions of PbO using $O_2(^3\Sigma)$

and $O_2(^1\Delta)$ as oxidizers. This comparison was the first step in determining if higher energy electronic states can be enhanced preferentially over lower energy states. In addition, the dependence of the relative intensities of the various states on oxidizer pressure was studied. Finally, the temperature dependence of the relative intensities was examined. This information allowed initial determination of the basic reaction mechanisms.

Approach

A chemiluminescent flame was generated in a flow tube reactor. $O_2(^1\Delta)$ was produced using a microwave generator and discharge cavity. Spectroscopy was performed conventionally using a 0.5 m monochromator. Temperature measurements were taken using a potentiometer and standard thermocouples.

II. Theory

This section will develop the concepts necessary to understand the spectroscopy of lead oxide and some of the kinetics involved in the reactions between lead and ground state oxygen and between lead and singlet delta oxygen. An overview of the spectroscopy of PbO will be given first. This will be followed by a discussion of the spectroscopy, gas handling, and generation of singlet delta oxygen. Finally, an introduction to the determination of kinetic mechanisms will be presented.

Overview of PbO Spectroscopy

The detailed theory of PbO spectroscopy has been developed previously at AFIT by Snyder and Glessner. The following synopsis is based on their work (Refs 2, 3).

Electronically excited lead oxide (PbO*) is formed by the reaction of lead vapor and an appropriate oxidizer. Emissions have been observed from six different electronic states (Refs 4, 5, 6). These states and their associated energies are shown in Table I.

Emission lines from these states are due to transitions from the vibrational energy levels of excited states to the vibrational energy levels of the ground state (Ref 7:284). The energies of each possible transition can be calculated using the equation

State	Energy (cm ⁻¹)	Reference
X	0	4
a	16024.9	5
b	16315	6
A	19862.3	6
B	22289	6
C	23820	6
C'	24947	6
D	30194	6
E	34455	6

TABLE I. Electronic State Energies

$$\begin{aligned}
 \bar{\nu}(v', v'') = & T'_e + w'_e(v'+0.5) - w'_e X'_e (v'+0.5)^2 + \dots \\
 & - w''_e(v''+0.5) + w''_e X''_e (v''+0.5)^2 + \dots \quad (1)
 \end{aligned}$$

where T'_e is the difference between the ground state energies of the two electronic states, v' and v'' are the upper and lower state vibrational quantum numbers, respectively, X_e is the anharmonicity constant, and

$$w_e = \frac{w}{2\pi c} \quad (2)$$

where w is the angular velocity (Ref 8: Sec III, 17).

Transitions can be broken down into groups called progressions and series. Transitions from the same upper state to different lower states form a v'' progression. Similarly, there are v' progressions. Transitions between upper and lower states that have the same vibrational quantum number are called series.

All the possible vibrational transitions between two electronic energy levels can be arranged in a Deslandres table (Ref 9:40). The table is arranged such that v'' progressions form rows, v' progressions form columns and series form the main diagonal. When the proper (v', v'') transition assignments have been made and the energies of the transitions arranged in a Deslandres table, the energy differences between successive pairs in a row will be equal. Similarly, the differences between successive pairs in a column will be equal within the accuracy of the experimental measurements (Ref 10:122). This relationship provides an excellent method for checking the accuracy of the transition assignments.

There is no strict selection rule for the vibrational transitions accompanying an electronic transition (Ref 9:194). In principle, transitions can occur between any two vibrational levels from different electronic states. However, not all transitions are observed and not all observed

transitions are of equal intensity. This can be explained by considering the Franck-Condon principle and the potential energy curves of two electronic states. The Franck-Condon principle states that an electronic transition takes place so quickly in comparison to the vibrational motion of the molecule that, immediately after the transition, the nuclei have the same relative position and velocity as before the transition (Ref 9:194). In terms of the potential energy curve, Figure 1, the electrons can only make vertical transitions. In Figure 1, the probability of the (0,1) and (0,0) transitions is very small due to the relative position of the two curves.

A wave mechanical treatment of the potential energy curves confirms this vertical transition assumption. The greatest probability of a transition occurs for the "best" overlapping of the eigenfunctions, shown in Figure 2. Each vibrational level has a probability density distribution. Therefore, the transition may occur over a given range of r (internuclear distance) values for both the upper and lower vibrational levels. This explains why, instead of a single band, a number of bands with differing intensities of the v'' progression where $v' = 0$ appear as in Figure 2 (Ref 9:199). Thus, the intensity of a transition is directly related to the number density of the upper vibrational level and the overlapping of the vibrational eigenfunctions (Ref 9:200).

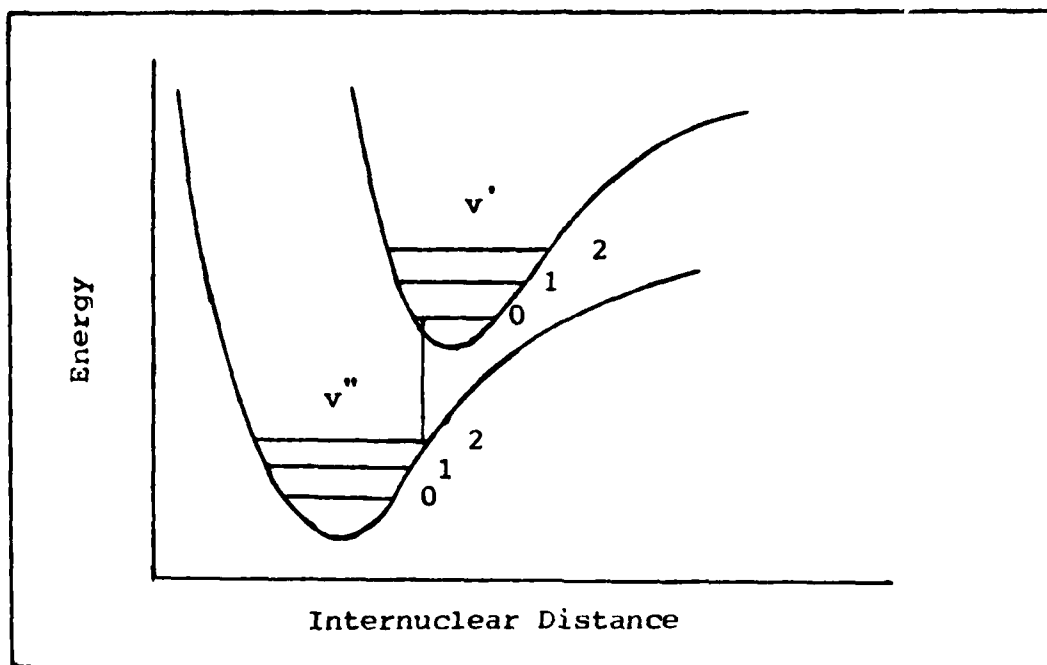


Figure 1. Vertical Transitions

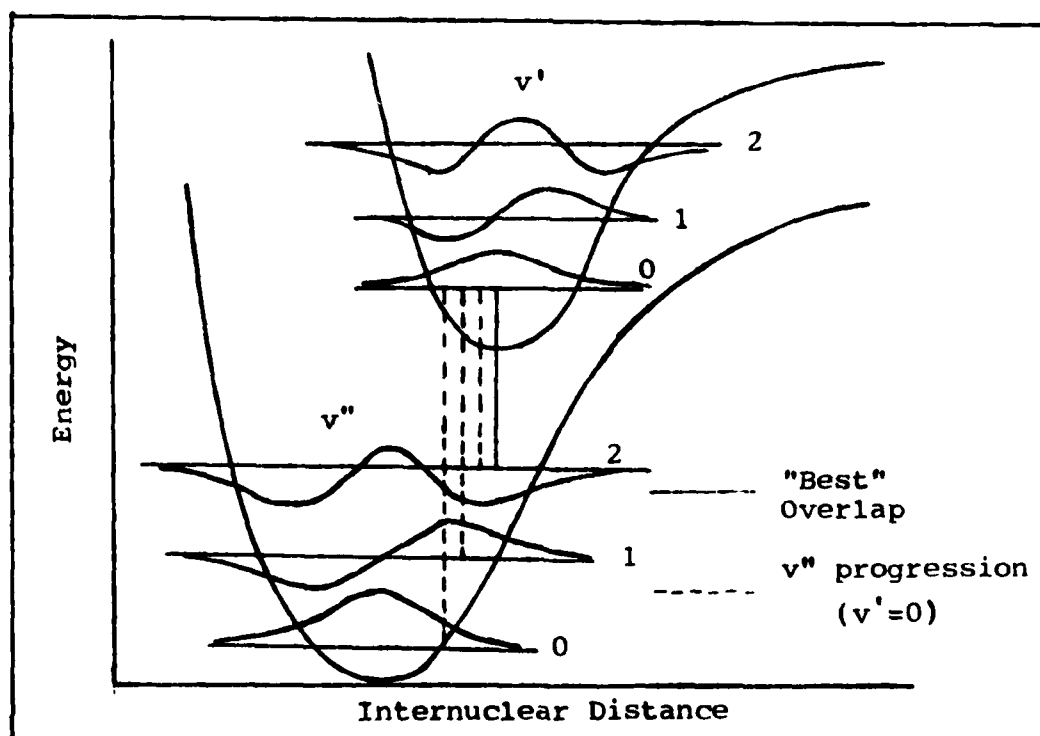


Figure 2. Overlapping Eigenfunctions

In low resolution spectroscopy, vibrational transitions appear as broad bands in a spectrum. These bands are due to the unresolved rotational transitions within the vibrational transitions. The bandhead, a sharply defined edge, is characteristic of these bands. The bandhead is usually close to the band origin and to a very good approximation can be used to determine the band origin (Ref 11:37).

In dealing with the electronic transitions of lead oxide, it is most convenient to start with the electronic configuration of the molecule. Lead contributes two 6p valence electrons and oxygen four 2p electrons to the electronic molecular orbitals of lead oxide. The ground state electronic configuration for the six valence electrons of PbO, following Mulliken's convention (Ref 9:22), is designated as

$$KKLMNO (Z\sigma)^2 (Y\sigma)^2 (W\pi)^4 (X\sigma)^2 \quad \text{or} \quad \sigma^2 \pi^4 \quad (3)$$

The first two excited states are $\pi^3 \pi$ and $\sigma \pi$. These electronic configurations correlate with electronic energy states as shown in Figure 3. The relative energies are as reported in the literature (Refs 4, 5, and 12). Because of the large spin-orbit coupling of PbO, the spin is no longer coupled to the internuclear axis and all the electronic states obey Hund's case c coupling (Ref 4:396).

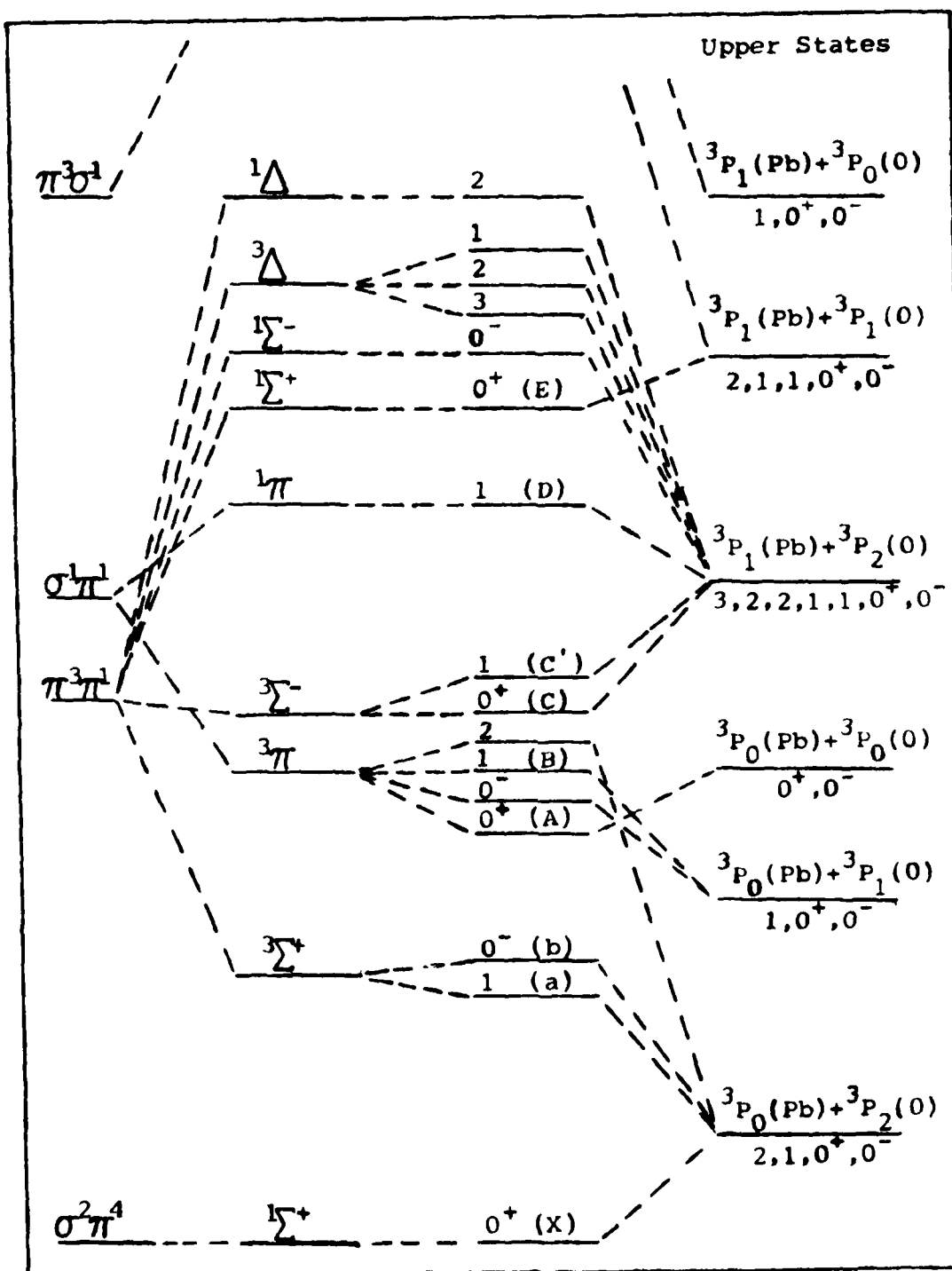


Figure 3. PbO Correlation Diagram (Refs 4, 5, 12)

The selection rules for case c coupling are $\Delta\Omega = 0, \pm 1$ with $0^+ \leftrightarrow 0^-$ (Ref 9:244). Based on these selection rules, all of the observed transitions from the states in Table I and shown in Figure 3 are allowed except for the $b0^- - x0^+$. This transition is forbidden because the reflection symmetry rule is violated. In case c coupling, this selection rule is not as strict as the selection rule for different multiplicities in Hund's case a coupling (Ref 9:242). Experimental observation of the $b - x$ transition lends credibility to the case c nature of the b state.

Singlet Delta Oxygen

Singlet delta oxygen, $O_2(^1\Delta)$, is the a state or lowest excited electronic state of molecular oxygen. The energy of $O_2(^1\Delta)$ is 7918.1 cm^{-1} above the energy of oxygen in the ground state (Ref 10:184). The electronic configuration of oxygen is

$$KK(\sigma_g 2s)^2 (\sigma_u 2s)^2 (\sigma_g 2p)^2 (\pi_u 2p)^4 (\pi_g 2p)^2 \quad (\text{Ref 9:343}) \quad (4)$$

Since there are the same number of odd and even parity electrons, all three lower states will have even parity. In homonuclear diatomic molecules, the $u \leftrightarrow g$ selection rule prevents transitions between states of the same parity (Ref 10:84). Therefore, the $O_2(^1\Delta)$ state is

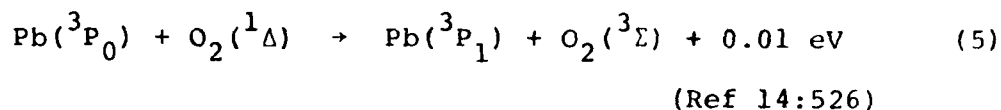
metastable. Experiment has shown that the $O_2(^1\Delta)$ state has a radiative half-life of 45 minutes at zero pressure (Ref 13:41). When operating in a conventional flow system at pressures of 0.5 to 10 Torr, the half-life decreases to about 1 sec. However, in 10-20 mm tubing, the gas stream can travel a centimeter in 1 to 2 msec. Therefore, $O_2(^1\Delta)$ can be transported more than a meter in such a flow system without significant losses (Ref 13:41).

$O_2(^1\Delta)$ is quenched rapidly upon contact with metal. The quenching efficiency of various other materials, however, is quite low. For instance, Pyrex has a quenching efficiency of 10^{-5} (Ref 14:526). A low quenching coefficient material must be used along the entire path that the $O_2(^1\Delta)$ will follow.

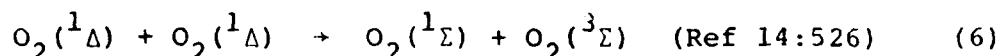
$O_2(^1\Delta)$ is produced in basically two ways: electrical discharge and chemical reaction. In electrical discharge, the primary mechanism for the creation of $O_2(^1\Delta)$ is electron collisions in a plasma generated by a 2450 MHz microwave discharge. Although this creates both $O_2(^1\Delta)$ and $O_2(^1\Sigma)$, the lifetime of $O_2(^1\Delta)$ is 10^3 times greater than $O_2(^1\Sigma)$, and the $O_2(^1\Sigma)$ concentration is negligible (Ref 13:24). Chemically, $O_2(^1\Delta)$ is produced by the reaction between hydrogen peroxide and hypochlorite ion (Ref 13:60). This reaction produces 30% concentrations of $O_2(^1\Delta)$ compared to 10% concentrations for the microwave discharge (Ref 14:526).

Kinetics

The primary mechanism for the reaction of $O_2(^1\Delta)$ with Pb, which has an energy of 7819 cm^{-1} in the 3P_1 state, is thought to be the resonant energy transfer process



As seen in Figure 4, $O_2(^1\Delta)$ has approximately the same energy as Pb in its lowest excited state 3P_1 . Further reactions of excited Pb with $O_2(^1\Delta)$ or $O_2(^1\Sigma)$ can yield even higher excited states of Pb. $O_2(^1\Sigma)$ is created via the energy pooling reaction



These excited forms of Pb can then react with $O_2(^3\Sigma)$ to produce PbO^* . The mechanism of this process is currently not well known (Refs 4, 14).

Specific information about the reaction kinetics can be obtained by observing the radiation emitted from products formed in highly energetic, single-collision chemiluminescent reactions. The temperature dependence of the reaction of a stream of metal atoms with an appropriate oxidizer can be used to deduce the activation energy for formation of

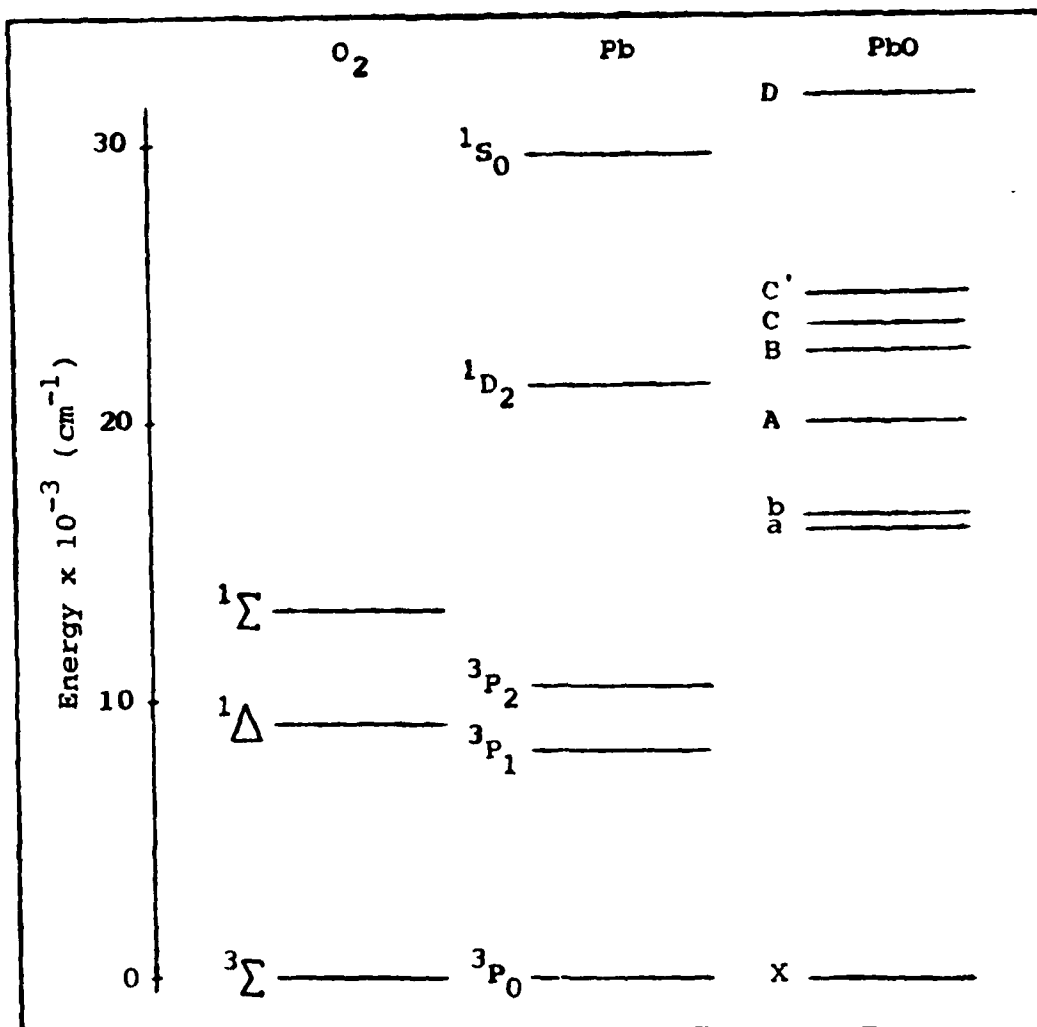


Figure 4. Energy Levels of O_2 , Pb, and PbO

product molecules (Ref 15:176). This information, in turn, can be used in a determination of the mechanism of the reaction.

To understand the kinetics of a reaction, the heats of formation, ΔH_f^0 is determined experimentally and the values are tabulated in the literature. ΔH_r can be found

using the following equation

$$\Delta H_r = \sum_p \Delta H_f^o - \sum_r \Delta H_f^o \quad (7)$$

where \sum_p is the summation over all products and \sum_r is the summation over all reactants. ΔH_f^o and ΔH_r are related to the activation energy, E_a , by the following equations

$$E_a = \Delta H_m + \Delta H_v \quad (8)$$

and

$$E_a = \Delta H_m + \Delta H_v + \Delta H_x \quad (9)$$

where m stands for melt, v for vaporization and x for excitation. Thus, the energy of one of the reactants can be determined. The relationship of the activation energy with respect to the reaction is shown in Figure 5.

The activation energy for a reaction is defined by the Arrhenius equation involving the reaction rate constant, $k(T)$ and a pre-exponential or frequency factor, A .

$$k(T) = A \exp(-E_a/kT) \quad (\text{Ref 15:177}) \quad (10)$$

where R is the universal gas constant and T is the

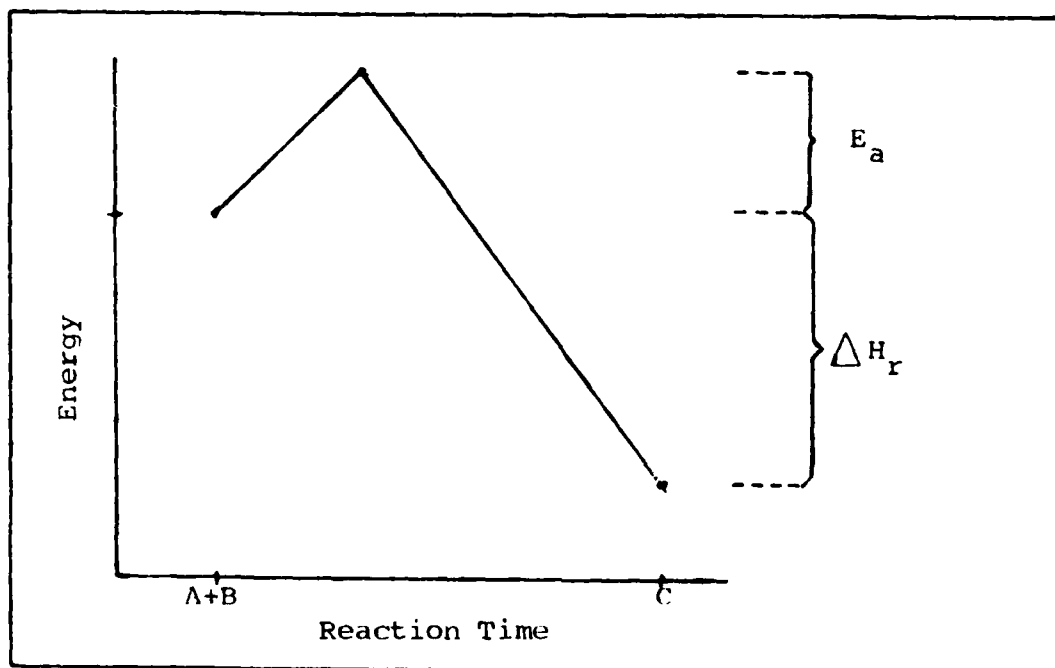


Figure 5. Reaction Process

absolute temperature. Assuming that A and E_a are independent of temperature, Eq (10) can be differentiated to yield

$$E_a = -R \frac{d[\ln k(T)]}{d[1/T]} \quad (11)$$

Therefore, a plot of $\ln k(T)$ versus $1/T$ should produce a straight line with negative slope (Ref 16:23). From Eq (11), E_a can easily be calculated once the slope is known.

Literature Review

The PbO system has been studied extensively for over 50 years. Early researchers used lead chloride gas flames

and carbon arcs using both lead chloride and uranium lead chloride. They observed emissions from the A, B and D states and were able to correlate, to good agreement with theory, the wavelength shifts due to the isotope effect (Ref 11).

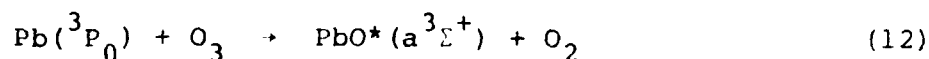
More recently, using a system called LABSTAR, Oldenberg, Dickson and Zare (Ref 7) were able to perform emission spectroscopy and laser induced fluorescence studies of the PbO system. By reacting atomic lead with O_3 under single collision conditions, they identified a series of 55 bands assigned to the a and b states from 450 - 850 nm. Their analysis showed that all bands were emissions to the ground state from excited electronic states. They were also able to perform radiative lifetime studies using pulsed laser excitation. Their results are shown in Table II.

State	Lifetime
a	$T > 10 \text{ } \mu\text{sec}$
A	$T = 3.75 \pm 0.3 \text{ } \mu\text{sec}$
B	$T = 2.58 \pm 0.3 \text{ } \mu\text{sec}$

Table II. Lifetimes of Excited States of PbO

Beattie et al (Ref 17) performed a similar study of the a state using laser excitation. They found the lifetime to be dependent on the vibrational energy level with higher levels having shorter lifetimes. The lifetimes of the $v' = 3$ and 4 levels were determined to be 81.8 ± 5.5 μ sec and 61 ± 14 μ sec, respectively, thus verifying the result of Oldenberg et al.

The bimolecular reaction between ground state lead atoms and ozone, shown in Eq (12), is responsible for the population of the a state.



To determine the order of this reaction, Oldenberg et al studied the chemiluminescent intensity as a function of oven temperature (T). By plotting the logarithm of the intensity versus $1/T$, they were able to find the activation energy. They concluded that (i) the chemiluminescence was first order in Pb, with no dependence on other components like Pb_2 , and that (ii) the reaction activation energy was small.

They observed unusual variations in chemiluminescent intensities of the B-X transition with changes in oven temperature. They found that the intensity decreased with increasing oven temperature over certain temperature ranges.

They attributed this phenomenon to a discharge near the oven which was exciting some Pb atoms to the metastable 3P_1 or 3P_2 levels. The reaction of these excited Pb atoms with O_3 produced the B-X chemiluminescent feature.

Kurylo et al (Ref 5) also studied the reaction of lead and ozone. They observed emissions from the a, b, A, and B states. Using laser excitation of the O_3 , they recorded a significant increase in A state emission intensity over the a, b, and B states. They have postulated two mechanisms for the enhancement. First, as a result of laser excitation of O_3 , the reaction with $Pb(J=1)$, where J is the total angular momentum quantum number, produces PbO^* in the B state in higher vibrational energy levels. This energy is then collisionally transferred to another molecule which is excited to the A state. Another possibility is that the vibrational energy in the excited O_3 directly increases the rate of A state production at the expense of other reaction channels. Their observation of chemiluminescence over several feet in their flow system indicates a slow reaction with $Pb(J=1)$ must compete favorably with its deactivation reaction points to a fast reaction for $Pb(J=1)$.

Linton and Broida (Ref 4) investigated the reactions of lead with N_2O , O, O_2 , and O_3 by studying the spectra of PbO from a flow system under a wide variety of conditions.

They found that spectral intensities were very dependent on the oxidizer used and on the oxidizer pressure. They tabulated eight band systems between 250 nm and 800 nm and observed 22 new bands in the PbO system.

Linton and Broida developed a technique for analyzing spectral data (Ref 4:398-399). They used logarithmic intensity ratio plots to illustrate on one graph the population behavior of electronic and vibrational states as system conditions were changed. This technique allows one to work directly from photomultiplier signals without any knowledge of electronic or vibrational probability parameters.

Brom and Beattie (Ref 18) used a flashlamp-pumped tunable dye laser to study the a-X band system of PbO. They were able to obtain high resolution spectra which allowed calculation of rotational constants. Observation of P, Q, and R rotational branches confirmed that Hund's case c is the angular momentum coupling scheme for the a state of PbO.

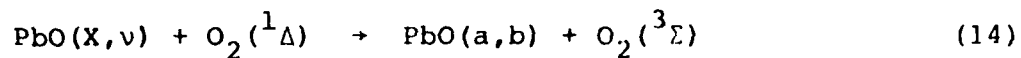
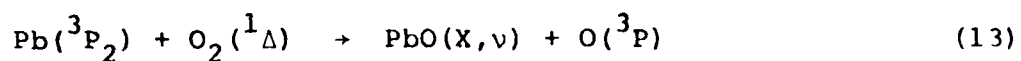
Lead oxide was first investigated at AFIT by Snyder (Ref 2) using a flow tube built by Koym (Ref 19). Low resolution spectra from 200 - 800 nm were obtained using O₂ and N₂O as oxidizers. Variations in spectral line intensities were recorded for different oxidizers and pressures. A significant enhancement of A and B states

was recorded at 0.4 Torr of O_2 . This low pressure phenomenon was previously unreported.

Glessner (Ref 3) performed a flame optimization of the system used by Snyder. Major modifications to the flow tube system increased flame intensity and decreased window contamination. Emissions from the a, b, A, and B states of PbO were observed. Spectroscopic constants for the respective states were calculated using the observed bandhead assignments and a linear regression technique. A slightly modified version of this system was used in the current work.

The most recent work with PbO was reported by Bachar and Rosenwaks (Ref 14). While studying the reaction of Pb with $O_2(^1\Delta)$, they observed emissions from the a, b, A, B, C, C', and D states, but did not report bandhead assignments. However, they were unable to observe a flame using $O_2(^3\Sigma)$ under their experimental conditions. Further, they made no attempts to adjust their experimental conditions to make such an observation. Using microwave and chemical sources of $O_2(^1\Delta)$, they were able to compare the effects of $O_2(^1\Delta)$ concentration on the relative intensities of the various states. In going from 10% concentration to 30%, they noted a significant increase in intensity from all the states with the enhancement of the high energy D state about twice that of the other states.

They also studied the kinetic mechanism of the reaction by taking into account the concentration of excited species and exothermicity of possible reactions. From their analysis, the main route for PbO* production is the following sequence



with higher states being formed by further reaction of the metastable a and b states with $\text{O}_2(^1\Delta)$. This mechanism is supported by the D state enhancement.

III. Experimental Equipment and Operational Procedures

The apparatus and procedures used during this thesis are discussed in this section. Modifications to the system will be described explicitly. All unique procedures will be explained fully.

Flow Tube System

The flow tube system used during this project was basically the same as that used by Glessner (Ref 3). A schematic of the system is shown in Figure 6, and a photograph is displayed in Appendix A. The system is comprised of four component systems:

- (1) Vacuum
- (2) Flow Tube
- (3) Optical
- (4) Detection and Recording.

Each of these systems will be discussed.

Vacuum. A complete description of the vacuum system is given in Reference 19 and will not be repeated here. However, an inherent problem with the current flow tube system is the constriction in the vacuum transition section from 2 and 7/8 in. ID to 1 and 1/2 in. ID. This reduction limits the amount of vacuum that can be achieved. With the acquisition of a new vacuum pump with a capacity

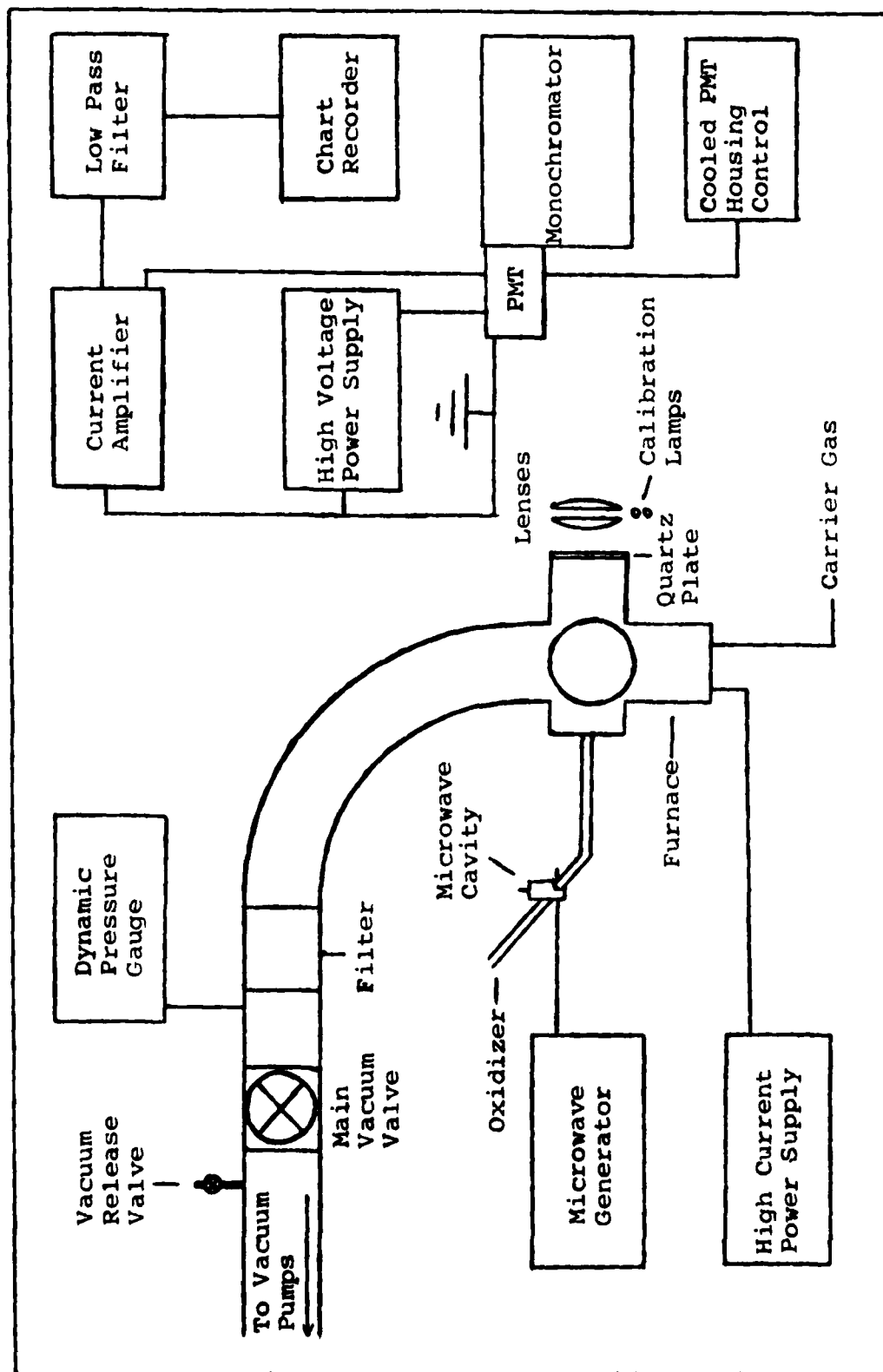


Figure 6. Flow Tube System

of 35 cubic feet per minute, a new transition section was designed and built. The old and new systems are compared in Figure 7. The new system maintains a minimum ID of 2 and 1/2 in. The particle filter is now the major limiting factor. In addition, a throttle valve was included to maximize system flexibility. The section of 3 in. fire hose provides vibrational isolation of the flow tube from the pump.

Flow Tube. The flow tube is constructed of 2 and 7/8 in. ID stainless steel sections (Alloy Products). The sections are interconnected by flanges and heavy duty clamps. This allows easy disassembly during cleanup. Rubber O-rings provide a vacuum seal between sections.

At the heart of the flow tube is a 6-way cross. The sixth arm of the cross was added to facilitate thermocouple experiments. The cross and back plate are anodized to prevent reflections while taking spectra. Each arm of the cross extends 3.5 in. from the center. The upper port of the cross is attached to the vacuum system. This design (Ref 3) allows efficient removal of reaction products and prevents window contamination. A glass wool particle trap (filter) prevents ingestion of contaminants into the vacuum pumps. An MKS Baratron 77 pressure meter was used to measure dynamic pressures downstream from the filter.

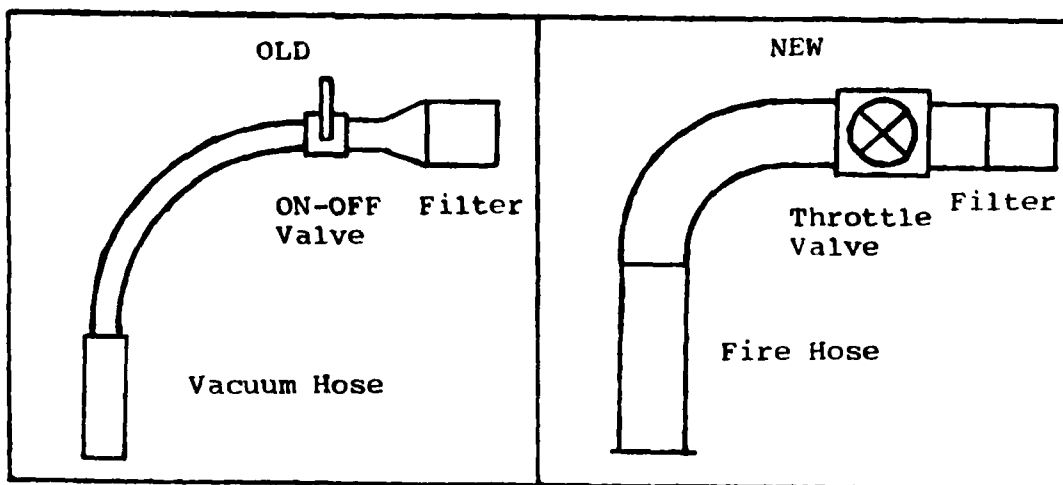


Figure 7. Vacuum Transition Sections

A water-cooled furnace assembly (Ref 3:28-30) is attached to the lower port of the cross. As recommended by Glessner (Ref 3:76), the furnace chamber was lined with Zirconia felt to provide a more stable temperature within the furnace. Expandable bands were used to secure the felt in the furnace. A photograph of the lined chamber is given in Appendix A.

Granular lead (Fisher-Scientific) was resistively heated in an alumina crucible (R.D. Mathis Co.). The crucible was held by a tungsten coil (R.D. Mathis Co.) attached to two brass electrodes. The electrodes were electrically insulated from the tube by Teflon swage-lock fittings (Nacon Industries, Tustin CA) capable of maintaining a vacuum seal. The electrodes were attached to a high current/low voltage power supply.

The previous power supply for the flow tube was a permanent fixture and could not be moved during relocation of the chemistry lab. A new power supply was designed and built specifically for use with the flow tube. The design includes a 115 V Variac power supply with a 15 A maximum output and three model RT-2012 transformers (Stankor Electronics, Inc., Chicago IL). A photograph and schematic diagram are included as Appendix B.

Lead vapor was entrained in Argon gas, and the mixture was passed via a chimney assembly (Ref 3:28-29) to the reaction region where it was mixed with the oxidizer. For the reaction of $O_2(^3\Sigma)$, the metal oxidizer manifold designed by Glessner was used. However, since $O_2(^1\Lambda)$ is deexcited upon contact with metal, a new manifold was designed and built from Pyrex. Pyrex was used because of its very low quenching coefficient (10^{-5}) (Ref 14:526). A cutaway diagram is shown in Figure 8.

The manifold consists of a section of 14 mm ID Pyrex tubing flared at one end. A series of 6 rows of 4 holes each were drilled in the tubing. The holes were 0.8 mm in diameter and were drilled with a diamond impregnated bit. The first row of holes was drilled in the flared edge at a 45° angle to the tube proper. The rows were spaced 3 mm apart, and each row was offset from the previous row by 45° to prevent stress fractures during drilling. Once the

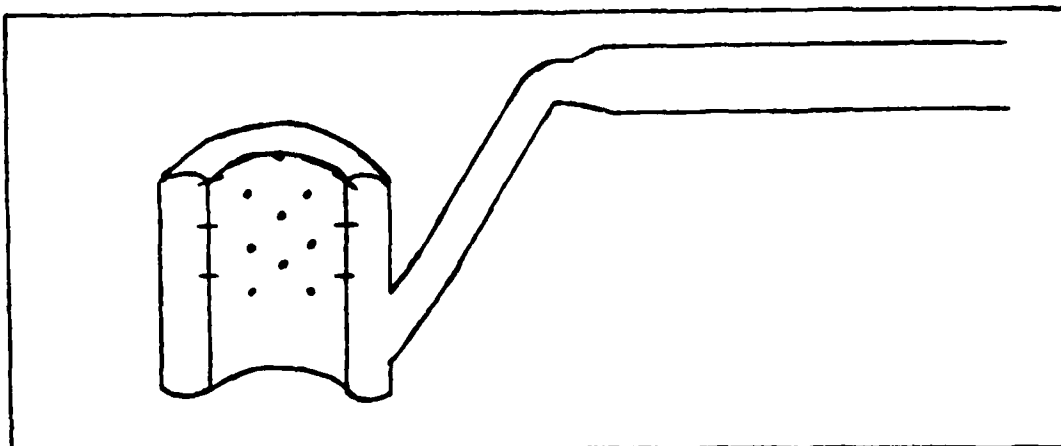


Figure 8. Pyrex Oxidizer Manifold

holes were drilled, a section of 28 mm OD tubing was placed over the smaller tubing, and the two sections were sealed together. This formed a double-walled cylinder with an open center. Finally, the Pyrex stem was attached to the lower edge of the cylinder. Appendix A shows a photograph of the metal and glass oxidizers.

The manifold was mounted over the chimney. The stem of the pyrex manifold was secured to the flow tube via a 1/2 in. Cajun connector welded on a stainless steel plate. The plate was attached to one of the side ports of the cross. Due to the fragility of the manifold, extreme care was taken when installing or removing the manifold.

The side port opposite the monochromator was used for introduction of thermocouples during temperature experiments. Four combination BNC/solder lug connectors were attached to a cover plate and provided thermocouple access.

The side ports opposite the oxidizer inlet and facing the monochromator were used for optical transmission. Extensions were added to these ports to prevent window contamination. Three inch quartz plates were mounted on the extensions.

$O_2(^1\Delta)$ was generated using a 2450 MHz microwave discharge. $O_2(^3\Sigma)$ was passed through an Evenson microwave discharge cavity via a 13 mm OD quartz tube. Quartz was used due to the extreme heat generated by the plasma within the cavity. The microwaves were produced by an Opthos MPG-4 microwave generator operating at 80 W forward power. Tuning of the cavity to reduce reflected power was performed as outlined in Reference 20. Appendix A shows a photograph of the discharge cavity assembly.

Optical. The optical system is comprised of two 3 in. quartz lenses and a Jarrell-Ash 0.5 m monochromator with an Ebert mount. Quartz lenses were used because they transmit down to 2000 \AA . A 25 cm focal length lens was used to collect the emissions from the flame region. A 50 cm focal length lens focused the emissions upon the entrance slit of the monochromator. The two lenses were mounted back-to-back in the same holder to simplify alignment. The lenses were positioned 25 cm from the flame region on a two dimensional translating stage. The monochromator was placed 75 cm from the flame region. An 1100 lines/mm grating blazed at 5000 \AA was used. The spectral response of the

grating is shown in Appendix C. The instrument has an exit slit dispersion of 16 \AA/mm with a maximum resolution of 0.2 \AA in first order. Available scanning speeds are 2, 5, 10, 20, 50, 125 and 500 \AA/min .

Detection and Recording. The major component in the detection and recording system is the photomultiplier tube (PMT). An RCA 7265 PMT was used for initial work. However, as Glessner reported (Ref 3:70), this PMT had slowly degraded to a signal-to-noise (S/N) ratio of 3 to 1 at the low light levels of this experiment. The 7265 was cooled by wrapping copper strips around the PMT housing and dipping them in a Dewar vessel filled with liquid nitrogen. Since the nitrogen level could not be kept constant, the response of the PMT drifted.

This problem was eliminated with the receipt of a new Model TE104TSRF cooled PMT housing (Products for Research, Inc.). The TE104TSRF is a thermoelectric refrigerated chamber which operates using water recirculation and can be operated down to 40° C below ambient. The housing also has quartz optics for low wavelength operation. An RCA C3103402 PMT was installed in the new housing. The characteristics and response of the 7265 and C3103402 are compared in Appendix D. Both PMTs were biased with a Keithley 244 high voltage power supply.

The signal from the PMT was input to a Keithley 427 current amplifier. The amplifier was placed as close to the PMT as physically possible to reduce the length of connection cable required. A doubly shielded cable wrapped with non-conducting tape was used to reduce stray noise. A low pass filter, built by Glessner (Ref 3:32-33), was modified and placed in the output line of the current amplifier. The modified design is shown in Figure 9. This design increased the filtering and allowed adjustment of the rise time constant from 1 msec to 1 sec.

From the filter, the signal was fed to an Omegaline Engineering strip chart recorder. The recorder has speeds available from 1 in./min to 10 in./min with speed reduction factors of 10 and 60. The full scale voltage is adjustable in factors of 10 from 0.001 V to 10 V.

Experimental Procedures

Procedures which were unique to this experiment are explained in this section. Start-up and shut-down procedures are given in Appendix E. General Operating procedures are presented in Reference 2. Alignment and calibration procedures will be presented first. This will be followed by signal-to-noise and resolution work. Finally, the procedures for using singlet delta oxygen and taking temperature measurements will be discussed.

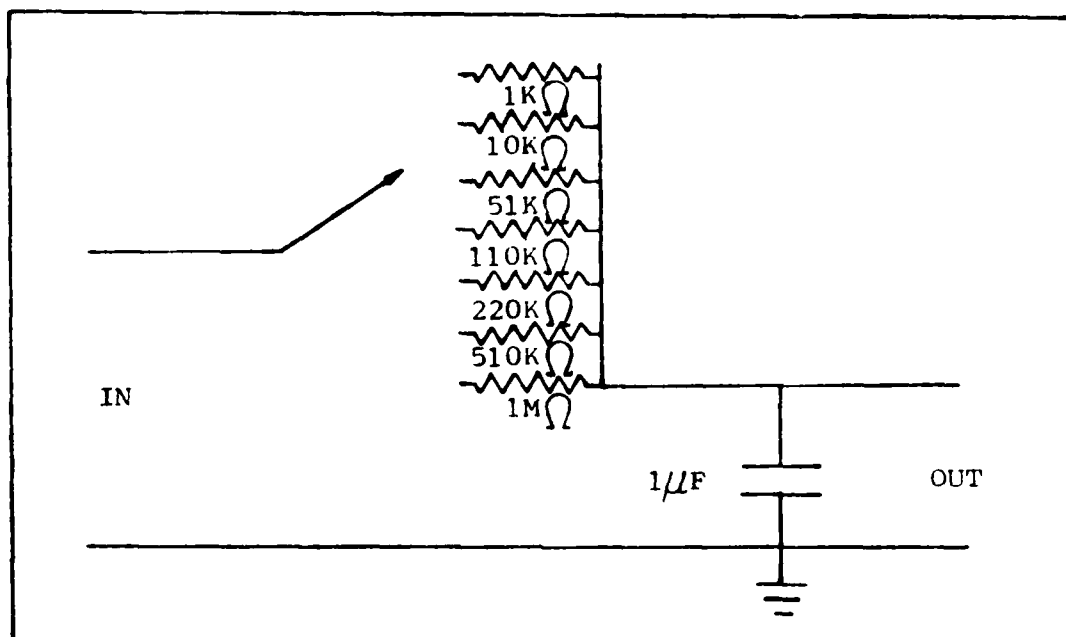


Figure 9. Low Pass Filter

Alignment. Initial alignment was accomplished using a 2 mW Spectra-Physics Helium-Neon laser. This alignment technique is detailed in Reference 3.

Once the initial alignment was complete, another method, more expeditious than laser alignment, was developed for realignment after each cleanup. Before disassembly, pencil marks were made across the two flange joints at the upper port of the cross and at the particle filter. As long as the lenses and monochromator were not moved during the cleaning operation, these two elements defined the optic axis. Upon reassembly of the components, the pencil marks were realigned. This ensured that the flow tube was returned to the same relative position on the optic axis.

Final, fine adjustments in the alignment were accomplished by inserting a mercury (Hg) calibration lamp into the flame region. A neutral density filter of 10^6 times attenuation was placed over the monochromator slit to prevent PMT saturation. With the monochromator tuned to the 5461 Å green line of Hg, the lens position was adjusted to maximize intensity. This technique cut the "down time" by 50%.

Calibration. Oriel pen lamps were used for calibration of spectra. Argon, krypton, mercury, neon, and xenon lamps were used. The lamps were positioned just off the optic axis beside the lenses. Each lamp was wrapped in an opaque sheath. Once the amplification settings for a particular run were established, pin holes were punched in each sheath. The number of pin holes per lamp was determined by the relative intensity of the calibration peak or peaks being used. A second sheath covered all of the lamps. During a spectral run, the outer sheath was removed momentarily as the monochromator scanned through the desired wavelength. Calibration peaks were placed every 500 Å when available to provide accurate band assignments. When possible, peaks were chosen to correspond to areas of the spectrum where no bands appeared. When overlap could not be avoided, sections of the spectrum were repeated without calibration lines.

Signal-to-Noise Ratio. Because of the low light levels, the S/N ratio was always a major concern. The PMT was determined to be the predominate noise source. The RCA 7625 used by Glessner (Ref 3) was initially used in the current work, but never gave better results than that reported by Glessner. With the arrival of a TE104TSRP cooled PMT housing (Products for Research, Inc.), the 7265 was replaced by an RCA C3103402 PMT. To minimize noise, the PMT was operated at -20° C throughout the project. A photograph of the new PMT housing is shown in Appendix D.

A search was made of the operating voltages of the PMT to determine the highest S/N ratio. A Hig pen lamp was placed in the flame region, and the monochromator was tuned to the 5461 \AA line. A neutral density filter of 10^6 times attenuation was placed over the slit to more closely resemble the PbO flame intensity. At each voltage setting from 800 V to 2000 V, the 5461 \AA line was scanned. The peak intensity was compared to the average peak-to-peak intensity of the noise. A graph of the results using maximum filtering and no filtering is shown in Figure 10. As shown by the graph, the optimum operating voltage is 1000 V.

Other attempts were made to increase the S/N ratio. Various grounding schemes were tried. Although grounding proved to be not very effective, grounding of the high voltage power supply to the current amplifier, the current

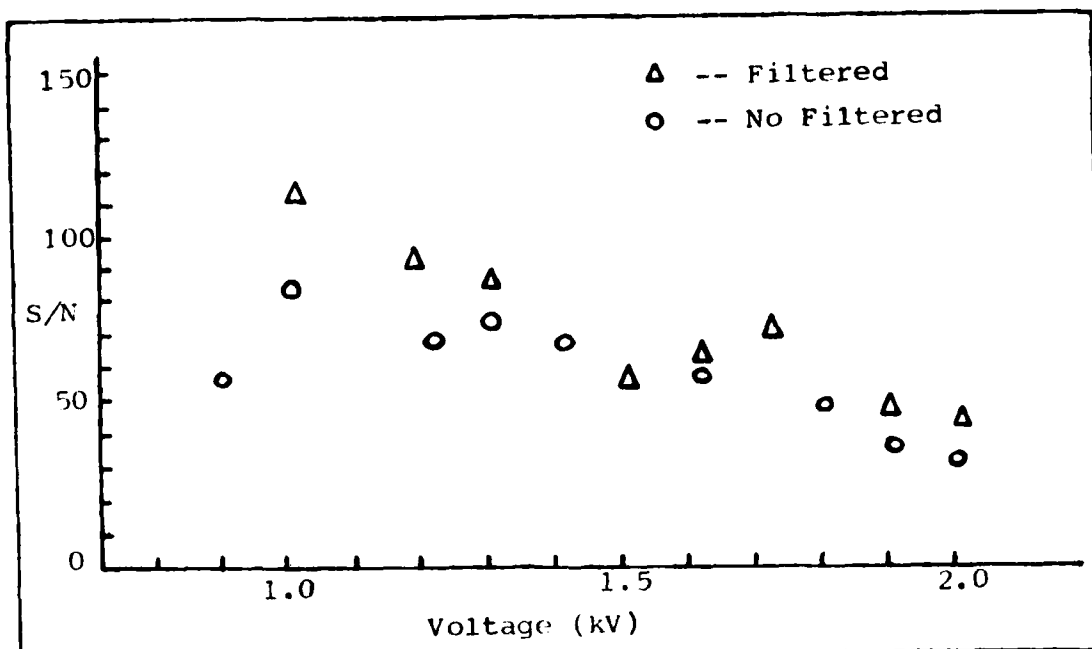


Figure 10. PMT Signal-to-Noise Ratios

amplifier to the PMT, and the PMT to a water line provided some decrease in the noise level. In addition, isolating the high voltage power supply and current amplifier on a separate AC circuit from all other components decreased noise still further.

Of significant note was the noise created by room lights. Even with the slit closed and all cracks on the monochromator sealed with tape, room lights caused excessive noise levels. Fluorescent lights caused the most noise. However, it was discovered that RF noise from the dimmer switch on the variable room lights was also significant. The hood light also caused noticeable noise in the system. Therefore, final readings were taken with all lights off.

Resolution. The theoretical resolution of the Jarrell-Ash 0.5 m monochromator with an 1180 lines/mm grating is 0.2 \AA . However, this resolution was not achieved during this work. Reasons for lower resolution include low light levels, low S/N ratios at narrow slit widths, and the wide range of wavelengths scanned. Using the 5780 \AA doublet of Hg, the full width half maximum (FWHM) of the peaks was determined at 15μ and 150μ slit widths. The resolution under these conditions was determined to be 1.6 \AA FWHM at 15μ slit width and 5.1 \AA at 150μ slit width.

Spectra. Spectra were taken with the flame at maximum intensity. This permitted using the narrowest slit widths for better resolution and gave higher S/N ratios.

Before spectra could be taken using $\text{O}_2(^1\Delta)$, a mercuric oxide (HgO) coating was applied to the discharge tube downstream from the microwave cavity. This coating removed oxygen atoms from the $\text{O}_2(^3\Sigma)/\text{O}_2(^1\Delta)$ mixture. The coating was applied by passing $\text{O}_2(^3\Sigma)$ over liquid Hg and passing the mixture through the microwave discharge. Application of the coating required about 30 minutes.

Temperature Experiments. A glass insulated Chromel-Alumel thermocouple was suspended in the crucible just above the boiling lead. Similarly, an Iron-Constantan thermocouple was placed in the flame region. The power

supply voltage was varied in 0.1 to 0.2 volt increments. Thermocouple voltages were recorded along with emission intensity variations of several PbO bands. Thermocouple readings were taken using a double-readout Honeywell portable potentiometer. The readings were converted to temperature using standard conversion tables from Reference 21.

IV. Results and Analysis

This section is presented in three parts. In the first part the results of system modifications are presented. In the second part the spectra are discussed in terms of the band assignments, relative intensities and pressure variations. Finally, the results of the kinetic analysis are presented and discussed in light of the theory and other current work in the field.

System Modifications

Several system modifications were tested during this project. The effectiveness of each is discussed.

Zirconia Felt Insulation. As recommended by Glessner (Ref 3:76), the inside of the furnace assembly was insulated with Zirconia felt. This effectively formed a heat reservoir around the crucible. Oven temperatures became more stable over long run periods. In addition, changes in carrier gas pressures did not affect the oven temperature as drastically as before the felt was added. This provided the necessary stability for accurate kinetic studies.

Flame Optimization. Glessner designed but did not have time to test a new oxidizer manifold whose design was based on the final dual-component oxidizer system used by Glessner (Ref 3:50). This metal manifold and the Pyrex

manifold discussed previously were subjected to a flame optimization during the current work. Oven temperature, oxidizer pressure and carrier gas pressure were systematically varied in an attempt to find the most intense, centralized but yet stable flame for spectroscopic examination.

The metal manifold was used exclusively for work with $O_2(^3\Sigma)$. The best flames using this manifold were extremely thin and very intense. These flames occurred at high oxidizer pressures (0.6 T - 1.2 T). However, these flames proved to be unstable and faded after only a few minutes. The most stable flames were found at low oxidizer and carrier gas pressures. However, these flames were not very bright and caused S/N problems. A compromise between the two extremes was sought. Unfortunately, exact system parameters are difficult to reproduce. This causes the conditions for obtaining an optimum flame to vary with each run. Therefore, it was necessary to set the parameters at nominal values to initially obtain the flame for each run. The conditions were then adjusted to maximize the flame. The nominal conditions for obtaining a flame using $O_2(^3\Sigma)$ as the oxidizer are given. Gas pressures were adjusted to 0.2 T of O_2 and 2.0 T of Ar, and the power supply to the furnace was set at approximately 7.0 V.

Flame optimization with the Pyrex manifold was simplified due to the dramatic increase in flame intensity when

using $O_2(^1\Delta)$. Flames were extremely bright and very stable. Again the optimum flame was obtained by establishing nominal parameters and then making minor adjustments to optimize the flame. The nominal conditions for obtaining a flame with $O_2(^1\Delta)$ are given. Gas pressures were adjusted to 0.8 T of O_2 and 0.4 T of Ar, and the power supply to the furnace was set to approximately 4.5 V. The significant reduction in Ar pressure and power supply voltage indicates a substantial increase in the efficiency of the $Pb + O_2(^1\Delta)$ reaction over the $Pb + O_2(^3\Sigma)$ reaction. A photograph of a typical flame is shown in Appendix A.

The only drawback of the Pyrex manifold is a limitation on the range of oxidizer pressures that can be used for a given carrier gas pressure. As oxidizer pressure was increased, the flame broke into four distinct arms. This phenomenon was caused by the four angled holes at the top edge of the manifold. As carrier gas pressure was increased, oxidizer pressure could be increased accordingly.

Vacuum Transition Section. Although never placed into actual operation with the flow tube due to a pump failure, the new vacuum transition section has been thoroughly tested. The new section was tested successfully to 35 μ of Hg (the limit of the pump). With the new throttle valve, the amount of vacuum can be varied from 1 Atm down to 35 μ of Hg.

The new system is ready for installation once a new pump is acquired.

Spectra

Spectra were observed from 3000 Å to 8500 Å. The vibrational band structure was observed in all spectra with the rotational structure being shaded toward the red. The narrowest slit widths possible were used to obtain the maximum resolution. The slit width for spectra of the $\text{Pb} + \text{O}_2(^3\Sigma)$ reaction was 150μ, and the slit width for spectra of the $\text{Pb} + \text{O}_2(^1\Delta)$ reaction was 15μ. The linear dispersion of all calibrated spectra was 10 Å/cm. Representative spectra from this work are shown in Figures 11-13. These figures show the increase in resolution as slit widths were decreased. Figure 13 represents the maximum resolution obtainable with the current system. The rotational structure is discernible, but is not resolved enough to do a rotational analysis.

Bandhead assignments were made with the aid of Deslandres tables. Spectroscopic constants for calculation of the tables were obtained from References 6 and 22. A computer program called SEARCH (Ref 3:82) was used to find close matches between the observed wavelengths and calculated values in the Deslandres tables. Where no ambiguities existed, the bandhead assignments were made directly from the computer printout. When two or more

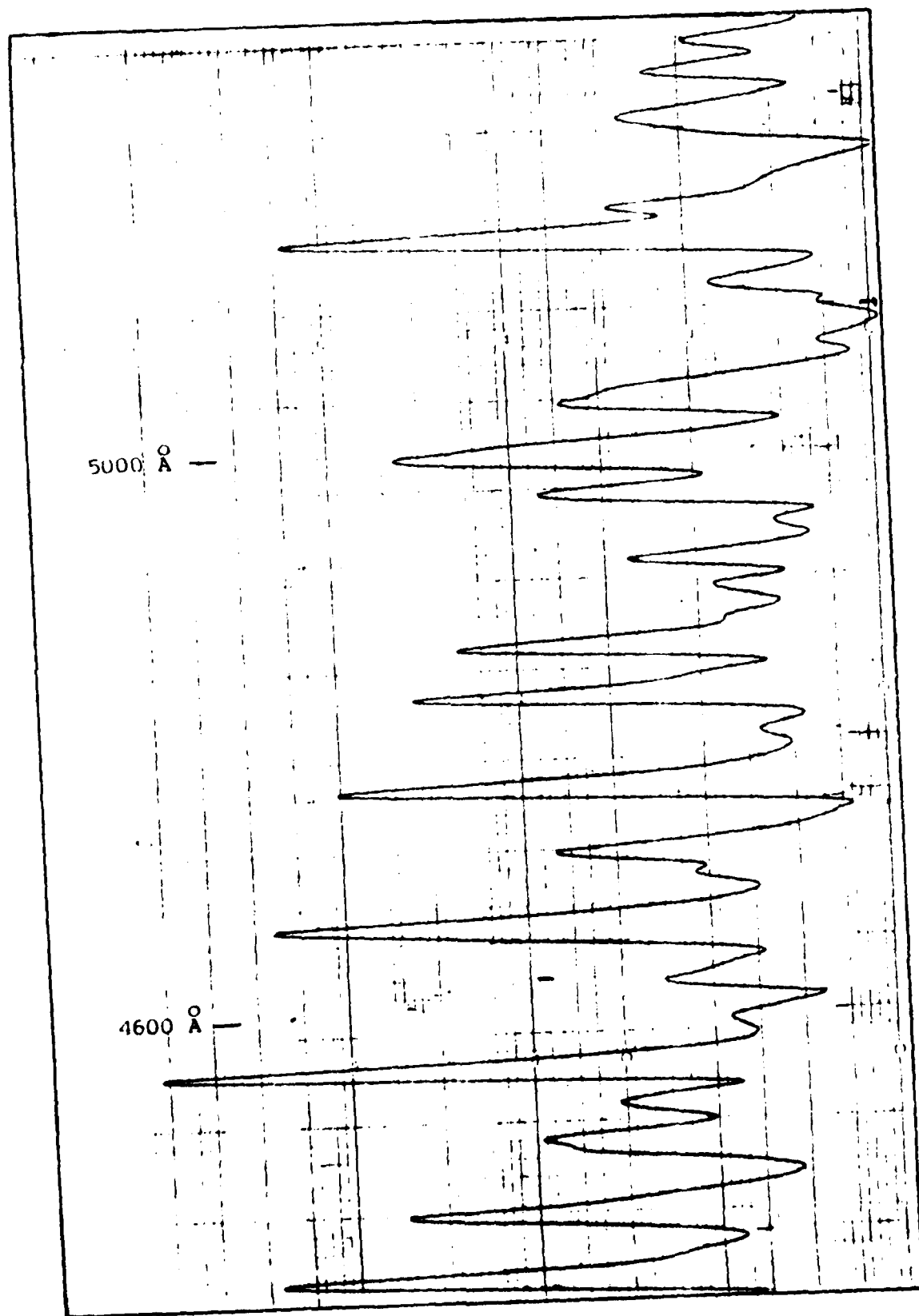


Figure 11. Low Resolution Spectrum

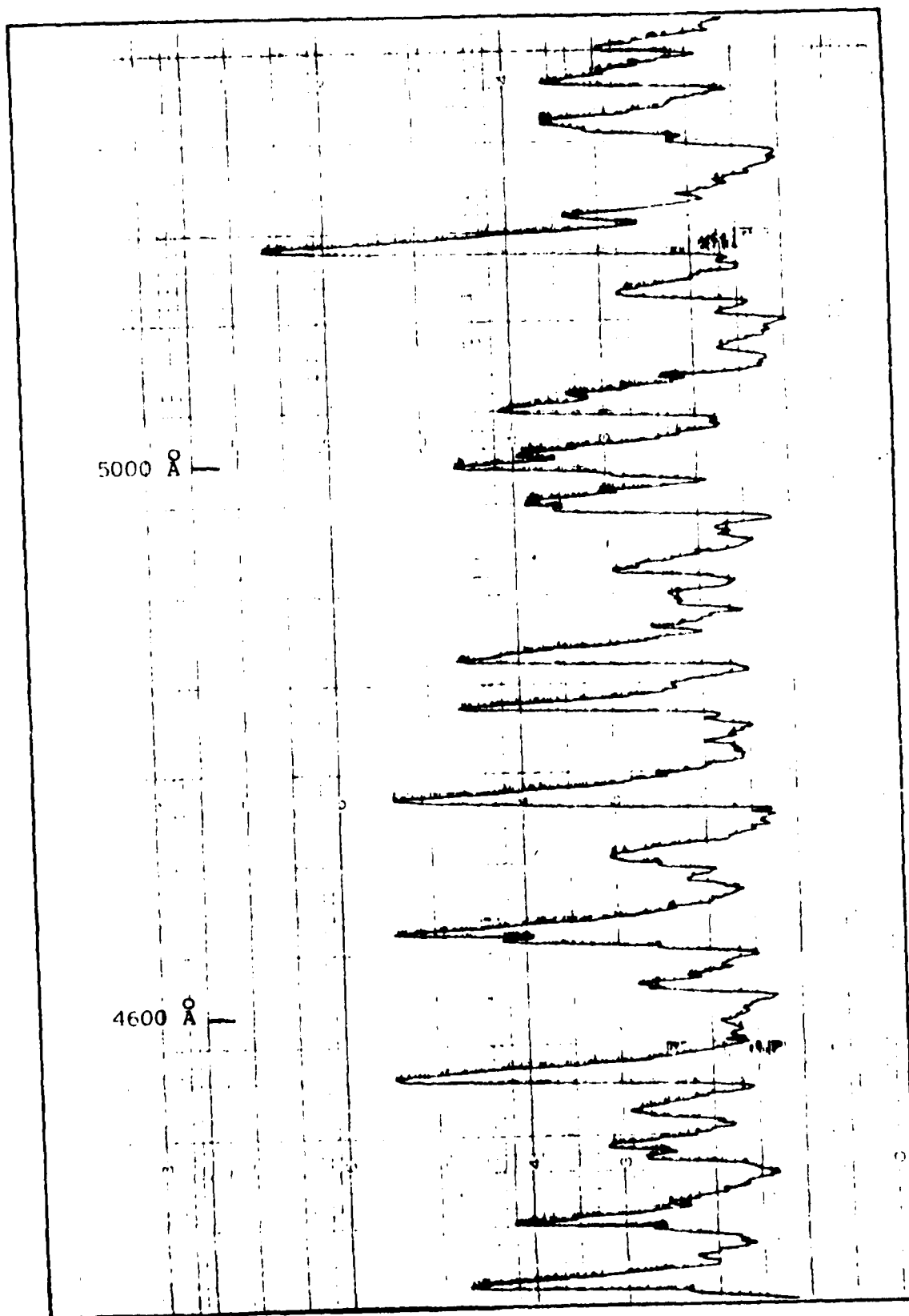


Figure 12. Medium Resolution Spectrum

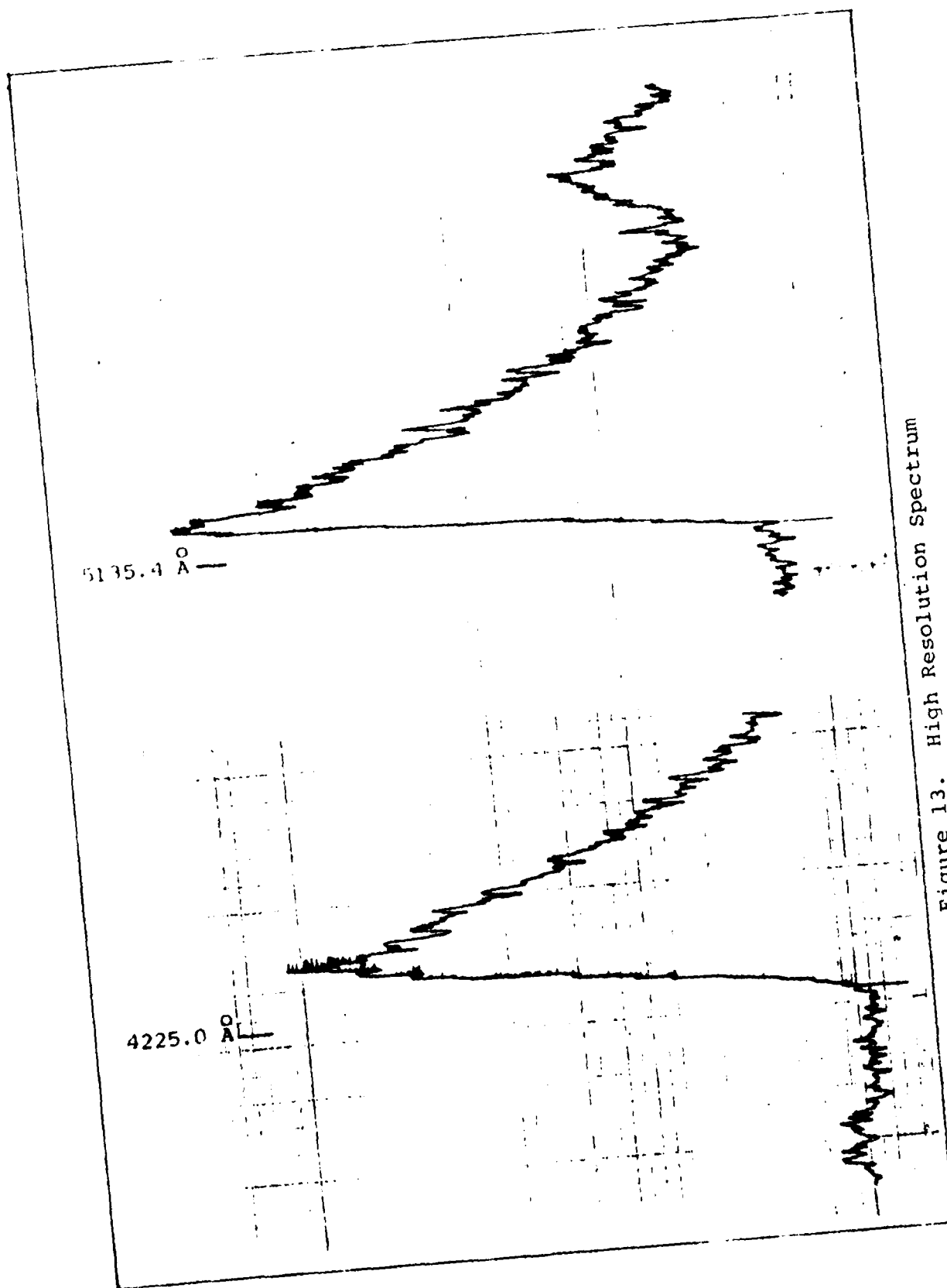


Figure 13. High Resolution Spectrum

wavelengths fell close to the same calculated value, additional information was used.

Pow (Ref 23) was able to calculate a complete set of Franck-Condon factors for the $a - X$, $b - X$, $A - X$, $B - X$, $C - X$, $C' - X$, $D - X$ and $E - X$ transitions of PbO^* . These factors were used extensively to discern proper assignments based on the relative intensity of the bands. Assignments were made in such a way as to continue a progression unless the Franck-Condon factors were unfavorable for a particular transition. In addition, assignments reported in the literature were used in making the determinations.

Analysis of the spectra from the $Pb + O_2(^3\Sigma)$ reaction yielded 67 transitions assignable to the a , b , A , B and C electronic states. A similar analysis of the spectra from the $Pb + O_2(^1\Delta)$ reaction led to the assignment of 225 transitions to the a , b , A , B , C , C' , D and E electronic states of PbO . The observed wavelengths and assigned transitions for each reaction are tabulated in Tables III and IV. The energies of the transitions have been corrected for vacuum operation and are reported along with the calculated energies and energy differences.

The accuracy of these assignments can be assessed with the aid of Deslandres tables. The transition energies for the $a - X$ transitions of the $Pb + O_2(^3\Sigma)$ reaction and

Observed (Å)	Corrected (cm ⁻¹)	Calculated (cm ⁻¹)	Cor - Cal (cm ⁻¹)	Assignment
5104.7	19584.4	19564.4	-19.9	a(8,0)
5219.3	19154.2	19127.4	-26.8	a(7,0)
5345.4	18702.4	18684.3	-18.1	a(6,0)
5475.8	18257.2	18235.5	-21.7	(5,0)
5590.3	17883.0	17872.8	-10.2	(9,3)
5615.9	17801.5	17780.9	-20.6	(4,0)
5699.9	17539.2	17520.8	-18.4	(5,1)
5767.2	17334.6	17320.2	-14.4	(3,0)
5851.8	17084.1	17066.0	-18.1	(4,1)
5927.0	16867.4	16853.7	-13.7	(2,0)
6014.9	16620.7	16606.5	-15.2	(3,1)
6099.1	16391.3	16381.1	-10.2	(1,0)
6190.5	16149.3	16138.9	-10.4	(2,1)
6283.8	15909.6	15897.7	-11.9	(3,2)
6377.9	15674.7	15666.3	- 8.3	(1,1)
6476.2	15436.9	15431.4	- 5.5	(2,2)
6579.0	15195.7	15188.1	- 7.6	(0,1)
6677.9	14970.7	14958.9	-11.8	(1,2)
6782.7	14739.3	14731.0	- 8.3	(2,3)
6899.2	14490.4	14480.6	- 9.8	(0,2)
7002.5	14276.7	14258.4	-18.3	(1,3)
7245.7	13797.5	13780.1	-17.3	(0,3)
7362.0	13579.6	13565.3	-14.2	(1,4)

Table III. Observed PbO Bandheads and Their
Assignments for the Pb + O₂(³Σ)
Reaction

Observed (Å)	Corrected (cm ⁻¹)	Calculated (cm ⁻¹)	Cor - Cal (cm ⁻¹)	Assignment
7632.1	13098.9	13087.0	-12.0	a(0,4)
8051.6	12416.5	12406.5	-10.0	b(4,8)
4446.5	22483.5	22515.4	31.9	A(8,1)
4612.3	21675.0	21650.2	-24.8	A(6,1)
4645.7	21519.3	21491.0	-28.3	A(4,0)
4749.8	21047.8	21051.3	3.5	(3,0)
4773.8	20942.0	20942.4	- 0.0	(6,2)
4846.3	20628.3	20609.6	-18.7	(2,0)
4916.3	20334.7	20336.8	2.1	(3,1)
4957.0	20167.8	20165.8	- 2.0	(1,0)
5022.1	19906.4	19895.0	-11.4	(2,1)
5070.2	19717.6	19720.0	2.4	(0,0)
5134.2	19471.9	19451.5	-20.4	(1,1)
5252.3	19033.8	19005.2	-28.5	(0,1)
5327.6	18764.9	18743.4	-21.5	(1,2)
5402.4	18505.1	18487.0	-18.1	(2,3)
5464.4	18295.2	18297.6	2.4	(0,2)
5537.1	18055.1	18043.0	-12.0	(1,3)
5553.1	18008.0	17989.2	-18.8	(4,5)
5671.8	17626.1	17597.3	-28.8	(0,3)
5758.2	17361.7	17350.0	-11.7	(1,4)
5905.3	16929.4	16903.9	-25.5	(0,4)
5993.8	16679.2	16663.9	-15.3	(1,5)

Table III. Observed PbO Bandheads and Their
Assignments for the Pb + O₂(³Σ)
Reaction (Continued)

Observed (Å)	Corrected (cm ⁻¹)	Calculated (cm ⁻¹)	Cor - Cal (cm ⁻¹)	Assignment
6155.0	16242.5	16218.0	-24.5	A(0,5)
6250.4	15994.6	15984.9	- 9.7	(1,6)
6428.3	15551.9	15539.0	-12.9	(0,6)
6522.7	15326.8	15313.5	-13.3	(1,7)
6817.7	14663.6	14649.0	-14.6	(1,8)
4063.5	24602.7	24610.5	7.8	B(5,0)
4143.0	24126.6	24122.5	- 4.1	B(4,0)
4223.8	23668.6	23634.0	-34.6	B(3,0)
4313.4	23177.1	23145.5	-31.6	(2,0)
4405.5	22692.7	22656.7	-36.0	(1,0)
4505.3	22189.7	22167.5	-22.2	(0,0)
4551.6	21964.0	21941.9	-22.1	(1,1)
4653.7	21482.3	21452.8	-29.5	(0,1)
4704.3	21251.3	21234.6	-16.7	(1,2)
4809.9	20784.8	20745.2	-39.6	(0,2)
4984.4	20057.0	20044.9	-12.0	(0,3)
5158.2	19381.3	19351.7	-29.6	(0,4)
5271.3	18965.3	18964.9	- 0.4	(2,6)
5410.5	18477.5	18476.0	- 1.5	(1,6)
4479.5	22317.4	22302.5	-14.9	C(0,2)
4628.1	21601.1	21602.5	1.4	C(0,3)

Table III. Observed PbO Bandheads and Their
Assignments for the Pb + O₂(³Σ)
Reaction (Continued)

Observed ° (Å)	Corrected (cm ⁻¹)	Calculated (cm ⁻¹)	Cor - Cal (cm ⁻¹)	Assignment
4889.0	20448.2	20450.8	2.6	a(10,0)
4993.4	20020.8	20020.1	-0.8	a(9,0)
5104.3	19586.0	19584.2	-1.8	a(8,0)
5221.8	19145.0	19143.1	-1.9	(7,0)
5299.0	18866.1	18869.1	3.0	(8,1)
5347.1	18696.5	18696.9	0.4	(6,0)
5424.3	18430.5	18428.0	-2.5	(7,1)
5480.1	18242.8	18245.5	2.7	(5,0)
5503.6	18165.0	18161.2	-3.8	(8,2)
5559.5	17982.4	17981.8	-0.6	(6,1)
5620.6	17786.6	17789.0	2.4	(4,0)
5639.0	17728.6	17720.1	-8.5	(7,2)
5702.6	17530.9	17530.5	-0.4	(5,1)
5768.5	17330.7	17327.3	-3.4	(3,0)
5784.3	17283.4	17273.9	-9.5	(6,2)
5854.5	17076.2	17073.9	-2.3	(4,1)
5871.9	17025.6	17019.4	-6.2	(7,3)
5930.6	16857.2	16860.5	3.3	(2,0)
5942.3	16824.0	16822.6	-1.4	(5,2)
6017.4	16613.8	16612.3	-1.5	(3,1)
6030.8	16576.9	16573.2	-3.7	(6,3)
6100.0	16388.9	16388.5	-0.4	(1,0)
6107.0	16370.1	16366.0	-4.1	(4,2)

Table IV. Observed PbO Bandheads and Their
Assignments for the Pb + O₂(¹Δ)
Reaction

Observed ° (Å)	Corrected (cm ⁻¹)	Calculated (cm ⁻¹)	Cor - Cal (cm ⁻¹)	Assignment
6192.4	16144.4	16145.4	1.0	a(2,1)
6199.2	16126.7	16121.8	- 4.9	(5,3)
6288.3	15898.3	15904.3	6.0	(3,2)
6378.5	15673.2	15665.3	- 7.9	(1,1)
*6378.5	15673.2	15673.4	0.2	(4,3)
*6475.8	15437.8	15437.5	- 0.3	(2,2)
6573.5	15208.4	15203.6	- 4.8	(3,3)
6677.4	14971.9	14971.7	- 0.2	(4,4)
6681.2	14963.3	14965.5	2.2	(1,2)
6784.1	14736.2	14736.8	0.6	(2,3)
6888.3	14513.4	14510.0	- 3.4	(3,4)
7003.4	14274.9	14285.3	10.4	(4,5)
7007.4	14266.8	14264.7	- 2.1	(1,3)
7126.4	14028.4	14043.2	14.8	(2,4)
7227.7	13831.8	13841.7	9.9	(6,7)
7249.7	13789.9	13787.6	- 2.3	(0,3)
7466.9	13388.7	13390.4	1.7	(5,7)
7632.1	13098.9	13094.0	- 4.9	(0,4)
5448.4	18349.	18358.8	9.8	b(5,0)
5663.5	17651.9	17643.7	- 8.2	b(5,1)
5718.6	17481.9	17488.8	6.9	b(3,0)
5808.6	17211.1	17208.1	- 3.0	(4,1)
5959.3	16775.7	16773.8	- 1.9	(3,1)

Table IV. Observed PbO Bandheads and Their
Assignments for the Pb + O₂(¹Δ)
Reaction (Continued)

Observed (Å)	Corrected (cm ⁻¹)	Calculated (cm ⁻¹)	Cor - Cal (cm ⁻¹)	Assignment
6055.9	16508.2	16500.2	- 8.0	b(4,2)
6118.4	16339.6	16340.9	1.3	(2,1)
6285.7	15904.8	15909.3	4.5	(1,1)
6392.6	15638.7	15632.9	- 5.8	(2,2)
*6573.5	15208.4	15201.4	- 7.0	(1,2)
6614.4	15114.4	15105.8	- 8.6	(4,4)
6692.5	14938.1	14932.2	- 5.9	(2,3)
6764.7	14778.5	14771.2	- 7.3	(0,2)
7102.5	14075.6	14070.5	- 5.1	(0,3)
7480.9	13363.6	13366.9	13.3	(0,4)
4302.2	23237.4	23242.5	5.1	A(8,0)
4383.3	22807.6	22810.2	2.6	A(7,0)
4438.5	22524.0	22527.5	3.5	A(8,1)
4468.2	22373.9	22376.3	2.4	(6,0)
4523.7	22099.4	22095.2	- 4.2	(7,1)
4556.6	21939.9	21940.6	0.7	(5,0)
4581.1	21822.6	21819.6	- 3.0	(8,2)
4613.4	21669.9	21661.2	- 8.7	(6,1)
4649.6	21501.2	21503.2	2.0	(4,0)
4708.7	21231.4	21225.5	- 5.9	(5,1)
4732.8	21123.3	21118.8	- 4.5	(8,3)
4746.2	21063.7	21064.1	0.4	(3,0)
4771.1	20953.8	20953.3	- 0.5	(6,2)

Table IV. Observed PbO Bandheads and Their
Assignments for the Pb + O₂(¹Δ)
Reaction (Continued)

Observed (\AA)	Corrected (cm^{-1})	Calculated (cm^{-1})	Cor - Cal (cm^{-1})	Assignment
4834.0	20681.2	20686.5	5.3	A (7,3)
4848.3	20619.8	20623.3	3.5	(2,0)
4872.5	20517.5	20517.6	0.1	(5,2)
4894.6	20424.8	20425.2	0.4	(8,4)
*4912.4	20350.8	20349.0	-1.8	(3,1)
4938.1	20245.0	20252.5	7.6	(6,3)
4954.1	20179.6	20180.8	1.2	(1,0)
4979.2	20077.9	20080.2	2.3	(4,2)
5021.7	19908.0	19908.3	0.3	(2,1)
5065.6	19735.5	19736.7	1.2	(0,0)
5091.5	19635.2	19641.1	5.9	(3,2)
5128.6	19493.2	19490.1	-3.1	(9,6)
5135.4	19467.4	19465.8	-1.6	(1,1)
5159.2	19377.6	19379.5	1.9	(4,3)
5178.1	19306.9	19306.5	-0.4	(7,5)
5228.4	19120.8	19123.3	2.5	(5,4)
5255.3	19023.0	19021.6	-1.4	(0,1)
5278.9	18938.0	18940.4	2.4	(3,3)
*5297.4	18871.8	18872.5	0.7	(6,5)
5330.1	18756.1	18757.9	1.8	(1,2)
5350.1	18686.0	18685.9	-0.1	(4,4)
5405.4	18494.9	18499.6	4.7	(2,3)
5422.3	18437.3	18436.8	-0.5	(5,5)

Table IV. Observed PbO Bandheads and Their
Assignments for the $\text{Pb} + \text{O}_2(^1\Delta)$
Reaction (Continued)

Observed ° (Å)	Corrected (cm ⁻¹)	Calculated (cm ⁻¹)	Cor - Cal (cm ⁻¹)	Assignment
5438.3	18383.0	18387.4	4.4	A (8,7)
5458.5	18315.0	18313.7	-1.3	(0,2)
5494.8	18194.1	18193.2	-0.9	(6,6)
5538.7	18049.9	18057.1	7.2	(1,3)
5553.5	18001.8	17999.4	-2.4	(4,5)
5567.5	17956.5	17955.1	-1.4	(7,7)
*5615.0	17804.4	17806.0	1.6	(2,4)
5631.0	17753.8	17757.5	3.7	(5,6)
5675.3	17615.2	17613.0	-2.2	(0,3)
5692.8	17561.1	17560.4	-0.7	(3,5)
5756.9	17365.6	17363.5	-2.1	(1,4)
5771.3	17322.3	17320.2	-2.1	(4,6)
5840.7	17116.5	17119.6	3.1	(2,5)
5850.5	17087.9	17085.4	-2.5	(5,7)
5907.6	16922.8	16919.4	-3.4	(0,4)
5923.0	16878.8	16881.1	2.3	(3,6)
5994.8	16676.4	16677.1	0.7	(1,5)
*6004.0	16650.8	16648.0	-2.8	(4,7)
6157.3	16236.4	16232.9	-3.5	(0,5)
6167.1	16210.6	16208.9	-1.7	(3,7)
6249.3	15997.4	15997.8	0.4	(1,6)
6252.8	15988.5	15983.1	-5.4	(4,8)
6341.2	15765.4	15768.2	2.8	(2,7)

Table IV. Observed PbO Bandheads and Their
Assignments for the Pb + O₂(¹Δ)
Reaction (Continued)

Observed ° (Å)	Corrected (cm ⁻¹)	Calculated (cm ⁻¹)	Cor - Cal (cm ⁻¹)	Assignment
6427.7	15553.3	15553.6	0.3	A(0,6)
6523.6	15324.7	15325.7	1.0	(1,7)
6619.5	15102.8	15103.2	0.4	(2,8)
6715.5	14886.7	14886.1	- 0.6	(3,9)
6717.5	14882.3	14881.5	- 0.8	(0,7)
6818.8	14661.3	14660.7	- 0.6	(1,8)
6921.8	14443.1	14445.4	2.3	(2,9)
7022.5	14236.1	14235.5	- 0.6	(3,10)
7032.3	14216.3	14216.5	0.2	(0,8)
7139.0	14003.6	14002.9	- 0.7	(1,9)
7247.7	13793.7	13794.7	1.0	(2,10)
7354.6	13593.2	13592.0	- 1.2	(3,11)
7461.9	13397.6	13394.7	- 2.9	(4,12)
7827.9	12771.2	12765.5	- 5.7	(4,13)
*3768.4	26528.7	26530.3	1.6	B(9,0)
*3838.3	26045.7	26055.3	9.6	B(8,0)
*3871.1	25825.1	25815.2	- 9.9	B(9,1)
*3909.8	25569.1	25578.3	8.7	(7,0)
3946.8	25337.0	25340.2	3.2	(8,1)
3984.8	25088.4	25099.3	10.9	(6,0)
4023.6	24846.6	24863.2	16.6	(7,1)
4059.8	24625.1	24618.4	- 6.7	(5,0)
*4102.1	24370.6	24384.3	13.7	(6,1)

Table IV. Observed PbO Bandheads and Their
Assignments for the Pb + O₂(¹Δ)
Reaction (Continued)

Observed ° (Å)	Corrected (cm ⁻¹)	Calculated (cm ⁻¹)	Cor - Cal (cm ⁻¹)	Assignment
4140.0	24147.6	24135.5	-12.1	B(4,0)
4182.9	23900.0	23903.3	3.3	(5,1)
4225.	23661.9	23650.7	-11.2	(3,0)
*4268.	23422.5	23420.5	- 2.0	(4,1)
4299.6	23251.5	23237.9	-13.6	(8,4)
4311.3	23188.4	23195.4	7.0	(5,2)
4313.7	23175.5	23163.9	-11.6	(2,0)
4340.5	23032.5	23026.5	- 6.0	(9,5)
4349.5	22984.8	22975.6	- 9.2	(6,3)
4358.3	22938.4	22935.6	- 2.8	(3,1)
4400.6	22718.0	22712.6	- 5.4	(4,2)
4407.0	22685.0	22675.1	- 9.8	(1,0)
4445.1	22490.6	22494.7	4.1	(5,3)
4453.0	22450.7	22448.8	- 1.9	(2,1)
4497.0	22230.6	22227.7	- 2.9	(3,2)
4505.8	22187.2	22184.4	- 2.8	(0,0)
4529.9	22069.2	22074.5	5.3	(7,5)
4551.0	21966.9	21960.1	- 6.8	(1,1)
4643.3	21530.4	21527.0	- 3.4	(3,3)
4656.4	21469.8	21469.4	- 0.4	(0,1)
4689.7	21317.4	21318.2	0.8	(4,4)
4702.5	21259.4	21252.2	- 7.2	(1,2)
4751.4	21040.7	21040.2	- 0.5	(2,3)

Table IV. Observed PbO Bandheads and Their
Assignments for the Pb + O₂(¹Δ)
Reaction (Continued)

Observed (Å)	Corrected (cm ⁻¹)	Calculated (cm ⁻¹)	Cor - Cal (cm ⁻¹)	Assignment
4813.2	20770.6	20761.4	- 9.2	B(0,2)
*4912.4	20350.8	20346.6	- 4.2	(2,4)
4961.5	20149.5	20147.0	- 2.5	(3,5)
4983.6	20060.2	20060.7	0.5	(0,3)
5034.3	19858.2	19857.8	- 0.4	(1,4)
5162.8	19364.1	19367.1	3.0	(0,4)
5211.6	19182.4	19171.4	-11.0	(1,5)
5264.9	18988.3	18980.9	- 7.4	(2,6)
*5350.1	18686.0	18680.7	- 5.3	(0,5)
*5405.4	18494.9	18492.1	- 2.8	(1,6)
5615.	17804.4	17820.0	15.6	(1,7)
5668.7	17635.8	17643.8	8.0	(2,8)
5828.8	17151.5	17155.0	3.5	(1,8)
5884.9	16988.0	16985.9	- 2.1	(2,9)
5945.7	16814.4	16822.1	7.7	(3,10)
6122.0	16330.	16335.3	5.3	(2,10)
3440.5	29048.7	29043.7	- 5.0	C(11,0)
3495.4	28600.8	28614.8	14.0	C(10,2)
3528.1	28335.8	28328.6	- 7.2	C(11,1)
*3547.8	28178.5	28174.7	- 3.8	(9,0)
*3606.2	27722.3	27723.3	1.0	(8,0)
*3666.9	27263.6	27260.7	- 2.9	(7,0)
3704.2	26988.4	27008.3	19.9	(8,1)

Table IV. Observed PbO Bandheads and Their
Assignments for the Pb + O₂(¹Δ)
Reaction (Continued)

Observed ° (Å)	Corrected (cm ⁻¹)	Calculated (cm ⁻¹)	Cor - Cal (cm ⁻¹)	Assignment
3732.0	26787.4	26786.9	- 0.5	C(6,0)
3768.4	26528.7	26545.7	17.0	(7,1)
3799.2	26296.6	26301.8	5.4	(5,0)
*3871.1	25799.8	25805.4	5.6	(4,0)
4067.5	24578.5	24582.8	4.3	(3,1)
4153.1	24071.4	24064.0	- 7.4	(2,1)
4281.2	23351.4	23356.1	4.7	(2,2)
4379.3	22828.4	22826.0	- 2.4	(1,2)
4634.5	21571.2	21583.9	12.7	(0,3)
4787.3	20882.9	20890.3	7.4	(0,4)
4947.1	20280.1	20203.9	- 4.2	(0,5)
5016.7	19927.9	19923.9	- 4.0	(2,7)
3255.0	30713.5	30714.9	1.4	C'(13,0)
3298.3	30310.4	30305.7	- 4.7	C'(12,0)
*3551.3	28158.7	28150.7	- 8.0	C'(7,0)
3591.6	27835.0	27881.1	46.1	(8,1)
*3610.9	27693.9	27697.9	4.0	(6,0)
*3666.9	27263.6	27238.0	-25.6	(5,0)
3838.3	26045.7	26055.8	10.1	(4,1)
*3909.8	25569.6	25581.4	11.8	(3,1)
*4100.3	24388.5	24391.8	3.3	(2,2)
*4182.9	23900.0	23902.9	2.9	(1,2)
4307.3	23209.9	23202.2	- 7.7	(1,3)

Table IV. Observed PbO Bandheads and Their
Assignments for the Pb + O₂(¹Δ)
Reaction (Continued)

Observed ° (Å)	Corrected (cm ⁻¹)	Calculated (cm ⁻¹)	Cor - Cal (cm ⁻¹)	Assignment
4541.7	22011.9	22012.5	0.6	C'(0,4)
*4689.7	21317.4	21326.0	8.6	(0,5)
3116.3	32080.1	32080.8	0.7	D(5,1)
3153.8	31698.7	31717.8	19.1	D(3,0)
3214.0	31105.2	31162.0	56.8	D(2,0)
3280.2	30477.6	30446.9	-30.7	(2,1)
*3298.3	30310.4	30294.8	-15.6	(3,2)
3331.3	30009.3	30016.8	7.5	(0,0)
3359.5	29757.5	29739.0	-18.5	(2,2)
3377.1	29602.4	29594.1	- 8.3	(3,3)
3426.2	29178.3	29172.0	- 6.3	(1,2)
3495.4	28600.8	28593.9	- 6.9	(0,2)
3606.2	27722.3	27777.7	55.2	(1,4)
3683.0	27144.4	27091.2	-53.2	(1,5)
3200.9	31232.4	31258.8	26.4	E(1,5)
3316.4	30144.1	30139.5	- 4.6	E(0,6)
3393.0	29463.8	29468.1	4.3	E(0,7)
3480.8	28720.8	28803.5	82.7	(0,8)

Table IV. Observed PbO Bandheads and Their
Assignments for the Pb + O₂(¹Δ)
Reaction (Continued)

for the A - X and B - X transitions of the $\text{Pb} + \text{O}_2(^1\Delta)$ reaction have been arranged in Deslandres tables and are shown in Figures 14-16. The energy differences between the rows and columns are shown in parentheses. The rows formed by the differences between successive pairs in the columns and the columns formed by differences between successive pairs in the rows agree within experimental error. This agreement substantiates the accuracy of the assignments. Deslandres tables for other states are not shown due to insufficient data points for a meaningful comparison.

The assignment of transitions from the C, C', D, and E states for the $\text{Pb} + \text{O}_2(^1\Delta)$ reaction was complicated by the fact that the intensities of the bands were relatively low. The spectra were rerun from 3000 Å to 4000 Å with the slit width increased by a factor of 10. This significantly reduced the resolution in the spectra and caused considerable overlap in the bands. In some cases, more than one transition was assigned to the same band. Overlaps are indicated by asterisks in Table IV. A representative spectra from 3000 Å to 4000 Å is shown in Figure 17.

To further check the validity of the assignments, the relative intensities of the bands in these transitions were compared to the Franck-Condon factors. For comparison purposes, the intensities were normalized by dividing each intensity by the sum of the intensities for a given electronic state. The intensities for the a - X, A - X, and

v'	v''				
	0	1	2	3	4
0		15196 (479)	14490 (481)	13798 (479)	13099 (481)
1	16391 (476)	15765 (716) (474)	14971 (704) (466)	14277 (694) (462)	13580 (697)
2	16867 (468)	16149 (718) (472)	15437 (712) (473)	14739 (698)	
3	17335 (467)	16621 (714) (463)	15910 (711)		
4	17802 (455)	17084 (718) (455)			
5	18257 (445)	17539 (718)			
6	18702 (452)				
7	19154 (430)				
8	19584				

NOTE: Energies are in cm^{-1}

Figure 14. Deslandres Table for the a - X Transition
of the $\text{Pb} + \text{O}_2(^3\Sigma)$ Reaction

v	v"					
	0	1	2	3	4	5
0	19736 (713) (444)	19023 (708) (444)	18315 (700) (441)	17615 (692) (435)	16923 (687) (443)	16236 (440)
1	20180 (713) (440)	19467 (711) (441)	18756 (706) (445)	18050 (684) (443)	17366 (690) (438)	16676 (441)
2	20620 (712) (444)	19908 (443)	19635 (697) (443)	18938 (440) (443)	18495 (691) (443)	17804 (687) (444)
3	21064 (713) (437)	20351 (716) (443)	19635 (697) (443)	18938 (440) (440)	18686 (684) (435)	18002 (435)
4	21501 (439)	21231 (713) (439)	20518 (436) (436)	19378 (692) (436)	19121 (684) (435)	18437 (435)
5	21940 (709) (434)	21670 (716) (429)	20954 (709) (429)	20245 (436) (436)	18872 (435)	18307 (435)
6	22374 (704) (434)	22099 (425)	21823 (700) (425)	21123 (698) (425)	20425 (425)	19307 (425)
7	22808 (709) (429)	22524 (701) (429)	21823 (700) (429)	21123 (698) (429)	20425 (425)	19307 (425)
8	23237 (713) (429)	22524 (701) (429)	21823 (700) (429)	21123 (698) (429)	20425 (425)	19307 (425)

Figure 15. Deslandres Table for the A - X Transition of the Pb + O₂(¹Δ) Reaction

v'	v''					
	0	1	2	3	4	5
0	22187 (717) (498)	21470 (699) (497)	20771 (711) (488)	20060 (696)	19364 (678) (494)	18686 (503)
1	22685 (718) (491)	21967 (708) (484)	21259		19858 (669) (493)	19189
2	23176 (725) (486)	22451 (487)		21041 (690) (489)	20351	
3	23662 (724) (486)	22938 (707) (485)	22231 (701) (487)	21530		20150
4	24148 (725) (477)	23423 (705) (477)	22718 (470)		21317 (475)	
5	24625 (725) (463)	23900 (712) (471)	23188 (697) (494)	22491 (699)	21792	
6	25088 (717) (482)	24371 (476)		22985		
7	25570 (723) (476)	24847 (471)				22069
8	26046 (728)	25318			23252	

Note: Energies are in cm^{-1}

Figure 16. Deslandres Table for the B - X Transition
of the $\text{Pb} + \text{O}_2(^1\Delta)$ Reaction

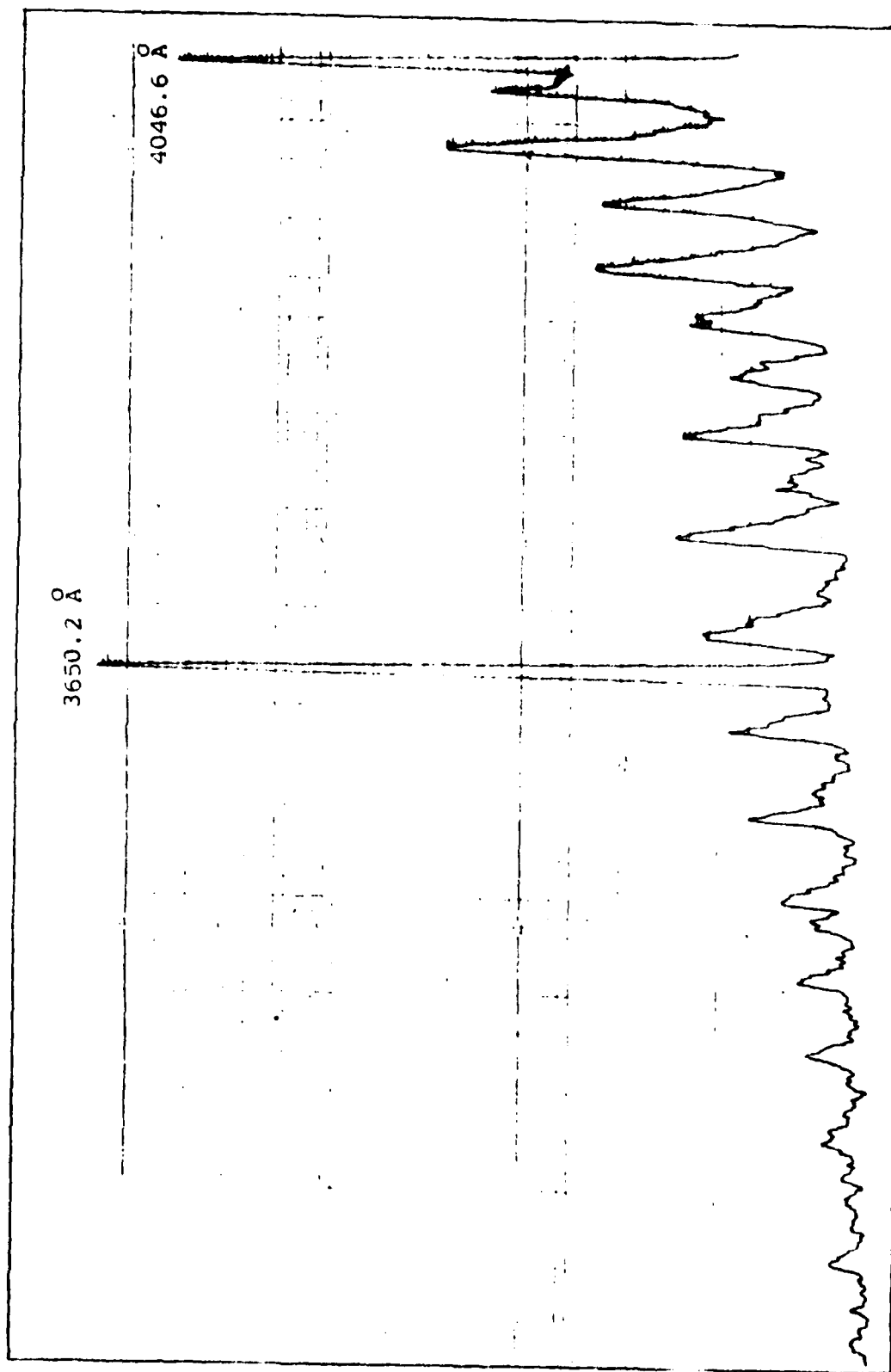


Figure 17. Spectrum from 3000 Å to 4000 Å
for the $\text{Pb} + \text{O}_2(^1\Delta)$ Reaction

B - X transitions mentioned earlier are shown in Figures 18-20. Although this allows only qualitative comparison, the relatively good agreement in the variation of the intensities and of the Franck-Condon factors supports the correctness of the assignments.

The Condon parabola is also shown in Figures 18-20. The width of the parabola is directly related to the difference in the internuclear separation distance of the upper and lower states (Ref 9:198). The relatively wide parabolas of Figures 18-20 indicate a large shift in the internuclear separation distances for the excited states of PbO and the ground state. This large shift was verified by Pow (Ref 23) who was able to plot potential energy curves for the X, a, b, A, B, C, C', D and E states of PbO.

Low dispersion spectra from the $\text{Pb} + \text{O}_2(^3\Sigma)$ and $\text{Pb} + \text{O}_1(^1\Delta)$ reactions were also taken during this work and are shown in Figures 21-22. The gain in Figure 21 is approximately 100 times greater than in Figure 22 due to factors of 10 in the slit width and in the carrier gas pressure (Pb flow rate). These spectra allow a qualitative comparison of the relative intensities of the different electronic systems. Taking into account the differences in gain, the $\text{Pb} + \text{O}_2(^1\Delta)$ reaction obviously caused a considerable increase in the intensity of emissions from all of the excited states. However, the A and B state emission intensities were increased much more than the a state

v'	v''				
	0	1	2	3	4
0		.020	.040	.055	.029
1	.018	.053	.108	.072	.028
2	.018	.062	.082	.032	
3	.033	.067	.036		
4	.055	.053			
5	.044	.022			
6	.033				
7	.026				
8	.009				

Figure 18. Deslandres Table of Intensities for the
a - X Transition of the $\text{Pb} + \text{O}_2(^3\Sigma)$ Reaction

v'	v''								
	0	1	2	3	4	5	6	7	8
0	.012	.034	.044	.069	.060	.031	.015	.004	.003
1	.029	.065	.040	.005	.003	.023	.029	.027	.018
2	.043	.029	.000	.019	.011	.013	.000	.009	.014
3	.041	.014	.008	.016	.000	.004	.009	.008	.000
4	.026	.000	.015	.004	.003	.011	.002	.003	.008
5	.023	.010	.006	.000	.008	.002	.005	.005	
6	.005	.022	.001	.005	.000	.002	.003	.000	
7	.002	.005	.000	.002	.000	.002	.000	.002	
8	.001	.004	.003	.002	.006	.000	.000	.002	
9							.001		

Figure 19. Deslandres Table of Intensities for the
A - X Transition of the $\text{Pb} + \text{O}_2(^1\Delta)$ Reaction

		v''								
		0	1	2	3	4	5	6	7	8
v'	0	.022	.046	.065	.035	.015	.004	.003	.001	.001
	1	.061	.074	.020	.000	.008	.024	.026	.014	.003
	2	.087	.034	.000	.030	.018	.000	.004	.000	.005
	3	.106	.007	.022	.020	.000	.007	.000	.000	.000
	4	.047	.007	.025	.000	.005	.000	.004	.000	.003
	5	.018	.005	.012	.017	.006	.000			
	6	.009	.005	.000	.014	.000	.000			
	7	.005	.009	.000	.000	.000	.014			
	8	.002	.005	.000	.000	.005	.000			
	9	.001	.002	.000	.000	.000	.003			

Figure 20. Deslandres Table of Intensities for the
B - X Transition of the $\text{Pb} + \text{O}_2(^1\Delta)$ Reaction

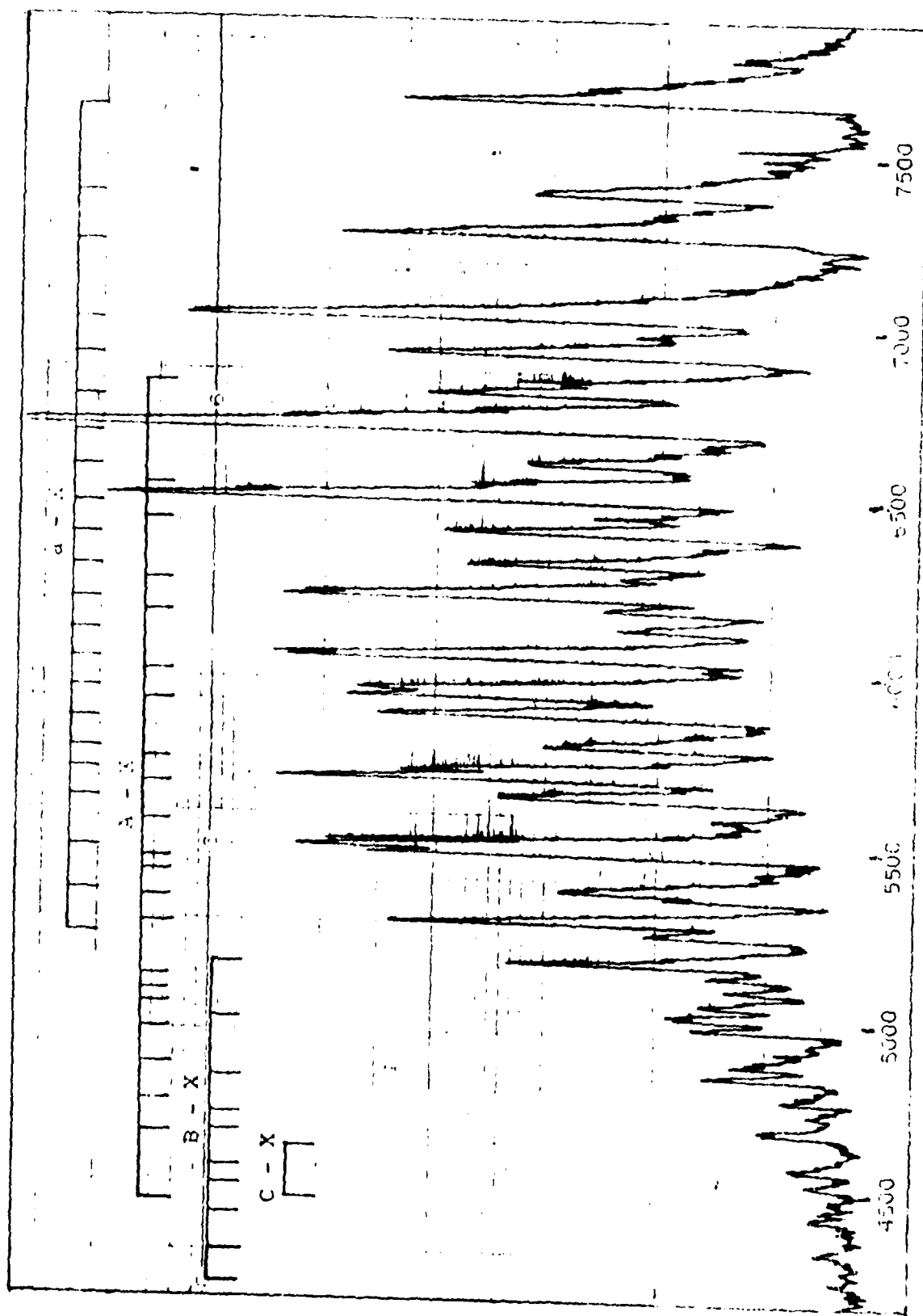


Figure 21. Low Dispersion Spectrum from
the $\text{Pb} + \text{O}_2(^3\Sigma)$ Reaction

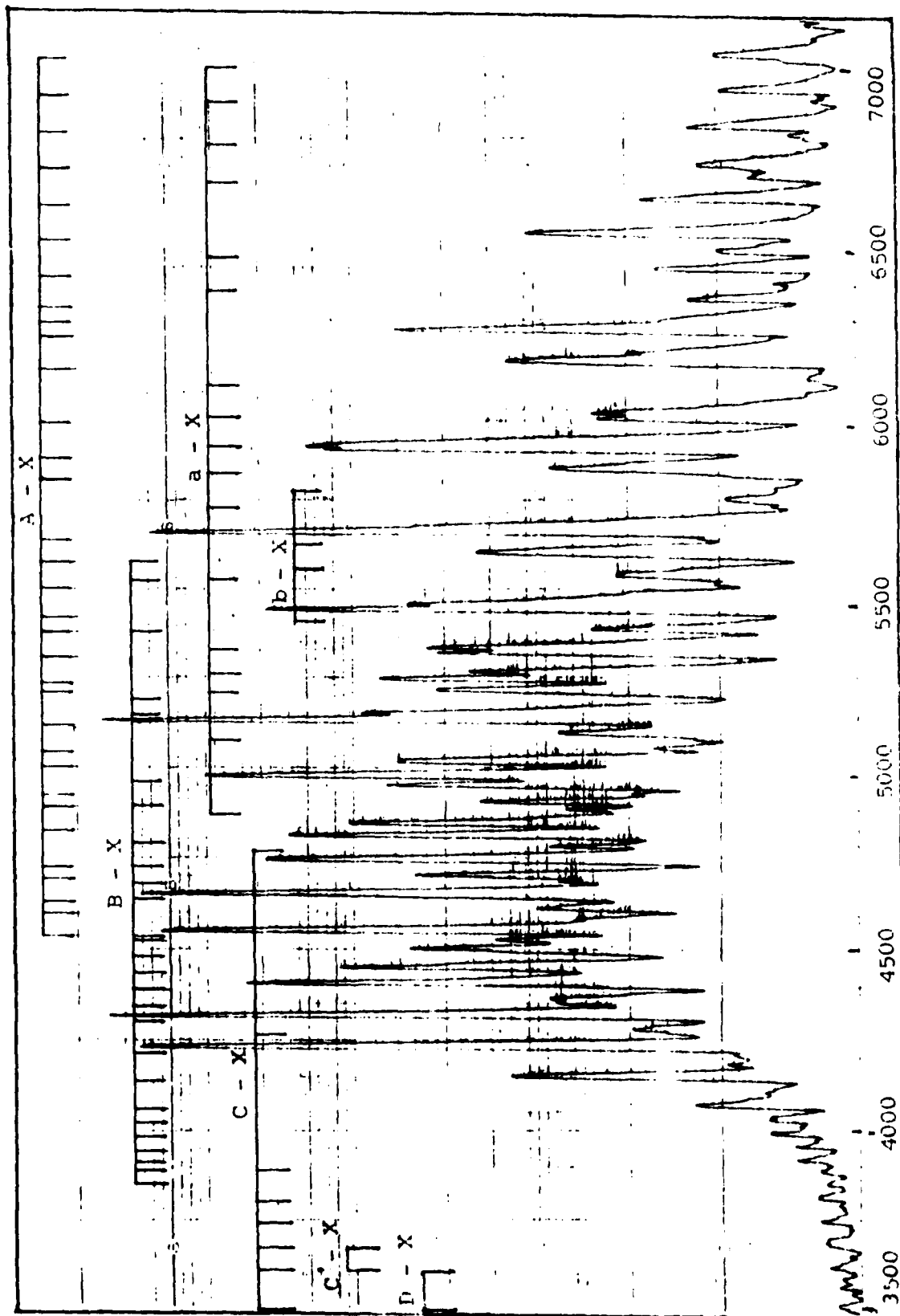


Figure 22. Low Dispersion Spectrum from
the $\text{Pb} + \text{O}_2(^1\Delta)$ Reaction

emission intensities. The ratio of intensities for several representative transitions is shown in Table V.

Transition	Energy (cm ⁻¹)	$I_{1\Delta}/I_{3\Sigma}$	Transition	Energy (cm ⁻¹)	$I_{1\Delta}/I_{3\Sigma}$
a(0,3)	13790	1	A(0,1)	19023	112
a(1,3)	14267	6	A(1,1)	19467	192
a(1,2)	14963	5	A(2,1)	19908	329
a(2,2)	15438	15	A(1,0)	20180	153
a(1,1)	15673	8	A(3,1)	20351	180
a(2,1)	16144	7	A(2,0)	20620	296
a(1,0)	16389	8	A(3,0)	21064	176
a(3,1)	16614	17	A(4,0)	21501	238
a(2,0)	16857	28	B(0,3)	20060	65
a(4,1)	17076	33	B(0,2)	20771	81
a(3,0)	17331	16	B(1,2)	21259	86
a(4,0)	17787	27	B(0,1)	21470	53
a(5,0)	18243	37	B(1,1)	21967	131
A(0,4)	16923	135	B(1,0)	22685	106
A(1,4)	17366	67	B(2,0)	23176	160
A(0,3)	17615	116	B(3,0)	23662	238
A(1,3)	18050	36	B(4,0)	24148	276
A(0,2)	18315	70	B(5,0)	24625	129
A(1,2)	18756	173			

Table V. Intensity Ratios for the a - X,
A - X and B - X Transitions

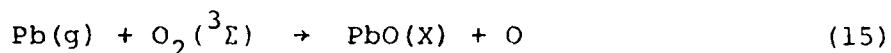
Based on these figures and after taking an average ratio for each state, the enhancement of the A state was calculated to be about 10 times that for the a state. Similarly, the enhancement of the B state was about 8.3 times that for the a state. These enhancements of the A and B states over the a state offer the first evidence that it may be possible to populate an upper electronic energy state at the expense of a lower lying energy state. If this upper state population could achieve greater than 50% of the lower energy state, a population inversion would be accomplished. The general trend of increasing intensity with increasing energy of the transition within a given electronic state remains to be explained.

Finally, an analysis was performed on the effect of variations in oxidizer pressure on spectral intensity for the $\text{Pb} + \text{O}_2(^1\Delta)$ reaction. Oxidizer pressures were varied from 0.3 T to 0.9 T at 0.5 T of Ar and from 1.0 T to 1.4 T at 0.9 T of Ar. The resulting spectra are shown in Appendix F. A slight enhancement of the B state over the A state was noted when pressure was increased from 0.3 T to 0.7 T. However, this enhancement subsided at 0.8 T and was not observed at the higher pressures. The major enhancement of the A and B states observed by Snyder (Ref 2:40, 46) for the reaction of $\text{Pb} + \text{O}_2(^3\Sigma)$ was not observed for the $\text{Pb} + \text{O}_2(^1\Delta)$ reaction.

Kinetics

The mechanisms of the reactions which lead to chemiluminescence from PbO are in doubt. Kurylo et al (Ref 5)

and Oldenberg et al (Ref 7) suggested that the presence of the 3P_1 excited state of Pb during reaction with ground state oxygen was responsible for the observed chemiluminescence. No evidence was given to substantiate this suggestion. Initial spectroscopic work on PbO at AFIT (Refs 2 and 3) led to the postulation of the following two-step mechanism for the reaction of Pb with $O_2(^3\Sigma)$.



where X indicates the ground electronic state, and g implies the gaseous state. The question as to how the 3P_1 state of Pb was generated has also arisen in the literature (Refs 5 and 7). Bachar and Rosenwaks showed that, for the case of the $Pb + O_2(^1\Delta)$ reaction, the main source of $Pb(^3P_1)$ was a reaction between $O_2(^1\Delta)$ and $Pb(^3P_0)$ (Ref 14:526). However, no evidence has been presented to indicate the source of Pb excitation or the mechanism leading to chemiluminescence in the reaction between Pb and $O_2(^3\Sigma)$. The first two parts of this section attempt to unravel the mechanism or mechanisms responsible for the observed emissions from the $Pb + O_2(^3\Sigma)$ reaction. The final part discusses the mechanism of the $Pb + O_2(^1\Delta)$ reaction.

Presence of Excited Pb. Two methods were used in an attempt to detect electrical excitation of Pb in the current work. First, one of the electrodes to the tungsten coil was grounded to the outside of the flow tube to prevent arcing across the electrodes. The emission intensities were recorded with and without the ground wire connected. No observable change occurred in the intensities.

The second method was to shut off the heater power supply and observe the resulting decay in emission intensity as a function of time and temperature. If electrical excitations were occurring, a sudden drop in intensity should have been observed. If no electrical excitations were occurring, the decay intensities should be gradual with time. Figure 23 shows a plot of intensity and temperature versus time. Note the linearity of the temperature and gradual decay of the intensity. A plot of the natural logarithm of the intensity versus time gives a linear plot as shown in Figure 24. These experiments are considered to be conclusive proof that no electrical excitations are occurring. The complete data set for these experiments is tabulated in Appendix G.

An experimental determination of the presence of thermally excited Pb was precluded due to a lack of necessary detection equipment. However, from a knowledge of the oven temperature and the energies of the states of Pb, the relative concentrations of the states can be determined using the Boltzman equation

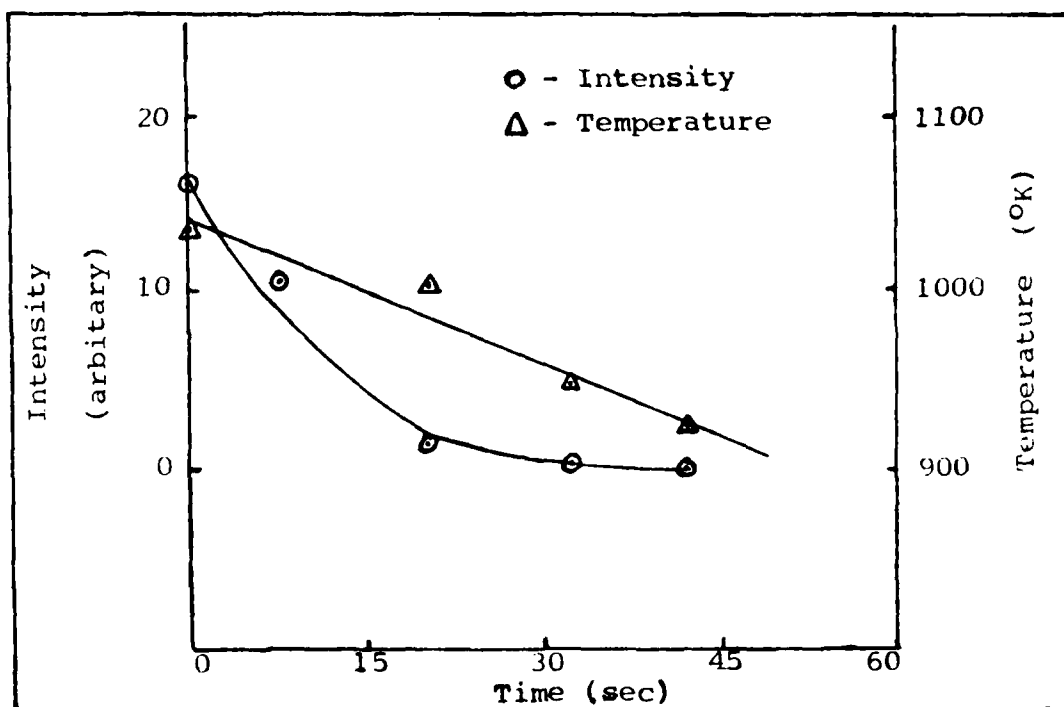


Figure 23. Intensity and Temperature Decay Versus Time for $\text{Pb} + \text{O}_2(^3\Sigma)$ Reaction

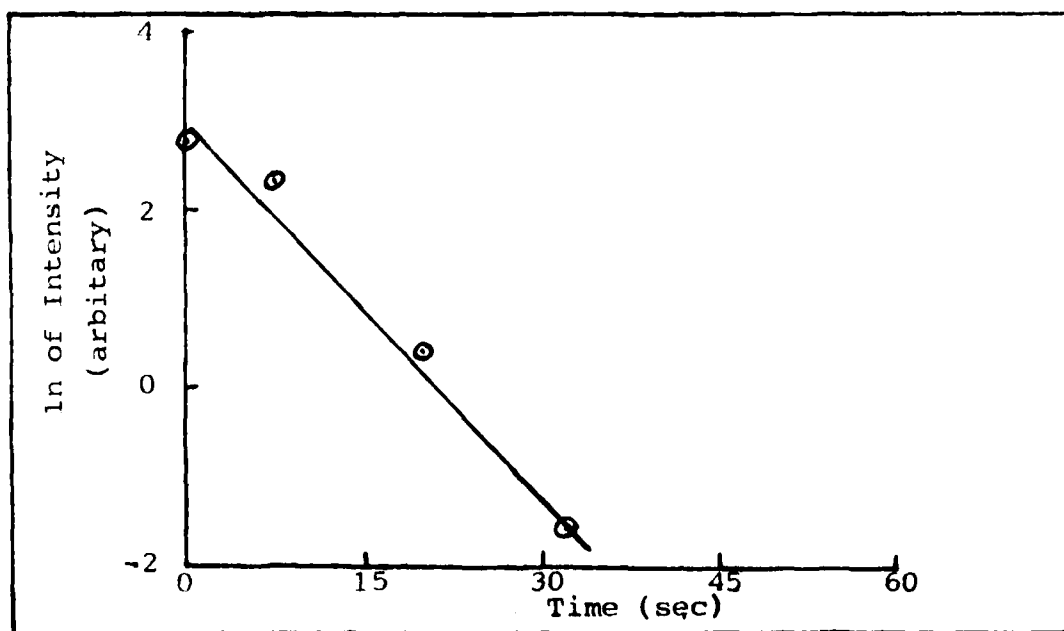


Figure 24. Logarithmic Intensity Decay Versus Time for $\text{Pb} + \text{O}_2(^3\Sigma)$ Reaction

$$N = N_0 \exp(-\Delta E / kT) \quad (17)$$

where N and N_0 are the number of atoms in the excited state and the ground state, respectively, ΔE is the energy difference between the excited state and the ground state, k is the Boltzman constant ($0.6952 \text{ cm}^{-1}/^\circ\text{K}$), and T is the oven temperature (1163°K). The energy levels for the first five states of Pb are shown in Table VI. Using Eq (17) and letting $N_0 = 1$, the values for N_{3P_1} and N_{3P_2} were found to be 6.3×10^{-5} and 1.9×10^{-6} , respectively. The concentration of Pb in the flame region was shown to be about 3.4×10^{14} atoms/cc (Ref 24:4). Assuming for the moment that all excited species created in the crucible reach the flame region, this would yield approximate concentrations of 2.1×10^{10} atoms/cc for $\text{Pb}(^3P_1)$ and 6.5×10^8 atoms/cc for $\text{Pb}(^3P_2)$. Concentrations of $\text{Pb}(^1D_2)$ and $\text{Pb}(^1S_0)$ are negligible (Ref 14:528).

To verify the previous assumption, a determination was made as to the amount of excited Pb remaining in the flame region. Transitions between the five lowest energy states of Pb are prohibited due to Laporte's rule (Ref 25:1089). Laporte's rule states that transitions between states of the same parity are forbidden (Ref 26:236). Thus, the first four excited states of Pb are metastable.

<u>State</u>	Energy (cm ⁻¹)
³ P ₀	0
³ P ₁	7819
³ P ₂	10650
¹ D ₂	21457
¹ S ₀	29466

Table VI. Energy Levels of Pb (Ref 10:45)

The transition probabilities for transitions between the three lower states of Pb have been reported by Garstang (Ref 27:67) and are tabulated in Table VII. A_m is the magnetic dipole transition probability and A_q is the electric quadrupole transition probability. Based on these values, the lifetime of the ³P₁ and ³P₂ states can be calculated from

$$T = 1/p \quad (18)$$

where p is the probability of a transition. This yields a lifetime of 136 msec for the ³P₁ state. Since the probabilities are additive for a given state (Ref 27:61), the lifetime of the ³P₂ state is 4.8 sec. For the current

Transition	Type	Probability (sec ⁻¹)
$^3P_1 - ^3P_1$	A_m	0.18
	A_q	2.5×10^{-4}
$^3P_2 - ^3P_2$	A_q	0.21
$^3P_1 - ^3P_0$	A_m	7.30

Table VII. Transition Probabilities Between Excited States of Pb

system, the Pb flow velocity was calculated to be 8150 cm/sec (Ref 24:4). Since the chimney of the flow tube is 4 in. long, the residence time of the Pb in the chimney is approximately 1.25 msec. Therefore, any 3P_1 or 3P_2 formed in the crucible will reach the flame region unless quenched by collisions with Ar molecules or the chimney walls.

The equation for the change in Pb(3P_1) concentration due to collisions with Ar can be written as

$$\frac{d[^3P_1]}{dt} = k'_{Ar} [^3P_1] \quad (19)$$

where $[\]$ indicate concentration and k' is a first-order collision rate constant. The constant k' is defined in terms of a second-order rate constant, k , and the concentration of Ar as

$$k' = k [\text{Ar}] \quad (20)$$

Hussain and Littler (Ref 28:68) reported a value for k of $0 \pm 1.0 \times 10^{-16}$ cc/molecule-sec at 300°K . The concentration of Ar can be determined from

$$[\text{Ar}] = P/RT \quad (21)$$

where R is the universal gas constant (82.056 cc-atm/ $^\circ\text{K}$ -mole), P is the pressure (~ 2 mm of Hg) and T is the temperature ($^\circ\text{K}$). The temperature extremes in the flow tube ranged from 300°K to 1163°K and correspond to the greatest and least concentration of Ar, respectively. Applying Eq (21) to both temperatures and multiplying by Avagadro's number yields the following Ar concentrations

$$[\text{Ar}]_{300^\circ \text{K}} = 6.439 \times 10^{16} \text{ molecules/cc} \quad (22)$$

$$[\text{Ar}]_{1163^\circ \text{K}} = 1.656 \times 10^{16} \text{ molecules/cc} \quad (23)$$

These concentrations were substituted into Eq (20) using the worst case for k (1×10^{-16}) and resulted in the following rate constants

$$k'_{300^\circ \text{K}} = 6.439 \text{ sec}^{-1} \quad (24)$$

$$k'_{1163^\circ \text{K}} = 1.656 \text{ sec}^{-1} \quad (25)$$

Upon taking the inverse of these rate constants, the following lifetimes were obtained

$$T_{300^\circ \text{ K}} = 155 \text{ msec} \quad (26)$$

$$T_{1163^\circ \text{ K}} = 603 \text{ msec} \quad (27)$$

A similar analysis for the $^3\text{P}_2$ state using $k = 2.0 \pm .5 \times 10^{-15}$ cc/molecule-sec (Ref 28:70) resulted in the following lifetimes

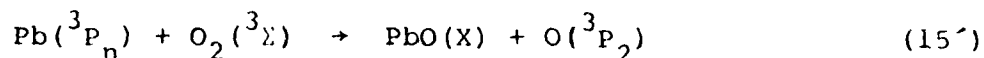
$$T_{300^\circ \text{ K}} = 6 \text{ msec} \quad (28)$$

$$T_{1163^\circ \text{ K}} = 20 \text{ msec} \quad (29)$$

As seen from these results, even in the worst case, the lifetimes of the $^3\text{P}_1$ and $^3\text{P}_2$ states are at least four times greater than the chimney residence time of lead.

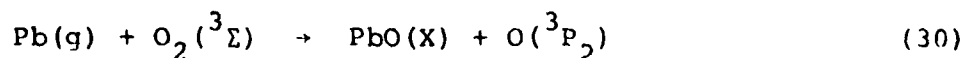
Since this analysis has neglected the effects of collisions with the chimney walls, these calculations represent an upper limit on the lifetimes. However, the effect of wall collisions is assumed to be negligible. Thus, any $^3\text{P}_1$ or $^3\text{P}_2$ created in the crucible will reach the flame region, and our original assumption is verified.

The effect of the presence of excited Pb on the reaction



where $n = 0, 1, 2$, can be assessed by studying the exothermicity of the reactions. The heats of formation of the reactants and products are given in Table VIII. Using the values in Table VIII, the various reaction exothermicities can be calculated. The exothermicities are tabulated by electronic state of Pb in Table IX. The plus and minus signs indicate endothermic and exothermic reactions, respectively. As can be seen from Table IX, only the reaction involving $^3\text{P}_2$ is exothermic. Still, the exothermicity of this reaction is far less than the $16,024.9 \text{ cm}^{-1}$ required to excite the a state of PbO. Therefore, the effect of excited Pb on the $\text{Pb} + \text{O}_2(^3\Sigma)$ reaction is negligible.

Pb + O₂(³Σ) Reaction Mechanisms. Reaction activation energies obtained during this experiment are listed in Table X. The activation energy for the reaction of Pb with O₂(³Σ) at the higher pressures is very close to the dissociation energy of ground state oxygen of 117.12 kcal/mole (Ref 9:558). Based on this value, it is plausible to suggest the following two-step mechanism for the formation of PbO*



Reactant/Product	Energy	
	(kcal/mole)	(cm ⁻¹)
Pb(³ P ₀)	46.34	16211.4
Pb(³ P ₁)	68.69	24030.4
Pb(³ P ₂)	76.78	26861.4
O ₂ (³)	0	0
PbO(X)	11.48	4016.1
O(³ P ₂)	59.56	20836.2

Table VIII. Heats of Formation (Refs 21; 29)

Electronic State of Pb	Energy	
	(kcal/mole)	(cm ⁻¹)
³ P ₀	+24.70	+8640.9
³ P ₁	+ 2.35	+ 821.9
³ P ₂	+ 5.74	-2009.1

Table IX. Reaction Exothermicities of
Pb(³P_n) + O₂(³Σ) Where n=0,1,2

Oxidizer	Pressure (O ₂)	Pressure (Ar)	Temperature (° K)	E _a (kcal/mole)
O ₂ (³ Σ)	.3 T	1.9 T	1040-1086	63.9±8.0
	.8 T	3.3 T	1062-1103	115.3±22.4
O ₂ (¹ Δ)	.7 T	1.0 T	929-1048	12.3
	.7 T	.9 T	940-1001	17.4
	.8 T	1.1 T	929- 974	19.2
	.7 T	1.0 T	929-1004	20.7
	1.3 T	1.0 T	984-1014	21.9
	.7 T	.9 T	937- 989	23.0
	.7 T	.9 T	809- 860	32.4

Table X. Activation Energies

The exothermicity of the reaction in Eq (31) is 33,051.5 cm⁻¹ (Ref 2:16). As seen in Figure 25, this energy is high enough so that states as energetic as the D state and possibly the E state could be formed as a result of this reaction.

When the oxidizer pressure is decreased, the activation energy also decreases. This decrease in activation suggests a change in the reaction mechanism. It is possible that Pb is condensing to the solid according to the reaction scheme



⋮

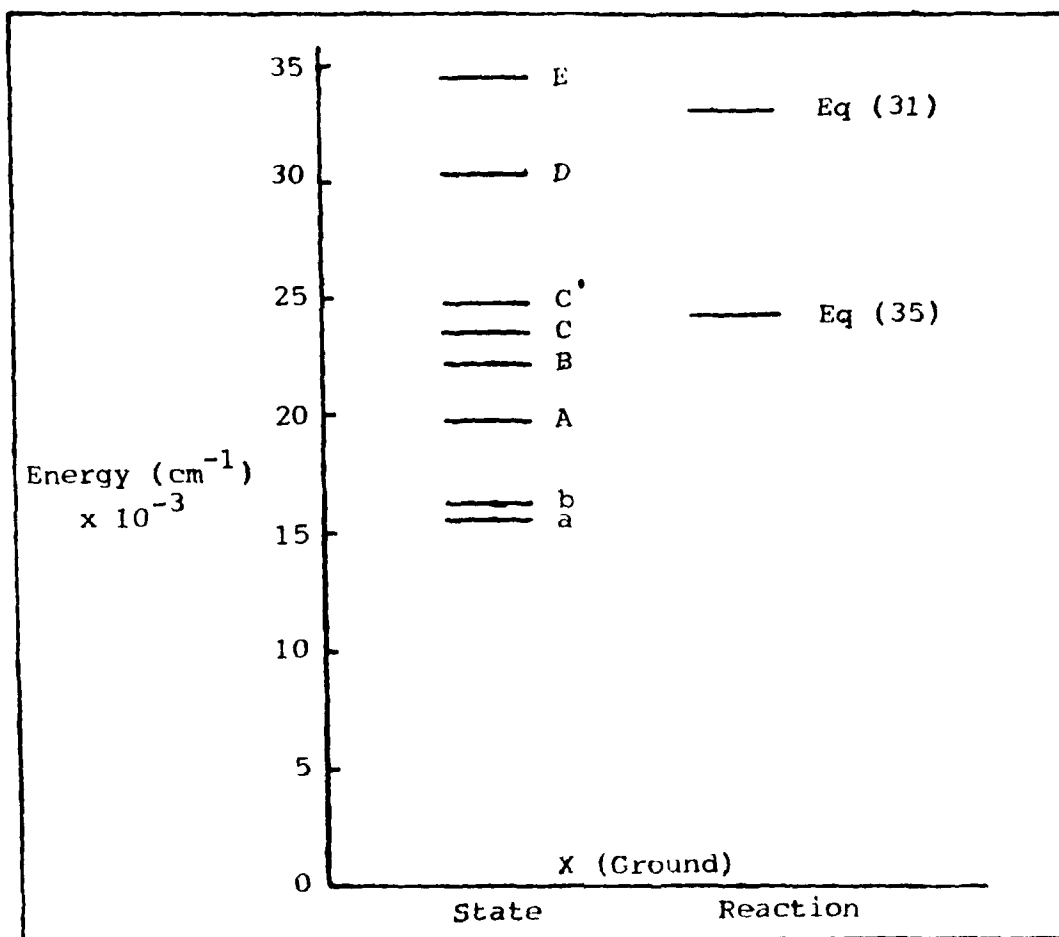
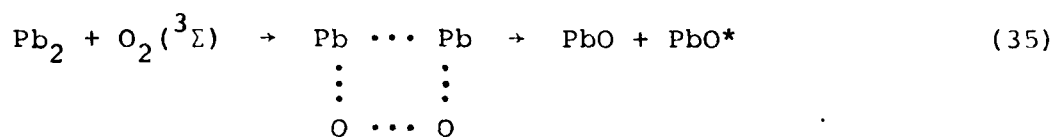


Figure 25. Excited State Energies and Reaction Exothermicities

where M is a third body necessary to provide decreasing stabilization for the reaction (Ref 30:681). It is known that, if the concentration of lead vapor exceeds the equilibrium saturated concentration by a factor of 50, then the condensation as shown in Eqs (32), (33), and (34) will occur (Ref 31:70). Shock tube studies have shown that, in the temperature range of current interest after about 0.5 msec

all the gaseous lead has condensed to small particles of solid (Ref 30:675). If this type of condensation is occurring to an appreciable extent, then the mechanism of the reaction is expected to change. A four-center type of reaction occurring on the surface of the particles as shown in Eq (35) is a possibility.

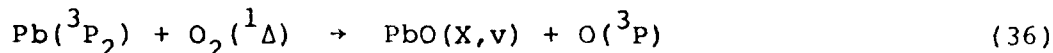


The exothermicity of this reaction is 24390.5 cm^{-1} (Ref 2:16). This energy is large enough to produce PbO^* only to the level of the C state as seen in Figure 25.

The variation in exothermicities in different pressure regimes corroborates Snyder's results. That is, he observed an increase in relative intensity of higher lying electronic states of PbO with an increase in oxidizer pressure (Ref 2:40, 46).

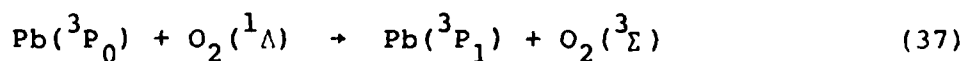
The activation energy for this four-center type of reaction may be roughly approximated by taking the average of the two bond strengths or chemical dissociation energies, D_0 . Herzberg reports values of 16.4 kcal/mole for $D_0(\text{Pb}_2)$ and 117.1 kcal/mole for $D_0(\text{O}_2)$ (Ref 9:561, 558). The activation energy is thus 66.6 kcal/mole. The experimental activation energy from Table X (63.9 ± 8.0 kcal/mole) is well within experimental error of this value.

Pb + O₂(¹Δ) Reaction. The reaction between Pb and O₂(¹Δ) has been studied by Bachar and Rosenwaks (Ref 14). They have proposed a mechanism for the formation of PbO* in which the rate controlling step is



where PbO(X,v) indicates PbO in vibrationally excited levels of the ground electronic state. This reaction is expected to have an activation energy much lower than that for the reactions shown in Eqs (30) and (31) or Eq (35). Experimentally (see Table X), this has been shown to be the case. For the reaction between Pb and O₂(¹Δ), the results in Table X reveal a very low activation energy (an average of 21.0 ± 6.1 kcal/mole). This value is much lower than the values determined for the reaction between Pb and O₂(³Σ).

In addition, the activation energy of the reaction between Pb and O₂(¹Δ) was found to decrease with increasing oven temperature. From a previous development, the concentration of Pb(³P₁) was shown to increase with oven temperature. Based on the mechanism presented by Bachar and Rosenwaks (Ref 14:526), a decrease in activation energy is expected. The first step in their mechanism is the production of Pb(³P₁) via the resonant energy transfer process



Since $\text{Pb}(^3\text{P}_1)$ is also being produced thermally, the reaction in Eq (37) is enhanced with an increase in temperature. The energy necessary for activation of the reaction sequence is reduced accordingly.

It is obvious that numerous mechanisms are contributing to the formation of PbO^* and the subsequent emissions. These mechanisms are dependent on the oxidizer being used, the oxidizer pressure and the operating temperature. Although the complete mechanism for the reaction of Pb and $\text{O}_2(^3\Sigma)$ remains to be determined, it is clear that Eqs (15) and (16) do not represent a complete picture. Further research and analysis are required before a final determination of the true mechanisms can be made.

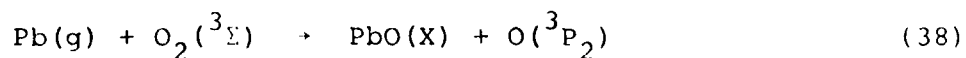
V. Conclusions and Recommendations

Conclusions

Chemiluminescent flames have been generated using a gas flow tube reactor for the $\text{Pb} + \text{O}_2(^3\Sigma)$ and $\text{Pb} + \text{O}_2(^1\Delta)$ reactions. Assignment of 67 transitions from the a, b, A, B and C electronic states were made for the $\text{Pb} + \text{O}_2(^3\Sigma)$ reaction. A similar analysis for the $\text{Pb} + \text{O}_2(^1\Delta)$ reaction led to the assignment of 225 transitions to the a, b, A, B, C, C', D and E electronic states. Relative intensities for transitions from the a state of the $\text{Pb} + \text{O}_2(^3\Sigma)$ reaction and from the A and B states of the $\text{Pb} + \text{O}_2(^1\Delta)$ reaction were tabulated in Deslandres tables. These values were compared to Franck-Condon factors (Ref 23) and found to be in excellent agreement. The relative intensities for transitions from the a, A, and B electronic states were compared for both reactions. Significant enhancements of the A and B states relative to the a state were observed for the $\text{Pb} + \text{O}_2(^1\Delta)$ reaction. By taking an average of the intensity enhancements for each electronic state, the enhancement factors for the A and B states were found to be 10 and 8.3, respectively. This enhancement is the first evidence that it may be possible to populate an upper electronic energy state at the expense of a lower lying energy state. A study of the dependency of transition intensity on oxidizer pressure was conducted for the $\text{Pb} + \text{O}_2(^1\Delta)$ reaction. Oxidizer

pressures were varied from 0.3 T to 1.4 T. A minor enhancement of the B state relative to the A state was noted from 0.3 T to 0.7 T. The low pressure enhancement of the A and B states observed by Snyder (Ref 2:40, 46) for the $\text{Pb} + \text{O}_2(^3\Sigma)$ reaction was not observed for the $\text{Pb} + \text{O}_2(^1\Sigma)$ reaction.

The presence of excited states of Pb in the flame region has been theoretically verified. However, due to the low exothermicities involved, the presence of excited Pb atoms was shown to have little effect on the mechanism of the $\text{Pb} + \text{O}_2(^3\Sigma)$ reaction. Activation energies for both reactions were determined. Based on the activation energies for the $\text{Pb} + \text{O}_2(^3\Sigma)$ reaction, two possible mechanisms have been proposed. At higher oxidizer pressures, the activation energy approximately equals the dissociation energy of O_2 . This evidence strongly supports the following two-step mechanism.



At lower oxidizer pressures, that is, lower activation energy, the following four-center mechanism was proposed to account for this result.

212

NL

UNCLASSIFIED

F/G 7/2

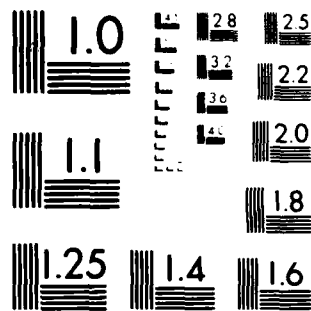
[illegible]

END

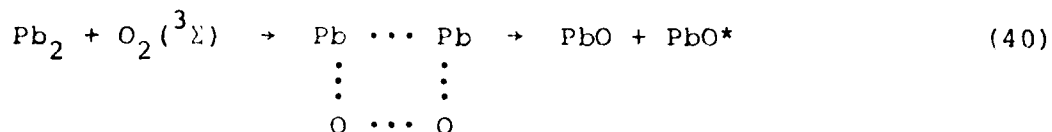
DATE _____

3 - 84

DTIC



MICROCOPY RESOLUTION TEST CHART
NATIONAL BUREAU OF STANDARDS-1963-A



Finally, the activation energies for the reaction of $\text{Pb} + \text{O}_2(^1\Delta)$ were found to be much lower than for the $\text{Pb} + \text{O}_2(^3\Sigma)$ reaction. This evidence is the first experimental verification of the mechanism proposed by Bachar and Rosenwaks (Ref 14) for the reaction of $\text{Pb} + \text{O}_2(^1\Delta)$.

Recommendations

New Grating. The new 1180 line/mm grating blazed at 3000 Å should be installed in the 0.5 m Jarrell-Ash. Spectra from the $\text{Pb} + \text{O}_2(^1\Delta)$ reaction should be rerun from 2000 Å to 4000 Å. The increased spectral response will allow finer resolution and, therefore, better bandhead assignments in this region.

New Manifold. A new Pyrex manifold should be constructed. The angled holes along the top edge should be eliminated. In addition, a series of holes directed vertically along the top surface should be added to create a gas curtain effect to prevent flaring of the flame.

Photon Counter. The C3103402 PMT should be utilized in the photon counting mode in conjunction with the new EG&G signal averager. This should significantly increase the signal-to-noise ratio and the resolution capabilities to allow more accurate determinations of bandheads.

Modulated Spectra. The modulation capabilities of the microwave generator should be utilized. The resulting spectra will illustrate the relative enhancements in intensity of the transitions from the $\text{Pb} + \text{O}_2(^3\Sigma)$ and $\text{Pb} + \text{O}_2(^1\Delta)$ reactions.

Flame Measurements. The flow tube should be modified to permit the taking of temperature and intensity measurements as a function of vertical position in the flame. This will allow the determination of the dependence of the kinetic mechanisms on the relative position in the flame.

Pb Concentration. The concentration of Pb in the $^3\text{P}_0$, $^3\text{P}_1$ and $^3\text{P}_2$ states should be determined. Excited atomic Pb should be produced via a microwave discharge. By measuring the absorption of Pb emissions from the discharge by the flame, the relative concentrations of the excited states of Pb can be determined.

Activation Energies. The activation energies of the $\text{Pb} + \text{O}_2(^1\Delta)$ reaction should be determined as a function of the electronic transition. From this information, the kinetic mechanism as a function of wavelength can be determined.

Bibliography

1. Fontijn, A, and W. Felder. "High Temperature Fast-Flow Reactor Study of $\text{Sn/N}_2\text{O}$ Chemiluminescence." Chemical Physics Letters, 34: 398-402 (May 1972).
2. Snyder, Stephen R. Spectroscopic Analysis of PbO Chemiluminescence. MS Thesis, Wright-Patterson AFB OH: Air Force Institute of Technology, December 1981.
3. Glessner, John W. Flame Optimization for the Spectroscopic Analysis of the Chemiluminescence from Lead Oxide. MS Thesis, Wright-Patterson AFB OH: Air Force Institute of Technology, December 1982.
4. Linton, C. and H.P. Broida. "Chemiluminescent Spectra of PbO Reactions of Pb Atoms." Journal of Molecular Spectroscopy, 62: 396-415 (1976).
5. Kurylo, M.J., et al. "A Study of the Chemiluminescence of the $\text{Pb} + \text{O}_3$ Reactions." Journal of Research of the NBS, 80A, (2): 167-171 (March-April 1976).
6. Suchard, S.N. Spectroscopic Data for Heteronuclear Diatomic Molecules, Vol II. Plenum Publications, 1975.
7. Oldenberg, R.C., C.R. Dickson, and R.N. Zare. "A New Electronic Band System of PbO." Journal of Molecular Spectroscopy, 58: 445-454 (1980).
8. Case, C.T. and L.S. Pedrotti. Atomic and Molecular Physics. Wright-Patterson AFB OH: Air Force Institute of Technology.
9. Herzberg, G. Spectra of Diatomic Molecules (Second Edition). New York: Reinhold Co., 1950.
10. Steinfeld, Jeffrey I. Molecules and Radiation. New York: MIT Press, 1978.
11. Bloomenthal, S. "Vibrational Quantum Analysis and Isotope Effect for the Lead Oxide Band Spectra." Physics Review, 35: 34-45 (January 1930).
12. Barrow, R.F., et al. Proceedings of the Physics Society of London, 81: 697-704 (1963)
13. Wasserman, H.H. and R.W. Murray. Singlet Oxygen. New York: Academic Press, 1979.

14. Bachar, J. and S. Rosenwaks. "Reactions of Chemically Produced $O_2(^1\Delta)$ with Pb Atoms." Chemical Physics Letters, 96(5): 526-531 (April 1983).
15. Wilson, L.E., S.N. Suchard, and J.I. Steinfeld. Electronic Transition Lasers II. Cambridge MA: MIT Press, 1977.
16. Frost, A.A. and R.G. Pearson. Kinetics and Mechanisms. New York: John Wiley and Sons, Inc., 1953.
17. Beattie, W.H., M.A. Revelli, and J.M. Brom, Jr. "Radiative Lifetime of $PbO\ a(1)$." Journal of Molecular Spectroscopy, 70: 163-164 (1978).
18. Brom, J.M., Jr. and W.H. Beattie. "Laser Excitation Spectrum of PbO ." Journal of Molecular Spectroscopy, 81: 445-454 (1980).
19. Koym, Vernon R. A Gas Flow Tube for Spectroscopic Studies. MS Thesis, Wright-Patterson AFB OH: Air Force Institute of Technology, December 1980.
20. Fehsenfeld, F.C., K.M. Evenson, and H.P. Broida. "Microwave Discharge Cavities Operating at 2450 MHz." The Review of Scientific Instruments, 36(3): 294-298 (March 1965).
21. Handbook of Chemistry and Physics (Fifty-Fourth Edition). Cleveland: The Chemical Rubber Company, 1973.
22. Rutger, Lyle L. Numerical Methods for the Preparation of Potential Energy Curves of Diatomic Molecules. MS Thesis, Wright-Patterson AFB OH: Air Force Institute of Technology, December 1982.
23. Pow, Joe J. Development of Computer Routines to Perform a Comprehensive Analysis of Spectroscopic Data from Diatomic Molecules. MS Thesis, Wright-Patterson AFB OH: Air Force Institute of Technology, December 1983.
24. Glessner, J.W., E.A. Dorko, S.R. Snyder, and L.L. Rutger. "Spectroscopic Analysis of the Chemiluminescence from Lead Oxide Flames." The Proceedings of the AIAA (Dayton-Cincinnati Section) 9th Annual Minisymposium on Aerospace Science and Technology, AIAA (Day/Cin) 83-1. Air Force Institute of Technology, Wright-Patterson AFB OH, 22 March 1983.
25. Mrozowski, S. "Hyperfine Structure and Intensities of the Forbidden Lines of Pb I." Physical Review, 34: 1086-1093 (1940).

26. Condon, E.U. and G.H. Shortley. The Theory of Atomic Spectra. Cambridge: University Press, 1963.
27. Garstang, R.H. "Transition Probabilities of Forbidden Lines." Journal of Research of the NBS, 68A(1): 61-73 (January-February 1964).
28. Hussain, D. and J.G.F. Littler. "The Collisional Behavior of the Spin Orbit States of the Lead Atom, $Pb(6^3P_{1,2})$, Studied by Time-Resolved Attenuation of Atomic Resonance Radiation." International Journal of Chemical Kinetics, VI: 61-75 (1974).
29. Thermo-Chemical Tables (Second Edition). USDC-NBS, JANAF, Washington DC: National Bureau of Standards, 1971.
30. Homer, J.B. and A. Prothero. "Nucleation of Highly Supersaturated Vapours." JCS, Faraday I, 69: 673-684 (1973).
31. Homer, J.B. and I.R. Hurle. "Shock Tube Studies on the Decomposition of Tetramethyl-lead and the Formation of Lead Oxide Particles. Proceedings of the Royal Society of London, A327: 61-79 (1972).
32. Photomultiplier Tubes. RCA, Electronic Components Division, Harrison NJ 07029.

Appendix A
Photographs

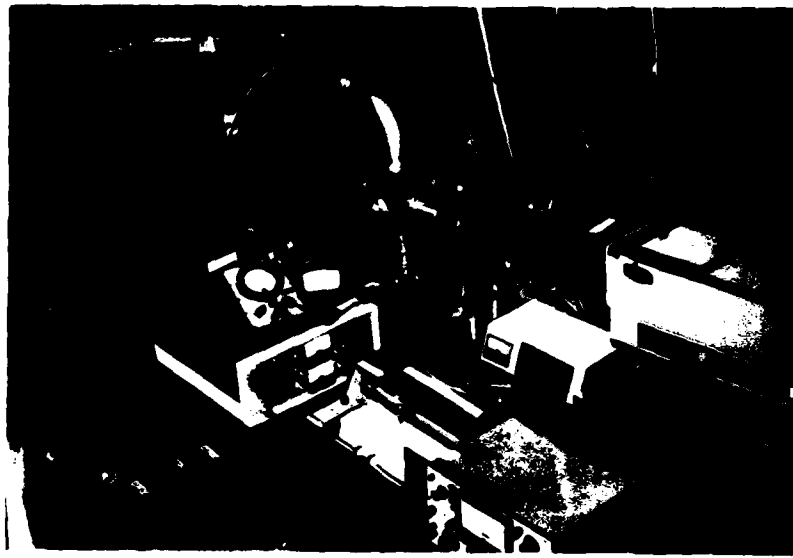


Figure A-1. Flow Tube System



Figure A-2. Furnace Chamber



Figure A-3. Oxidizer Manifolds



Figure A-4. Discharge Cavity Assembly

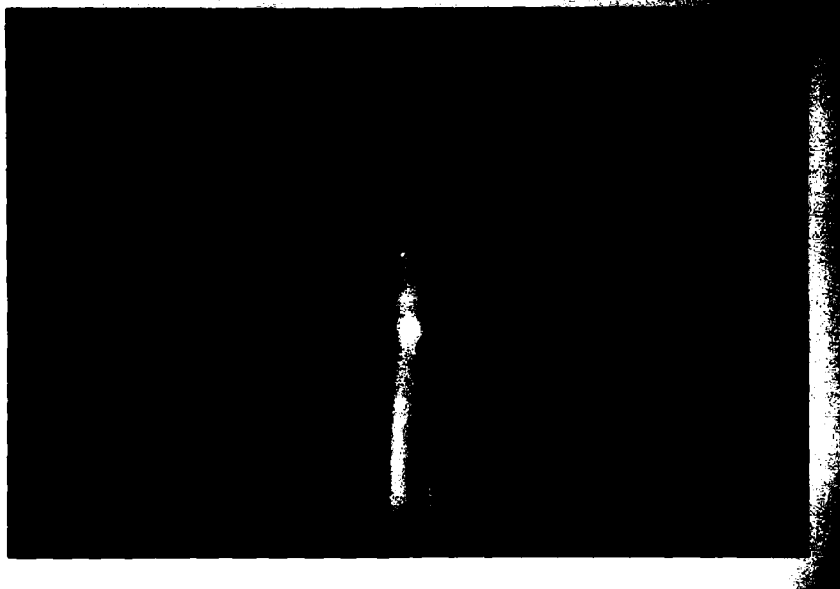


Figure A-5. Chemiluminescent Flame

Appendix B
Power Supply

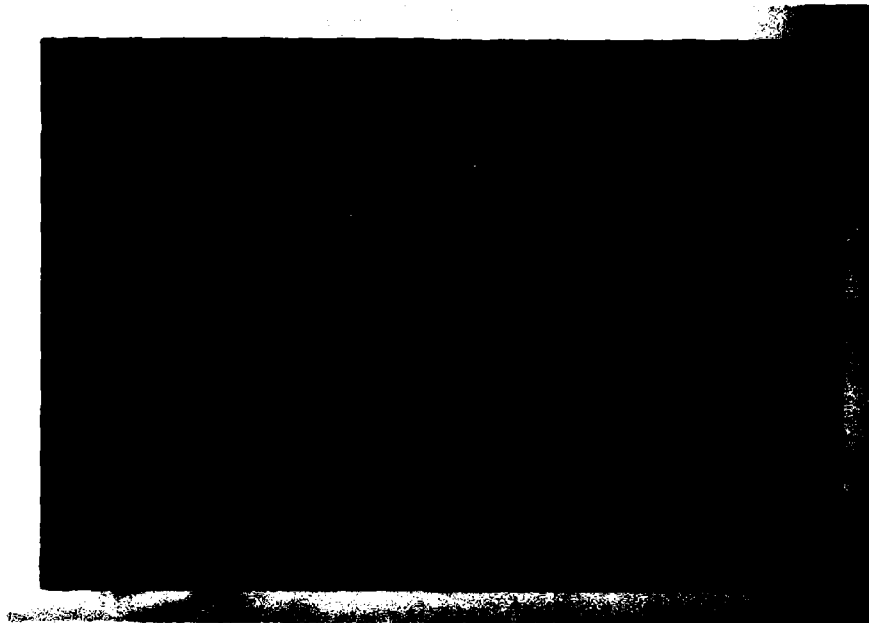


Figure B-1. Power Supply

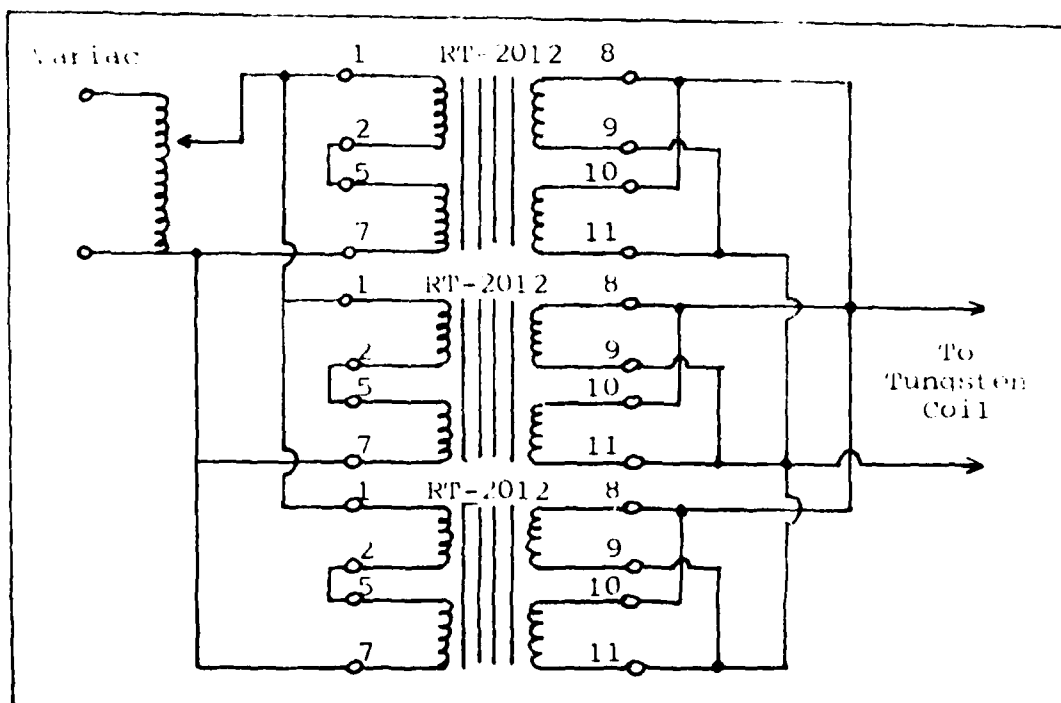
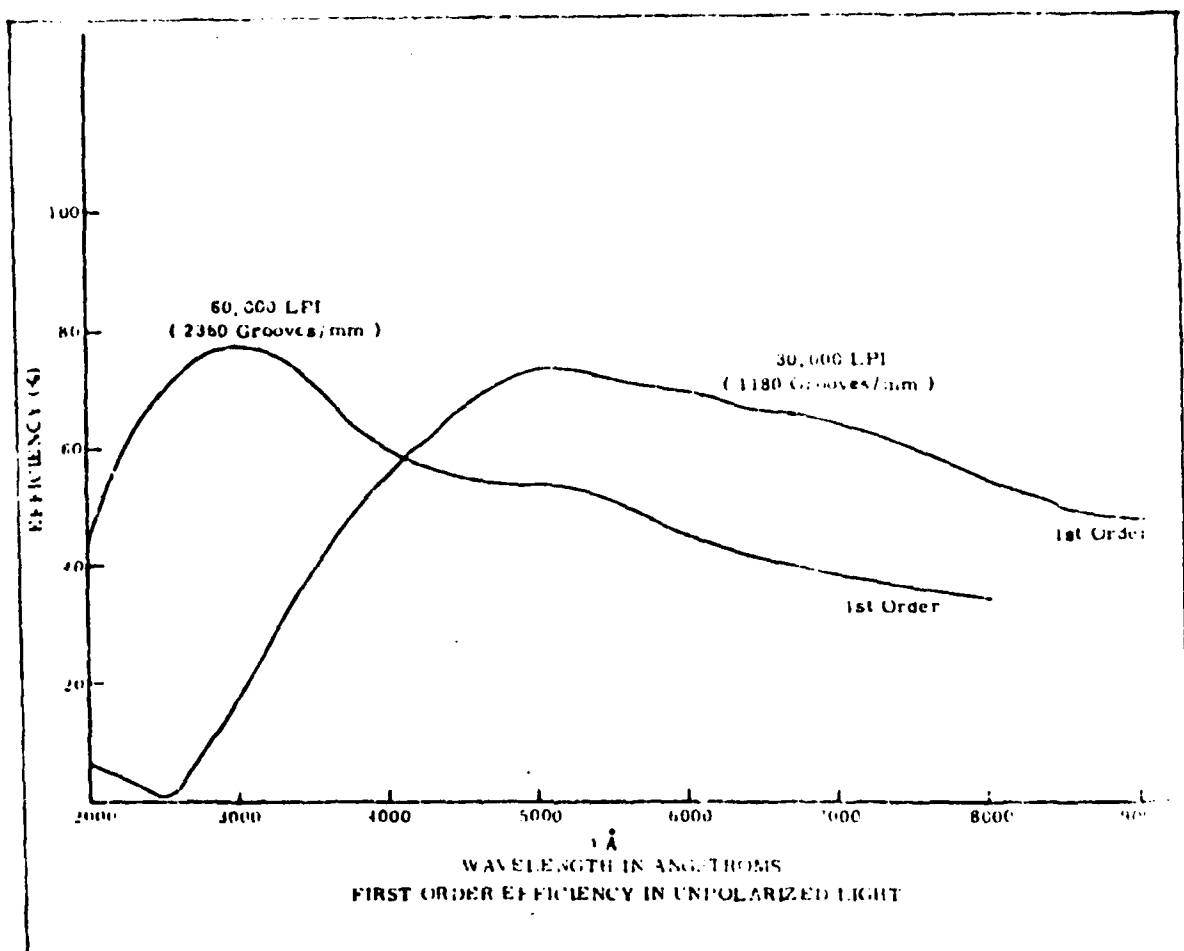


Figure B-2. Power Supply Schematic

Appendix C
Grating Response



Appendix D Photomultiplier Tubes

Mechanical				Maximum Ratings		Typical Characteristics at specified operating supply voltage, voltage distribution, and 22°C							
Spectral Response	RCA Type No.	No. of Stages and Cage Structure ^a	Dynode Secondary Emitting Surface Material	Supply Voltage V	Average Anode Current mA	Operating Supply Volts and Distribution ^f	Sensitivity				Gain (Approx.) $\times 10^6$	Anode Dark Current nA ^g	Anode Pulse Rise Time ^h ns
							Radiant ^d		Luminous ^e				
							Anode A/W	Cathode mA/W	Anode A/lm	Cathode μ A/lm			
							Anode A/W	Cathode mA/W	Anode A/lm	Cathode μ A/lm			
12B	C31034	11	B+O	2000	0.01	1500 L	41,000	68	300	500	0.6	3 ϕ 100	< 2.5
110 (S 20)	7265	14	B+O	3000	1.0	2400 W	3,100,000	64	7200	150	48	50 ϕ 1000	< 3.0

Figure D-1. PMT Characteristics (Ref 32)

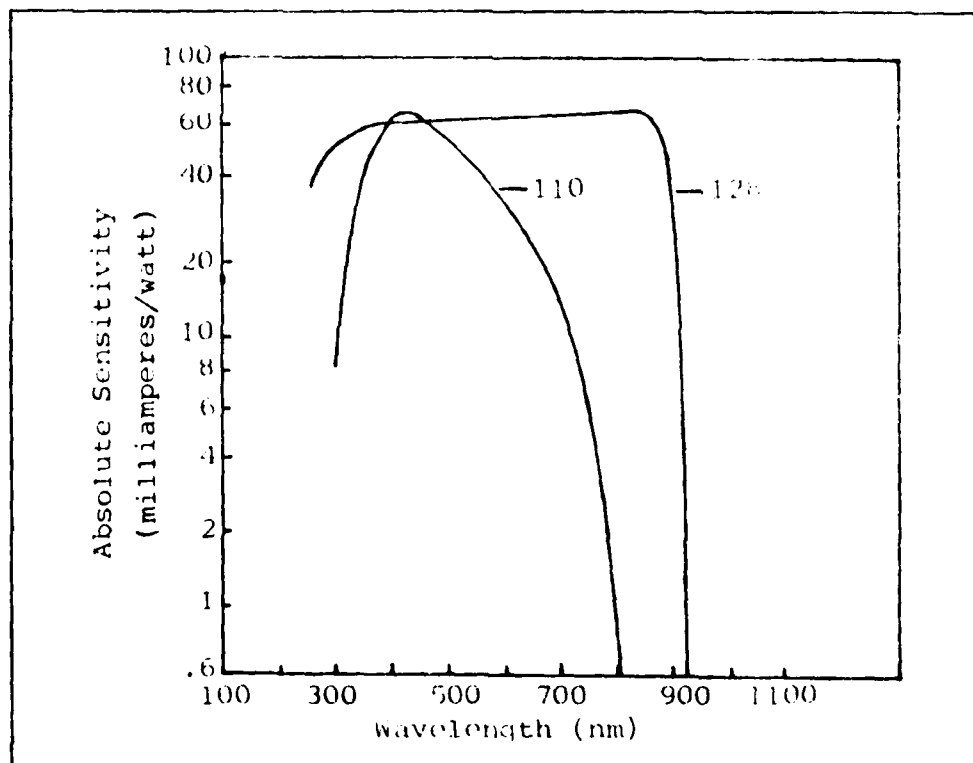


Figure D-2. PMT Response

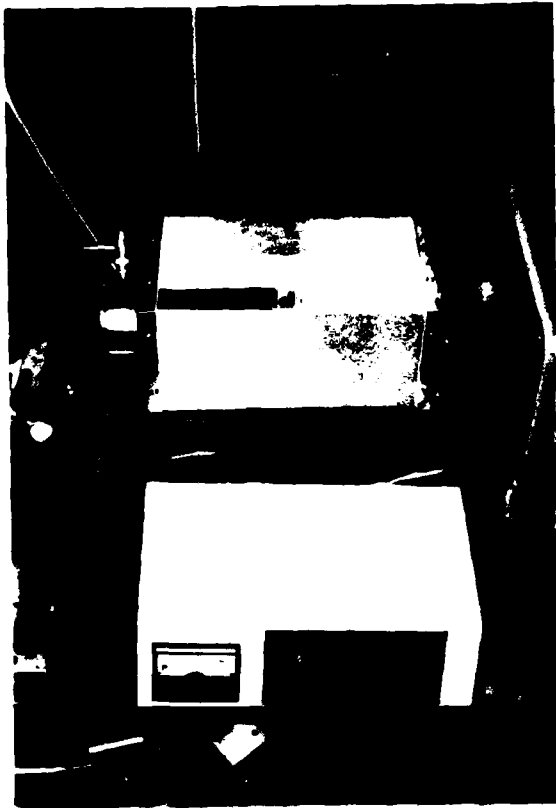


Figure 1-1. Low Power Reactor

Appendix E

Start-up and Shut-down Steps

After the aluminum oxide crucible has been filled with lead and the flow tube assembled, then the following start-up procedures should be used to generate a flame.

1. Turn on the PMT power supply and current amplifier at least 30 minutes prior to a run in order to stabilize these electronic systems.
 2. Tighten all vacuum clamps.
 3. Close the vacuum release valve (see Figure 6).
 4. Turn on the cooling water to the furnace cooling coils.
 5. Start the main vacuum pumps (one at a time due to high current demand).
 6. Open the main vacuum valve (see Figure 6).
 7. Start the vacuum pump connected to the reference side of the MKS Baratron 77 pressure head.
 8. Turn on the Baratron gauge (see Instruction Manual for bakeout and operational procedures).
 9. When the pressure is less than 200μ of Hg, open the valves to the Baratron pressure head and to the reference pump.
 10. Increase the voltage to the furnace heater power supply to the desired level (~ 1 V per 2 minutes).
 - 11* Turn on the main power switch to the microwave generator. Wait three minutes and turn on the high voltage switch.
- CAUTION: Never turn on the generator without a properly terminated load.
12. With the Baratron gauge zeroed, adjust the oxidizer pressure.
 - 13* Increase microwave power to maximum and ignite the plasma with a Tesla coil.

CAUTION: Never operate the generator for more than a few minutes with a S.W.R. greater than 3 where

$$S.W.R. = \frac{1 + \sqrt{\frac{\text{Reflected Power}}{\text{Forward Power}}}}{1 - \sqrt{\frac{\text{Reflected Power}}{\text{Forward Power}}}}$$

- 14.* Adjust the microwave cavity for minimum reflected power.
- 15.* Adjust the microwave generator to desired output power.
16. Adjust the carrier gas pressure.

Shut-down

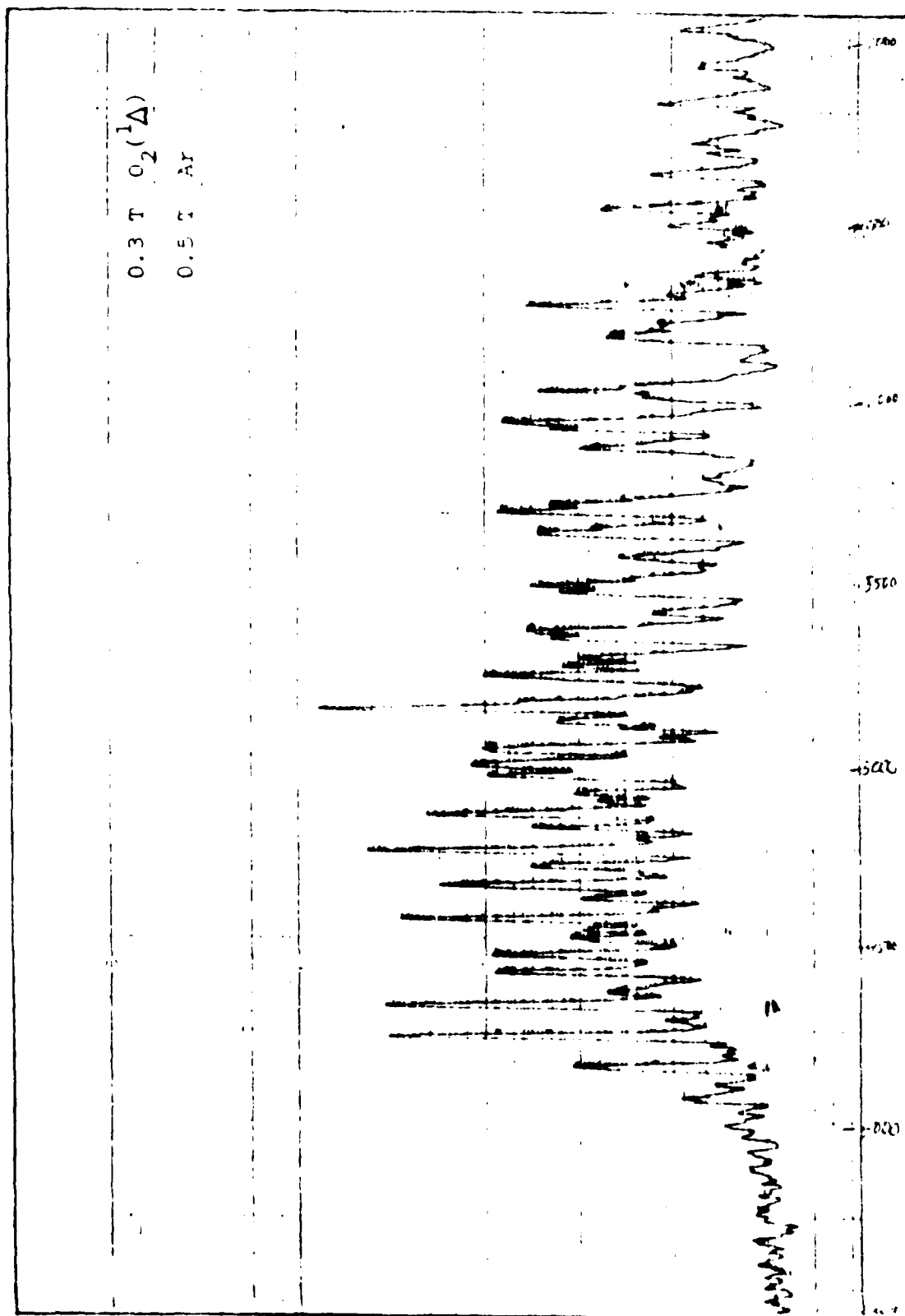
1. Turn off the main power supply to the furnace heater.
- 2.* Turn microwave power to zero at the generator.
- 3.* Turn off the high voltage switch and then the power switch of the microwave generator.
4. Turn off the oxidizer.
5. Allow 10 to 15 minutes for the furnace section of the flow tube to cool and for the reaction products to be removed from the flame region.
6. Close the valves to the Baratron pressure head and to the reference pump. Turn off the reference pump.
7. Close the main vacuum valve.
8. Shut off the pumps and open the vacuum release valve.
9. When the tube is at positive pressure, turn off the carrier gas.

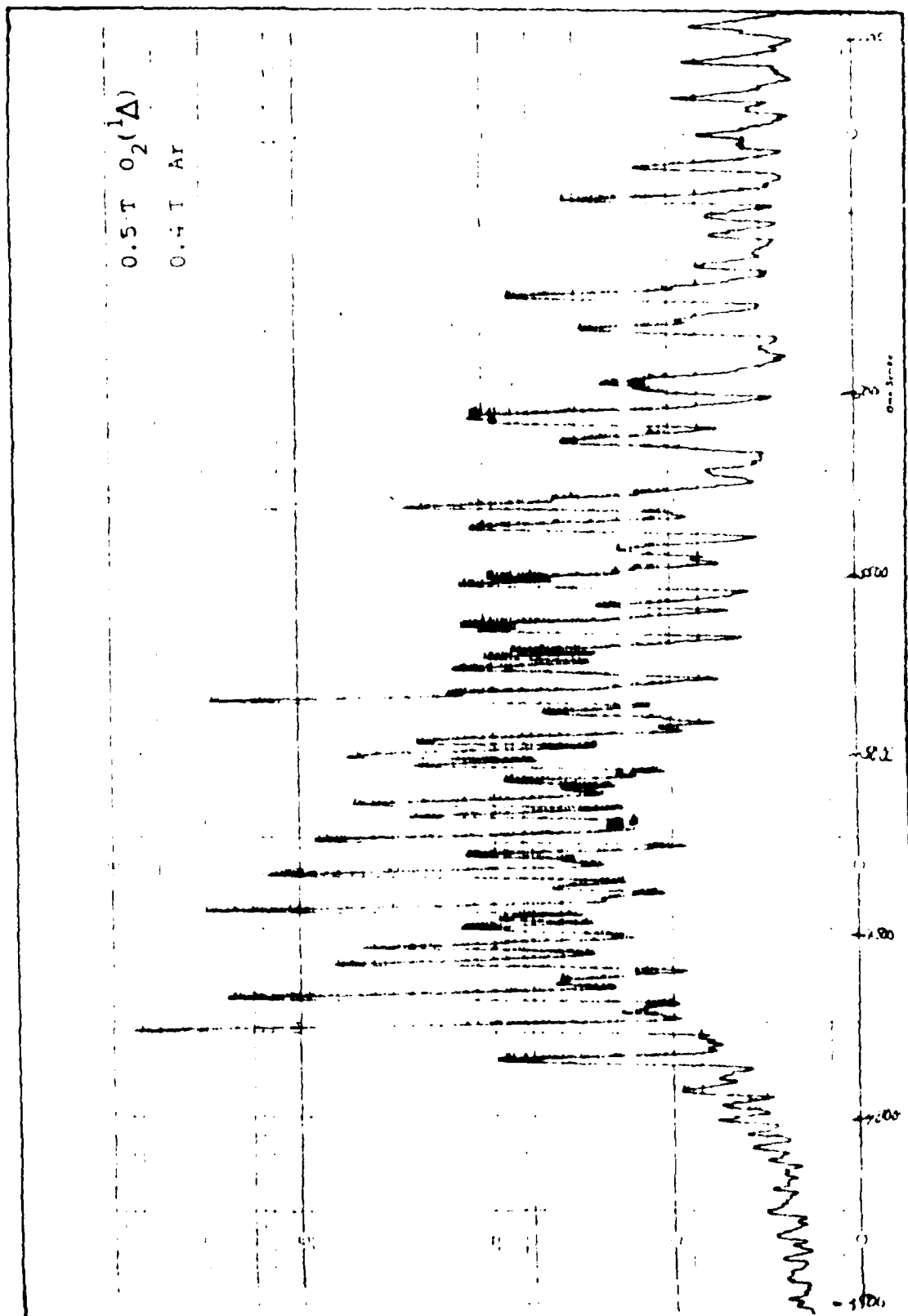
* These steps are followed when microwave excited oxidizers are being used.

Appendix F

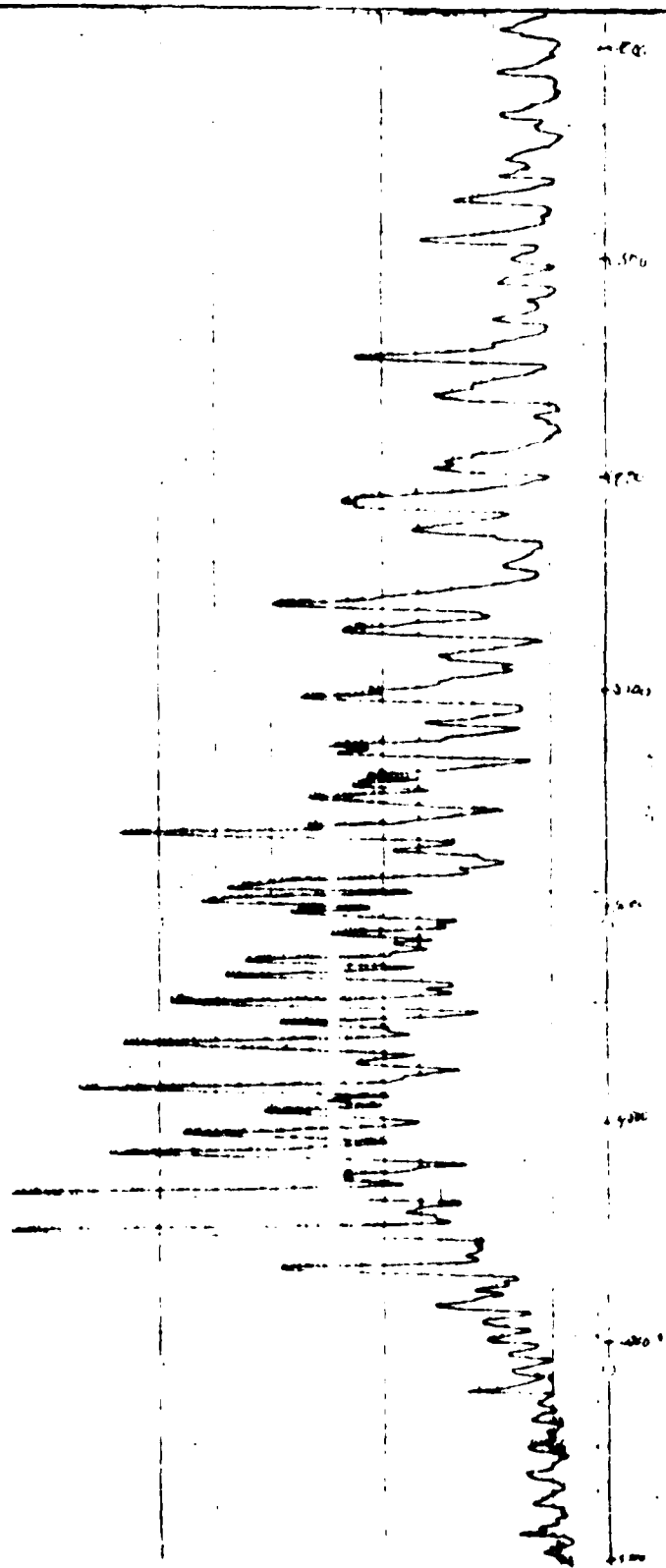
Pressure Variation Spectra

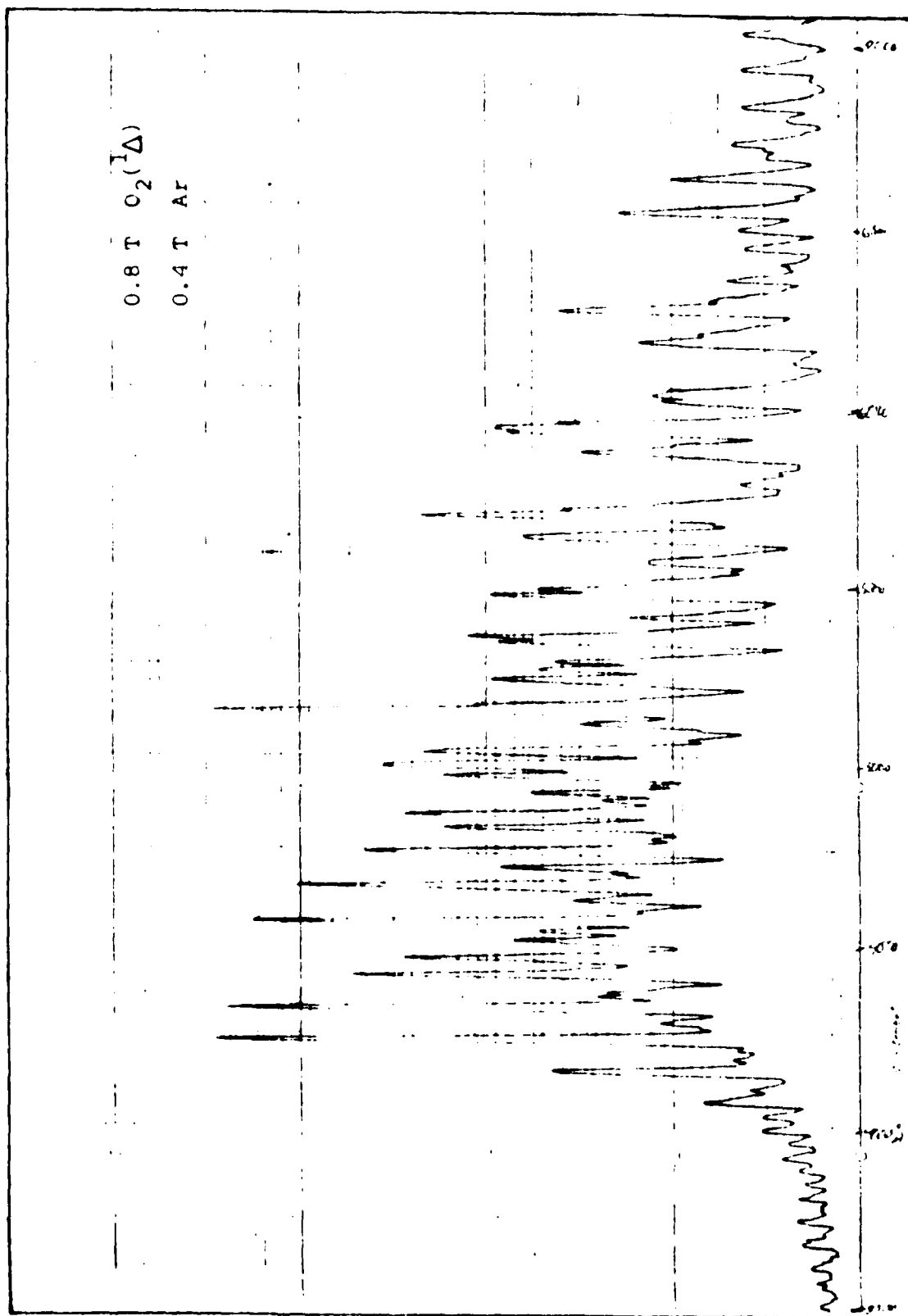
The following eight pages display spectra from the pressure variation runs of the $\text{Pb} + \text{O}_2(^1\Lambda)$ reaction.

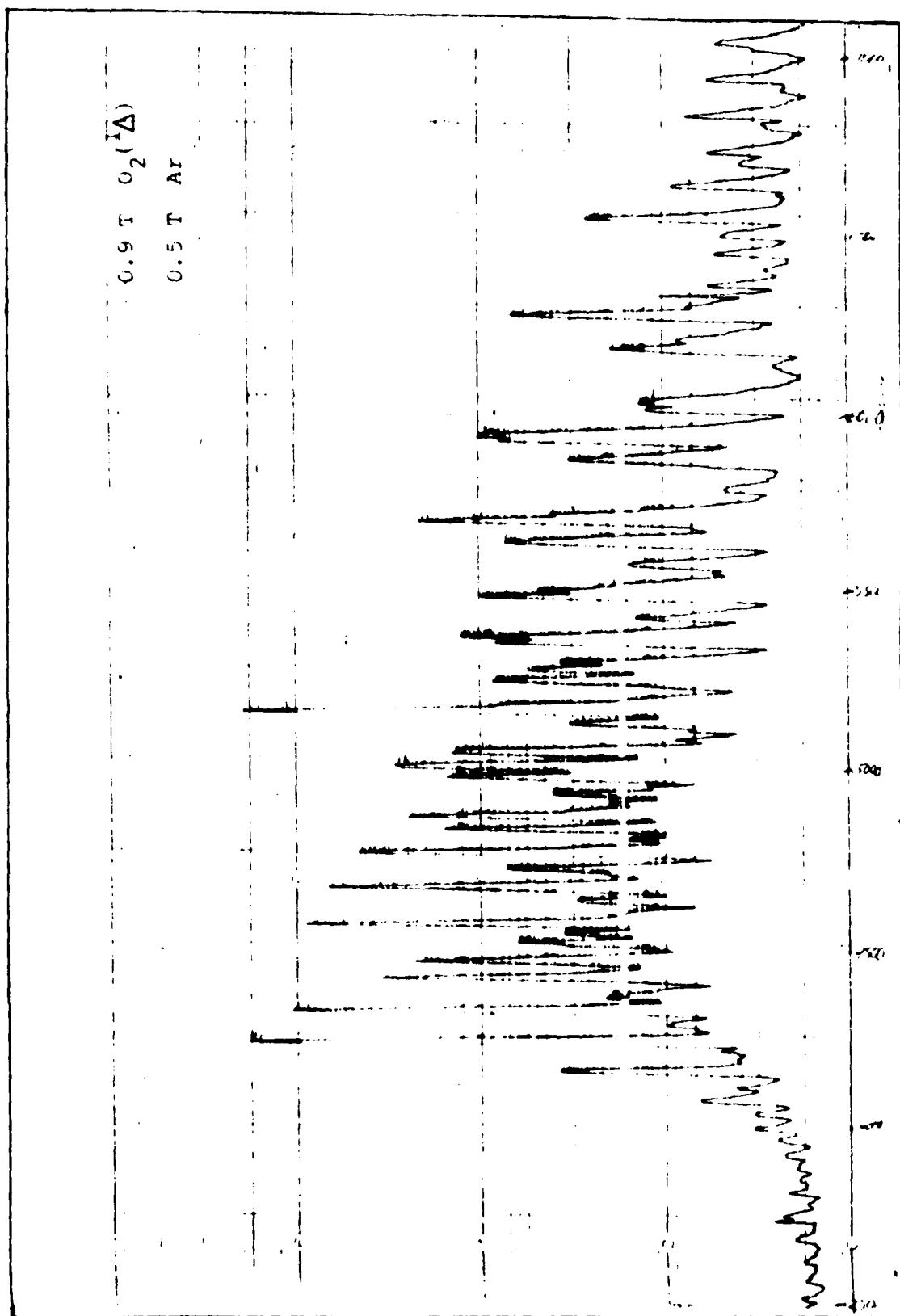


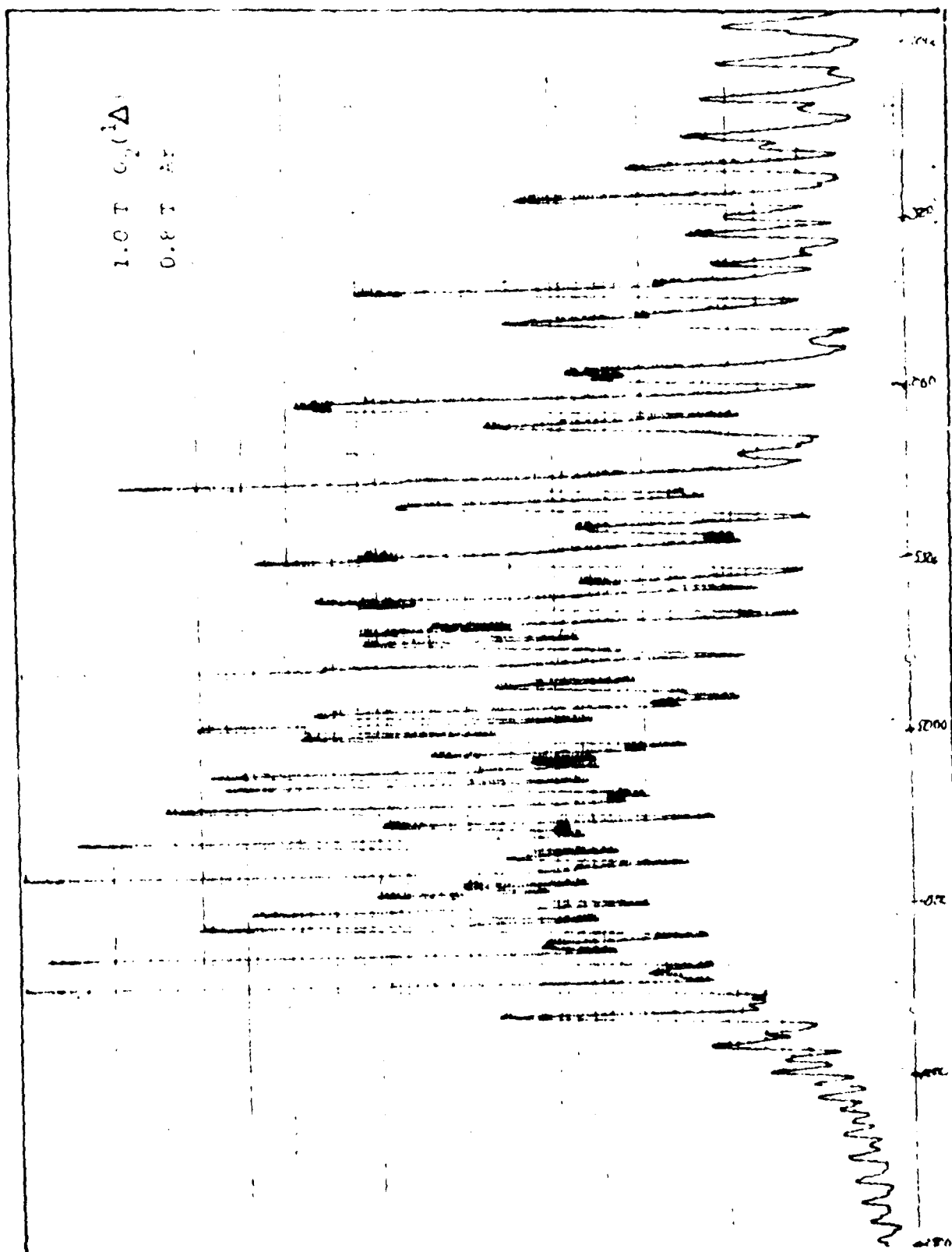


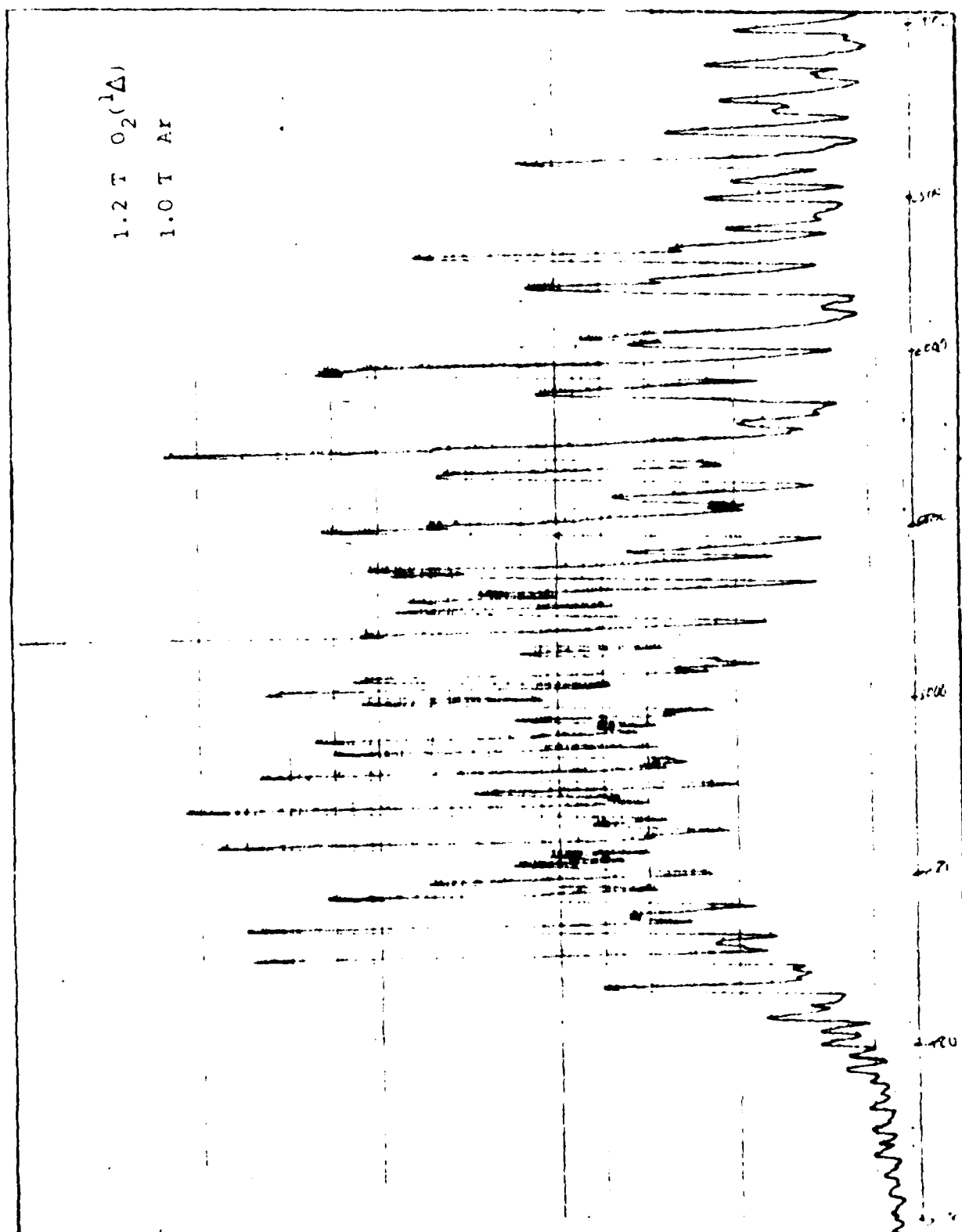
0.7 T $O_2(^1\Delta)$
0.5 T Ar

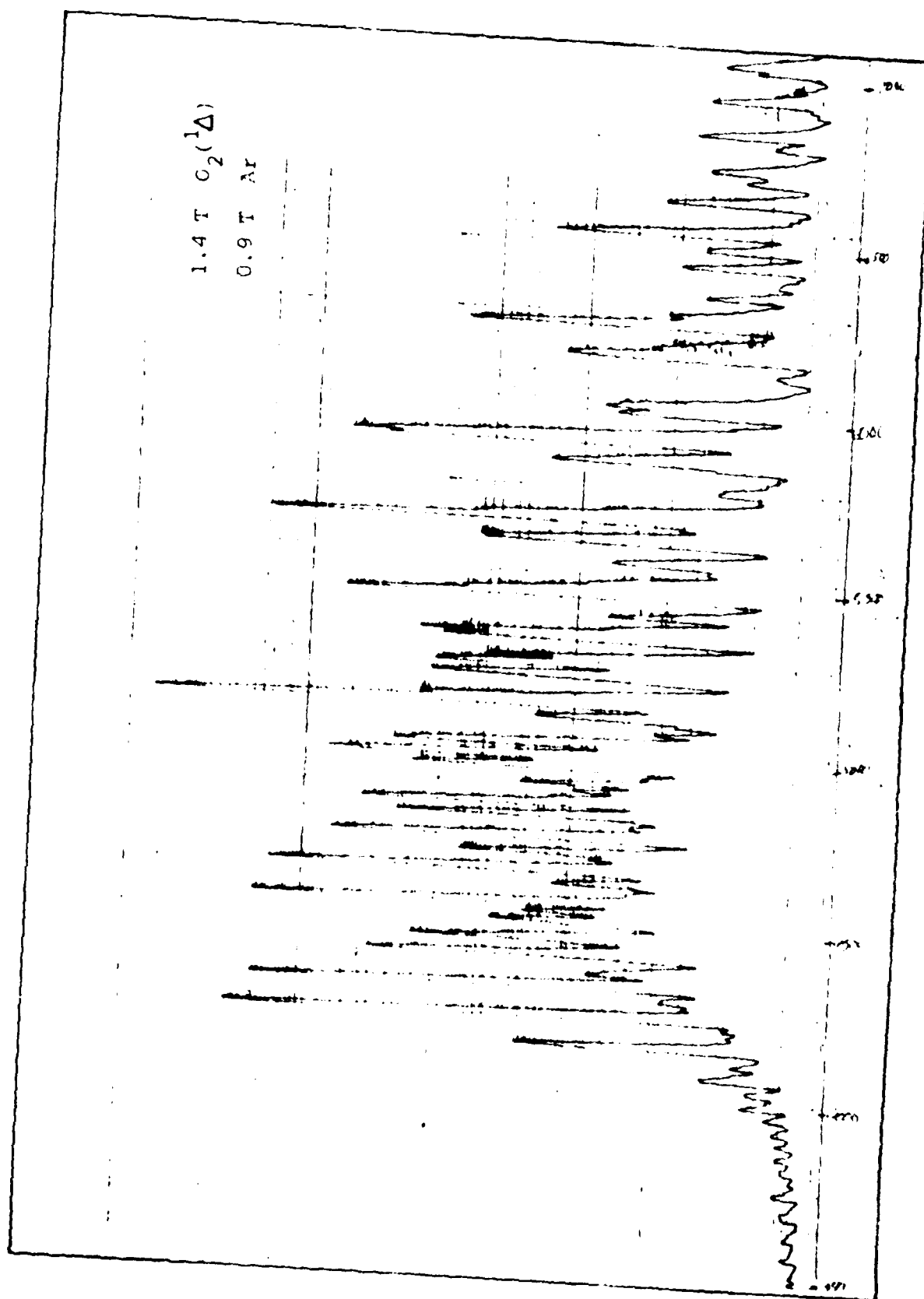












Appendix G

Temperature Measurements

with Heater Off - $O_2(^3\Sigma)$

Run #	Time (sec)	Voltage (V)	Temperature (°K)	Intensity (I)	ln I
1	0	30.6	1033	16.0	2.77
	7.5			10.4	2.34
	20.0	29.3	1002	1.5	0.41
	32.0	27.5	959	0.2	-1.6
	42.0	26.1	926	0	
2	0	32.7	1084	17.0	2.83
	8.0	31.7	1060	11.2	2.42
	14.0	30.0	1019	4.1	1.41
	25.0	27.9	969	0.5	-0.69
	40.0	25.4	910	0	

Vita

Conrad Merritt Ritchey was born in Camden, Arkansas, on 20 May 1955. He graduated from high school in Stephens, Arkansas, in 1972. He graduated Suma Cum Laude from Southern Arkansas University in 1977 with a Bachelor of Science degree in Math and Physics. He received his Air Force commission through the Officer Training School in June of 1978. He served four years as a systems analyst/project officer for tactical, theater and strategic war simulations with the Air University at Maxwell AFB, Alabama. He entered the Graduate Engineering Physics program at the Air Force Institute of Technology in June 1982.

Permanent Address: 301 Onyx Street
Stephens, Arkansas 71764

UNCLASSIFIED

SECURITY CLASSIFICATION OF THIS PAGE

REPORT DOCUMENTATION PAGE

1a. REPORT SECURITY CLASSIFICATION UNCLASSIFIED		1b. RESTRICTIVE MARKINGS	
2a. SECURITY CLASSIFICATION AUTHORITY		3. DISTRIBUTION/AVAILABILITY OF REPORT Approved for Public Release; Distribution Unlimited	
2b. DECLASSIFICATION/DOWNGRADING SCHEDULE			
4. PERFORMING ORGANIZATION REPORT NUMBER(S) AFIT/CEP/PH/83D-10		5. MONITORING ORGANIZATION REPORT NUMBER(S)	
6a. NAME OF PERFORMING ORGANIZATION Air Force Institute of Technology	6b. OFFICE SYMBOL (If applicable) AFIT-EN	7a. NAME OF MONITORING ORGANIZATION	
6c. ADDRESS (City, State and ZIP Code) Wright-Patterson Air Force Base, Ohio 45433		7b. ADDRESS (City, State and ZIP Code)	
8a. NAME OF FUNDING/SPONSORING ORGANIZATION	8b. OFFICE SYMBOL (If applicable)	9. PROCUREMENT INSTRUMENT IDENTIFICATION NUMBER	
8c. ADDRESS (City, State and ZIP Code)		10. SOURCE OF FUNDING NOS.	
		PROGRAM ELEMENT NO.	TASK NO.
		PROJECT NO.	WORK UNIT NO.
11. TITLE (Include Security Classification) Spectroscopy and Kinetics of Lead Oxide Chemiluminescence (Unclassified)			
12. PERSONAL AUTHOR(S) Conrad M. Ritchey, Capt, USAF			
13a. TYPE OF REPORT MS Thesis	13b. TIME COVERED FROM _____ TO _____	14. DATE OF REPORT (Yr, Mo., Day) 83-12-12	15. PAGE COUNT 122
16. SUPPLEMENTARY NOTATION <i>Sign Wilson. 7 Feb 84</i>			
17. COSATI CODES		18. SUBJECT TERMS (Continue on reverse if necessary and identify by block number)	
FIELD	GROUP	SUB. GR.	
19. ABSTRACT (Continue on reverse if necessary and identify by block number) Chemiluminescence from lead oxide has been observed from the reaction between lead (Pb) vapor and $O_2(^1\Delta)$. The spectrum obtained from this emission has been compared to that obtained from the chemiluminescence observed during the reaction between Pb and ground state $O_2(^3\Sigma)$. A significant enhancement of the A and B states over the a state was noted. Spectral analysis has led to the assignment of 225 transitions from the a, b, A, B, C, C', D and E excited states to the ground state. A simple kinetic analysis was performed for the two reactions in which a plot of the logarithm of the intensity of a spectral band vs $1/T^\circ K$ was prepared. From the slope of the straight lines produced, the activation energies of the two reactions were calculated. The activation energy for the $Pb + O_2(^1\Delta)$ reaction was found to be about 21 Kcal/mole with a strong inverse dependency on oven temperature. The activation energy for the $Pb + O_2(^3\Sigma)$ reaction			
20. DISTRIBUTION/AVAILABILITY OF ABSTRACT UNCLASSIFIED/UNLIMITED <input checked="" type="checkbox"/> SAME AS RPT. <input type="checkbox"/> DTIC USERS <input type="checkbox"/>		21. ABSTRACT SECURITY CLASSIFICATION UNCLASSIFIED	
22a. NAME OF RESPONSIBLE INDIVIDUAL Ernest A. Dorko, Professor		22b. TELEPHONE NUMBER (Include Area Code) (513)-255-2012	22c. OFFICE SYMBOL AFIT/ENP

DD FORM 1473, 83 APR

EDITION OF 1 JAN 73 IS OBSOLETE.

UNCLASSIFIED

SECURITY CLASSIFICATION OF THIS PAGE

UNCLASSIFIED

SECURITY CLASSIFICATION OF THIS PAGE

Block 19.

was determined for two oxidizer pressure regimes. The activation energies ranged from 64 Kcal/mole at low oxidizer pressures to 115 Kcal/mole at high oxidizer pressures. The significance of these results is discussed.

UNCLASSIFIED

SECURITY CLASSIFICATION OF THIS PAGE

END

DATE
FILMED

3-84

DTIC